DETAILED STUDY OF THE TRANSIENT ROD PNEUMATIC SYSTEM ON THE ANNULAR CORE RESEARCH REACTOR

A Thesis
Presented to
The Academic Faculty

by

Brandon M. Fehr

In Partial Fulfillment
of the Requirements for the Degree
Master of Science in Nuclear Engineering in the
School of Nuclear and Radiological Engineering and Medical Physics Program, George W. Woodruff School of Mechanical Engineering

Georgia Institute of Technology
May 2016

DETAILED STUDY OF THE TRANSIENT ROD PNEUMATIC SYSTEM ON THE ANNULAR CORE RESEARCH REACTOR

Approved by:

Dr. Farzad Rahnema, Advisor
School of Nuclear and Radiological Engineering
Georgia Institute of Technology

Mr. Michael Black
R&D S&E Mechanical Engineering
Sandia National Laboratories

Dr. Tristan Utschig
School of Nuclear and Radiological Engineering
Georgia Institute of Technology

Dr. Bojan Petrovic
School of Nuclear and Radiological Engineering
Georgia Institute of Technology

Date Approved: April 11, 2016

ACKNOWLEDGEMENTS

I would like to give the utmost appreciation to my colleagues at Sandia National Laboratories for their support, with special thanks to Michael Black, James Arnold, and Paul Helmick for their technical guidance. I would also like to thank Dulce Barrera and Elliott Pelfrey for their encouragement and support, and Bennett Lee for his help with proofreading and formatting.

Special thanks to Dr. Farzad Rahnema for his guidance and contract support, as well as, Dr. Bojan Petrovic and Dr. Tris Utschig for serving on my committee.

Lastly, I would like to thank my parents for their support and encouragement during the whole journey.

This research was funded by Weapons Science & Technology (WS&T), Readiness in Technical Base and Facilities (RTBF). This document is approved for Unclassified Unlimited Release (UUR) with SAND#: SAND2016-2828T.

TABLE OF CONTENTS

LIST OF TABLES

Page

LIST OF FIGURES

NOMENCLATURE

ACRR – Annular Core Research Reactor

ACRRF – Annular Core Research Reactor Facility

FREC-II - Fuel Ringed External Cavity II

KAFB – Kirtland Air Force Base

PL-PCB – Pulse Logic – Printed Circuit Board

Razorback – Coupled point kinetics – thermal hydraulics research reactor code for transient analysis

RU – Rod Unit

SNL - Sandia National Laboratories

TR – Transient Rod

TRIGA – Training, Research, Isotopes, General Atomics

SUMMARY

Throughout the history of the Annular Core Research Reactor (ACRR), Transient Rod (TR) A has experienced an increased rate of failure versus the other two TRs (B and C). Either by pneumatic force or electric motor, the transient rods remove the poison rods from the ACRR core allowing for the irradiation of experiments. In order to develop causes for why TR A is failing (rod break) more often, a better understanding of the whole TR system and its components is needed. This study aims to provide a foundational understanding of how the TR pneumatic system affects the motion of the TRs and the resulting effects that the TR motion has on the neutronics of the ACRR.

Transient rod motion profiles have been generated using both experimentally-obtained pressure data and by thermodynamic theory, and input into Razorback, a SNL-developed point kinetics and thermal hydraulics code, to determine the effects that TR timing and pneumatic pressure have on reactivity addition and reactivity feedback. From this study, accurate and precise TR motion profiles have been developed, along with an increased understanding of the pulse timing sequence. With this information, a safety limit within the ACRR was verified for different TR travel lengths and pneumatic system pressures. In addition, longer reactivity addition times have been correlated to cause larger amounts of reactivity feedback. The added clarity on TR motion and timing from this study will pave the way for further study to determine the cause for the increased failure rate of TR A.

CHAPTER 1
INTRODUCTION

Due to a recent failure of the 13-8 PH rod (also referred to as the dashpot rod) of transient rod (TR) A, it was determined that a full study of the TR system on the ACRR was needed in order to prevent (or mitigate) this failure from occurring in the future. From this, the ACRR TR Pneumatic System Design Study was spawned with the intention of determining why TR A was failing more often than the other two TRs (B and C). By figuring out why TR A is failing more often, the ACRR will be able to operate with less down time and conduct more experiments to further the field of radiation science.

Two previous attempts to study the failures by Clovis and Lippert, and Trinh provided some clarity to the problem, but were not able to make any definitive conclusions. Their research is discussed in more depth later in the study.

Missing from the previous attempts of study were clearly defined motion profiles of the transient rods. Given the motion of the TRs, it will become clearer how each of the TRs react (both mechanically and neutronically) during a pulse by being able to predict stresses on certain components and how the poison rods are ejected from the ACRR core.

The core problem approached in this study is to fully understand how the TR Pneumatic System behaves during operation. As of currently, it is thought that the operation of TR Pneumatic System is a possible reason why TR A is associated with more frequent failures. This study will try to determine if this thought has any merit.

This study will deliver a better understanding of overall TR performance. A more detailed background of the TR system and its components will be given in Chapter 2. Chapter 3 studies the data available to develop an estimate of TR motion, while Chapter 4 derives, from first principles, an understanding of the TR system in both motion and timing. The motion profiles developed in Chapter 3 will be extended to study the neutronic effects in Chapter 5. Chapter 6 will take the same motion profiles developed in Chapter 3 and apply them to study the impact of a broken TR on the dust cap. Lastly, concluding remarks and future work are provided in Chapter 7.

CHAPTER 2
BACKGROUND INFORMATION

ACRRF Overview

The Annular Core Research Reactor Facility (ACRRF) is located in Technical Area-V (TA-V) at Sandia National Laboratories (SNL) on Kirtland Air Force Base (KAFB) in Albuquerque, NM. The ACRRF consists of two separate cores: the Annular Core Research Reactor (ACRR) and the Fuel Ringed External Cavity (FREC-II) (shown in Figure 1).

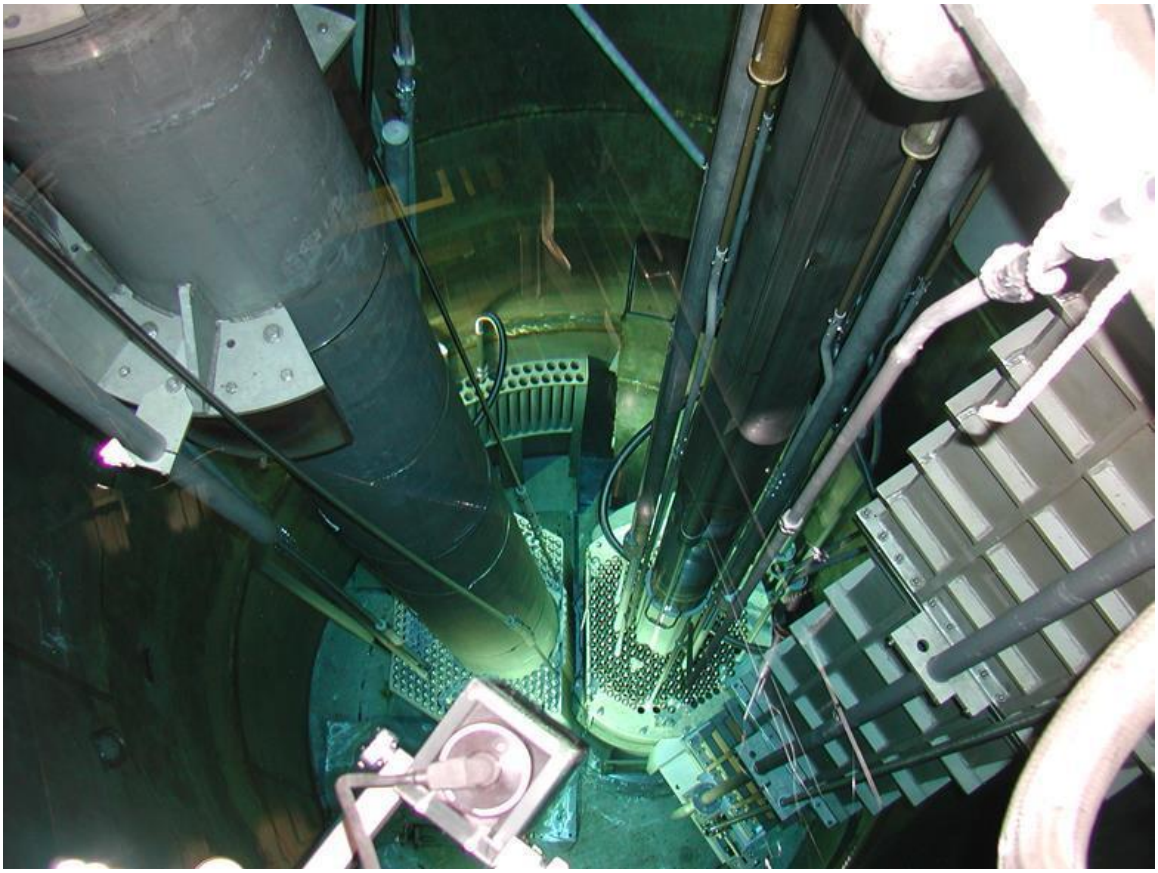

Figure 1. ACRR (right) with FREC-II (left) Decoupled [1]

The ACRR is an open-pool, modified TRIGA-type design that uses light water as the coolant and moderator with cylindrical fuel elements arranged in a triangular-pitched grid located within a hexagonal core grid. Within the core sits a 233 mm dry central cavity for irradiation. The core consists of 200-250 UO_2–BeO fuel elements, six fuel-

followed control rods, two fuel-followed safety rods, and three void-followed transient rods (arrangement shown in Figure 2). The ACRR allows for both steady state and pulse operations, which are limited to 4 MW and 45,000 MW respectively [2]. ACRR also allows for a transient operation, which can tailor the reactor pulse shape for a reactor energy deposition of up to 300 MJ. The primary mission of the ACRR is to provide a means to subject various components or systems to pulse and steady-state neutron irradiation environments.

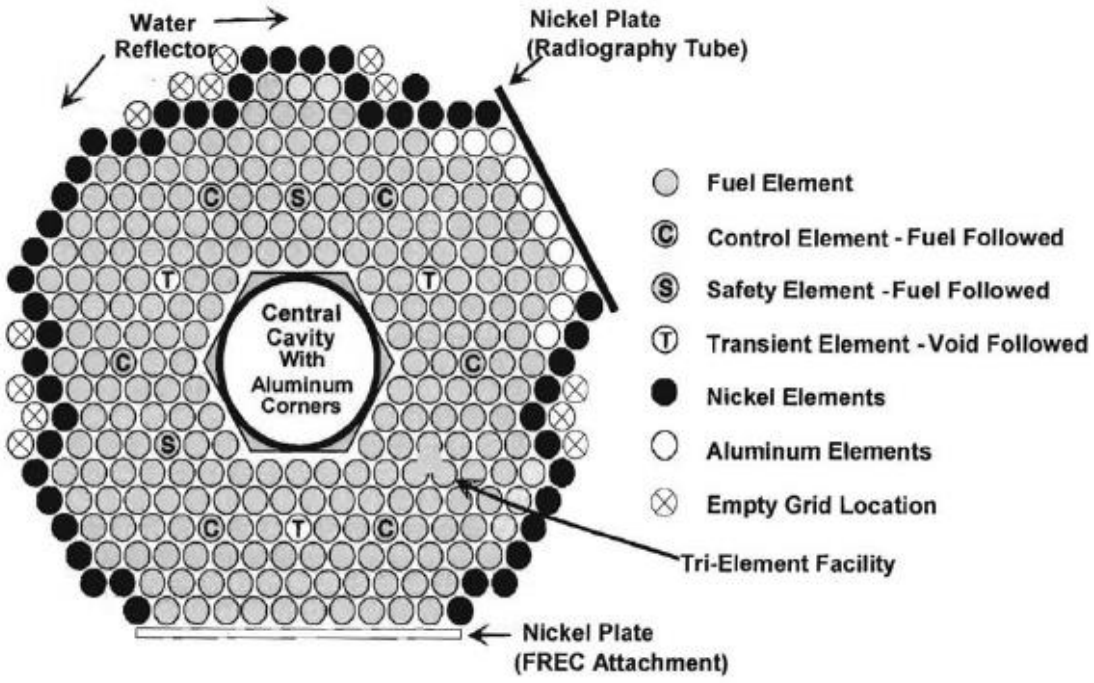

Figure 2. Standard ACRR 236 Fuel Element Core Loading

Technical Area Five (TA-V) has existed at Sandia National Laboratories since 1961, when the first reactor building was built to house the Sandia Engineering Reactor (SER). The Annular Core Pulsed Reactor (ACPR) replaced SER in 1967. The ACPR was a modified TRIGA Mark F design with uranium zirconium hydride fuel and the ability to operate in steady state and pulse modes. After operating for 10 years, the ACPR was replaced with the ACRR in its current state. After upgrading to the ACRR, the uranium zirconium hydride fuel was repurposed to create FREC-II, which can be coupled to the ACRR. The advantage of FREC-II is its large (20 inch) dry central cavity.

A pulse or transient operation in the ACRR is driven by the withdrawal of the three transient rods (TRs) out of the core. The three transient rods combine to have a reactivity worth of \$4.25, while the control and safety rod banks combine for reactivity worths of \$12.00 and \$2.15 respectively. The ACRR provides the capability of tailoring the pulse size (up to \$4.25) by varying the starting position of the TRs by driving them up or down using a stepper drive motor. For more information on how the reactivity is inserted into the core during a pulse, see Chapter 5. The TRs are driven out of the core by either pneumatic ejection or by the stepper motors.

For a pulse or transient operation, the ACRR can operate in one of three modes: pulse, pulse-reduced tail (PRT), or transient rod withdrawal (TRW). In both the pulse and PRT modes, the TRs are pneumatically ejected from the core at a rapid rate (tens of ft/s); whereas, in TRW mode the TRs are driven out of the core using the stepper motors at roughly 0.4 in/s. The difference between pulse and PRT modes is the time at which the TRs are dropped back into the core. By allowing the TRs to drop back in the core earlier, the pulse shape is manipulated to reduce the tail of the reactivity insertion (hence the name pulse-reduced tail).

Transient Rod Assembly Overview

The transient rod assembly consists of three major sections:

- TR Pneumatic System (shown in Figure 3 and Figure 4)
- TR Mechanical Linkages (shown in Figure 5)
- TR Drive Motor Assembly (shown in Figure 6)

It should also be noted that this part of the TR assembly is composed of only the mechanical components. There is also an electronic control system aspect to the TR assembly that is not studied in as much detail.

Transient Rod Pneumatic System

The TR pneumatic system supplies the force to eject the poison rods out of the core. The TR pneumatic system starts at the nitrogen bottles and is routed through ~ 100 feet of piping via a regulator to the accumulators. The regulator provides the set pulsing pressure of 65 psig and can be vented through relief valves in case of a failure. The accumulator volume is much larger (~ 700 in^3) than all other components in the

pneumatic system. The solenoid valve, which is the driver of the whole TR pneumatic system, controls the release of nitrogen pressure from the accumulator to the cylinder via controls set by the operators. Nitrogen flows into the pneumatic cylinder at the manifold block, and then connects into the TR mechanical linkages at the pneumatic piston.

TR Mechanical Linkages

Composed of both moving and stationary components, the TR mechanical linkages provide the structure and moving components to allow for the rapid ejection of the poison rods (which are a part of the mechanical linkages). The moving components of the mechanical linkages consist of the pneumatic piston, piston rod, upper aluminum connecting rod, dashpot rod (or 13-8 rod), lower aluminum connecting rod and the poison rod (seen in Figure 5). The structure of the mechanical linkages helps prevent the moving rods from misaligning and moving transversely. Consisting of upper and lower guide tubes, the dashpot and the pneumatic cylinder assembly, the structure of the mechanical linkages is rigidly bolted to the ACRR bridge plates. Also included in the mechanical linkages are upper and lower stops to the TR pneumatic system. The upper stop is composed of the dashpot and aluminum piston and inhibits the upward motion of the TRs by relying on a hydro-lock brake, which is designed to uniformly slow the TRs to a stop. The lower stop is made up of an air cushion in either the pedestal or pneumatic manifold block (if no pedestal is installed). This air cushion works by trapping nitrogen pressure between the air cushion and piston seal, thereby forcing the pressure to be vented out of a small vent hole in either the pedestal or manifold block. These stops are designed to slow the TRs down significantly thereby reducing loading to the structure and moving components contained within the mechanical linkages.

Transient Rod Drive System

The TR drive system allows for the operators to customize the size of the pulse by adjusting the starting position of the TR bank. The TR drive system connects into the mechanical linkages via a yoke located underneath a knob on the upper aluminum connecting rod. Using a stepper motor, the yoke is driven upwards or downwards to adjust the height of the transient rods. The TRW method of pulsing uses the TR drive system rather than the pneumatics to force the poison rod out of the core.

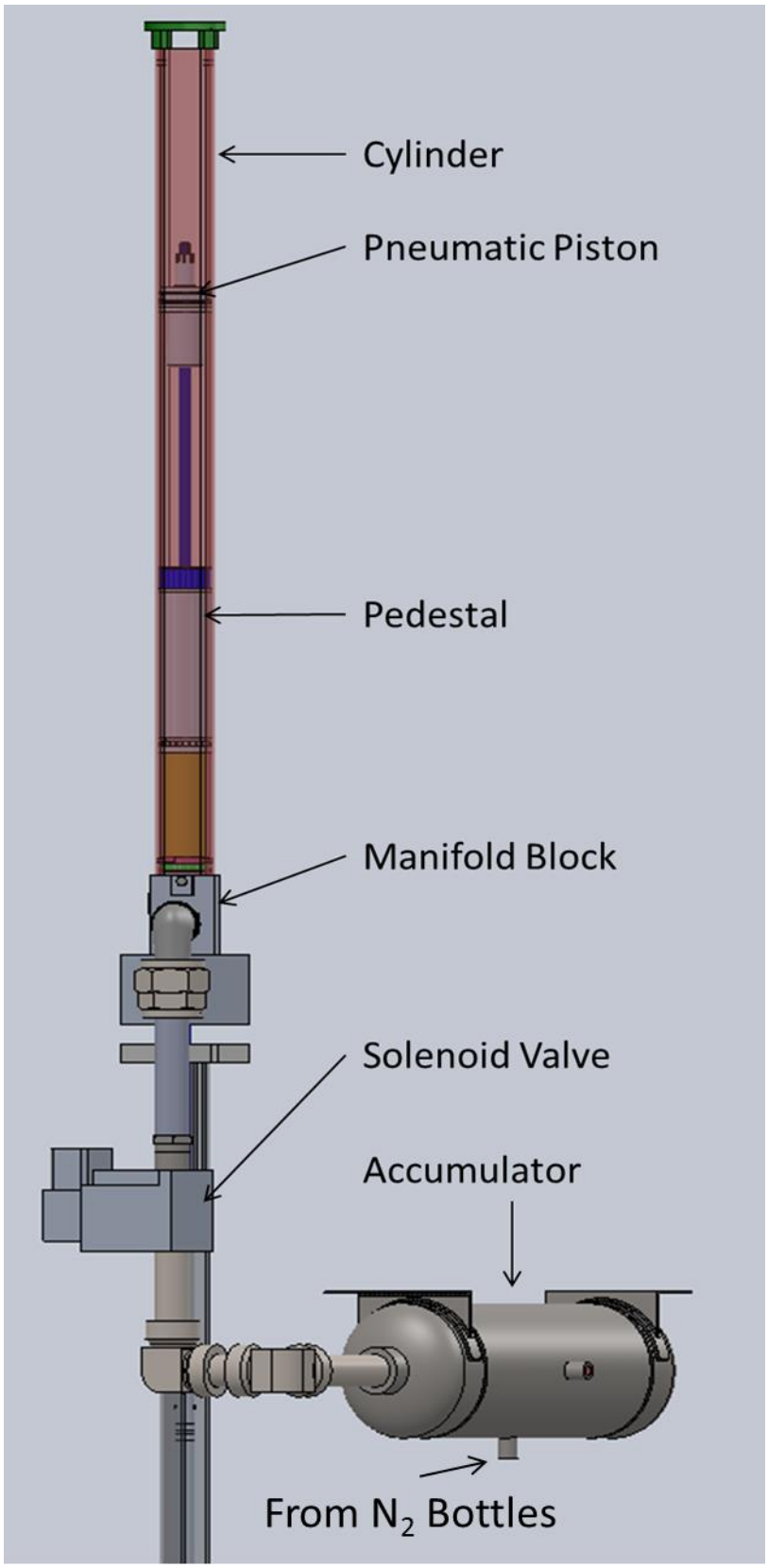

Figure 3. Connection of TR Pneumatics System to the TR Mechanical Linkages

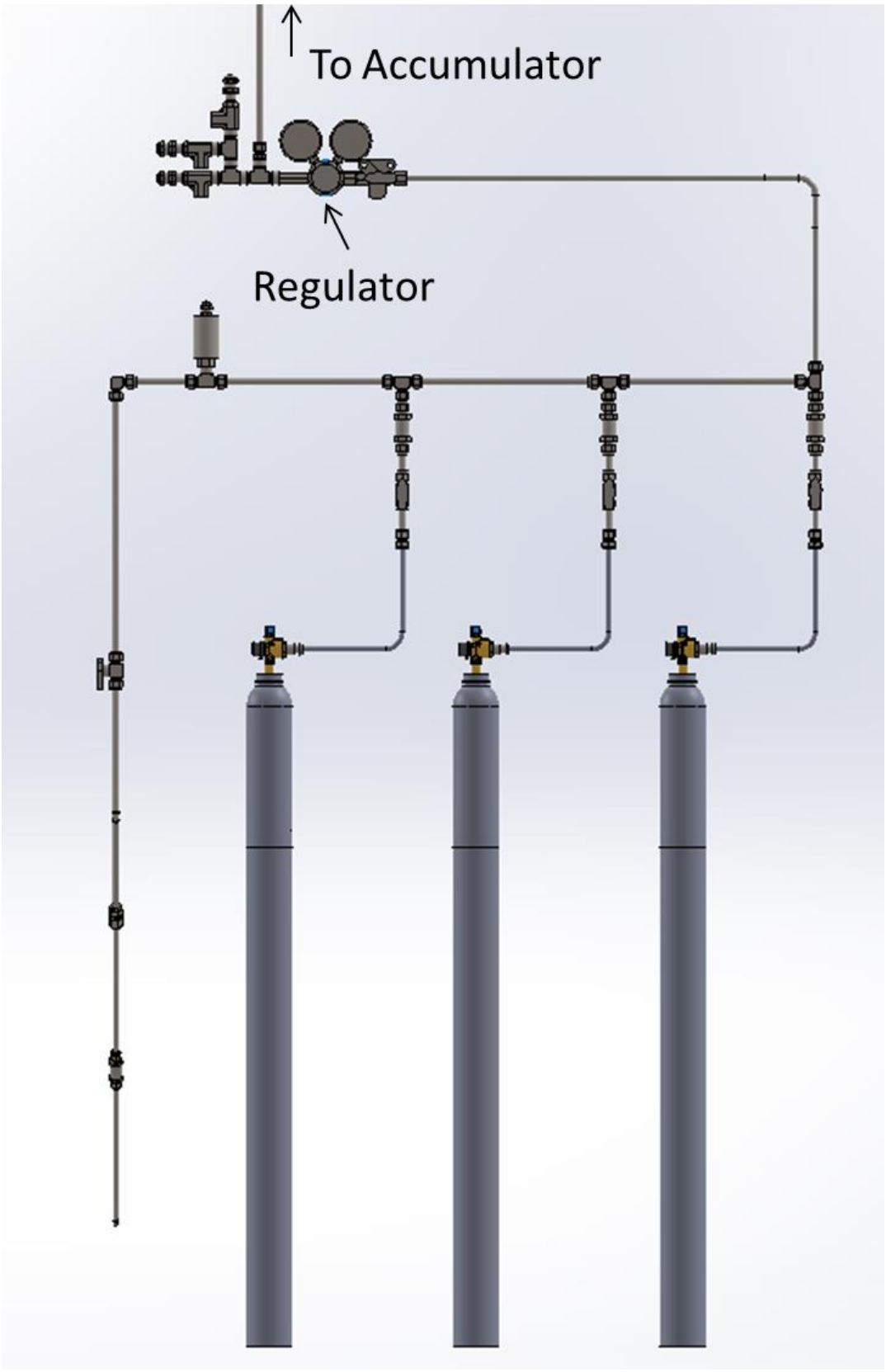

Figure 4. Nitrogen Bottles and Regulator; Beginning of TR Pneumatic System

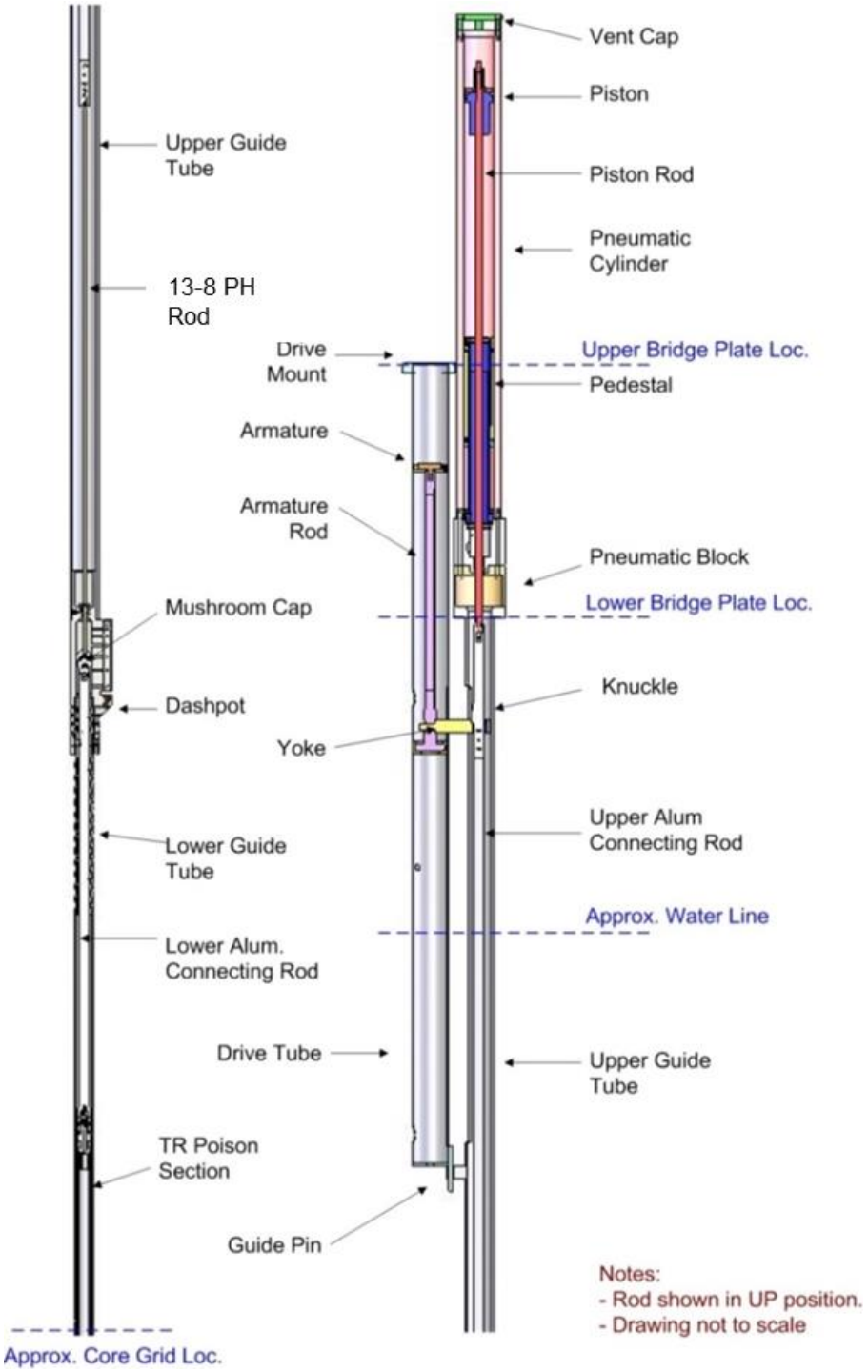

Figure 5. TR Mechanical Linkages Layout

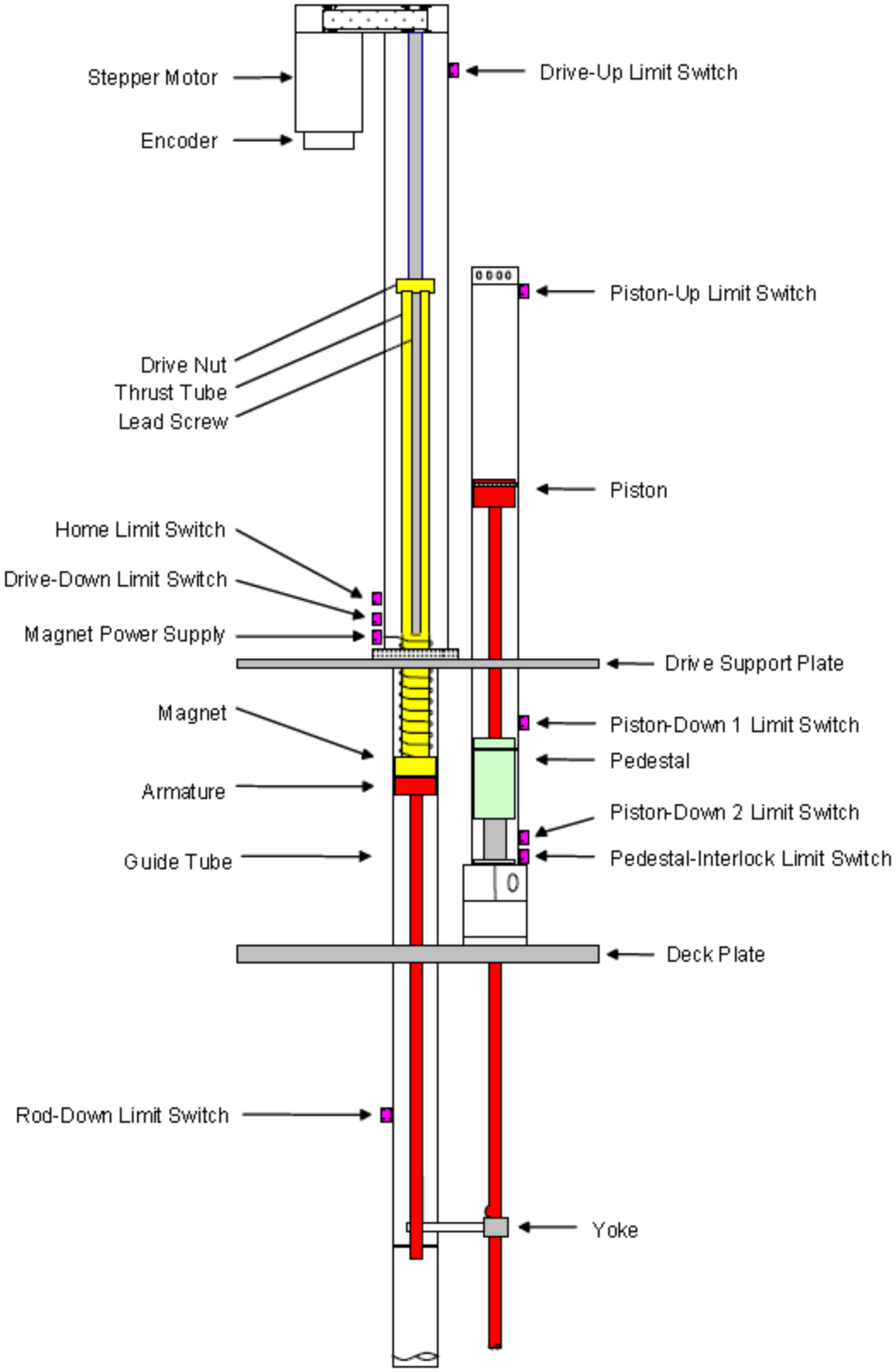

Figure 6. TR Drive Assembly

Previous Work

Two previous attempts to study TR performance were performed in the past decade. The first, competed by Dave Clovis and ACRR facility operations during October and November of 2008, had the intention to study the motion of the TRs and perform a design study on the dashpot rod itself. The second study, completed by Tri Trinh and Russell DePriest in late 2009, was aimed at studying pulse repeatability and verifying the accuracy of the pulse worth.

Clovis and Operations

To study the motion of the TRs, Clovis and operations installed accelerometers on all three TRs to measure approximate acceleration during both rod ejection and drop. The wide variety of parameters tested includes:

- Varying accumulator pressure (30, 45, 65 psig)
- Pulsing rods from wildly different starting positions
- Changing the bleed valve position to allow for quicker or slower drop times in the pedestal
- Measuring both fire and drop times
- Replacing the muffler on the solenoid valve (for reference, a new muffler has less gunk buildup allowing a quicker rate of nitrogen exhaust out of the cylinder)

Even though the experiment seemed to have a good estimation of what parameters will lead to a better understanding of the TR operation, there are a couple of points that make the data unsuitable for further study in this analysis. The worries include:

- Rigidity of the connection of the accumulator to the piston (bolted instead of fixed)
- Unreliability of accelerometer (most data was clipped above 730g)

However, the one definitive result to come from this study was that the dashpot rod was redesigned with 13-8 PH stainless steel instead of 17-4 PH stainless steel. Also, the threads were now to be rolled rather than cut.

Some of the initiatives to be completed with further study include:

- Develop a method to measure TR displacement/velocity/acceleration

- Vary nitrogen accumulator pressure to determine effect on rod motion and pulse repeatability
- Provide more description to the ACRR Safety Basis on how the TR system works and how it impacts reactivity of the reactor [3]

  All three initiatives are studied in greater detail in the following study.

Trinh and DePriest

Part of the analysis completed by Trinh involves the construction of a test platform to test the effect of varying accumulator pressure and the pipe length from the accumulator to the pneumatic manifold on both TR travel time and dashpot forces. As with the study by Clovis and operations, details regarding the accelerometer lead to suspicion with the data and results. Trinh concluded that different accumulator pressures did not have much effect on the total travel time of the TR [4]. Due to the difference in test setup versus the ACRR, it is difficult to say whether the results are truly believable; however, the ACRR TR Pneumatic System Design Study intends to build a full scale test stand of the ACRR (similar to Trinh's) to test parameters like these.

CHAPTER 3
EXPERIMENTAL PRESSURE DATA

Purpose

Pressure transducers were installed with the intent of isolating pressure behavior between TR A versus B and C, as the pressure behavior between the three rods is thought to be a cause to the increased failure rate of A. The following section discusses the processing, methodology and results derived from the data collected from the pressure transducers located on the TR pneumatic system. This data provides a large basis for the sum of all work completed during this thesis.

Gathering of Data

Pressure Transducers

The pressure transducers installed at the accumulators (see Figure 7) are Endevco Model 8530B-200, while the transducers installed on the pneumatic manifold block (see Figure 8) are Endevco Model 8530BM37-200-1. Note, the numbered tags on Figure 7 and Figure 8 connect to the bill of materials for the other components in the system. The only difference between the two models are the connections, otherwise, both models have the same operating parameters. Each transducer was sent to the Primary Standards Lab at SNL for calibration (traceable to NIST). The data from the transducers is processed through a Yokogawa DL850E oscilloscope, where the data is output to a waveform (.wvf) data file. These files are converted to a .csv file using Yokogawa's free viewer software.

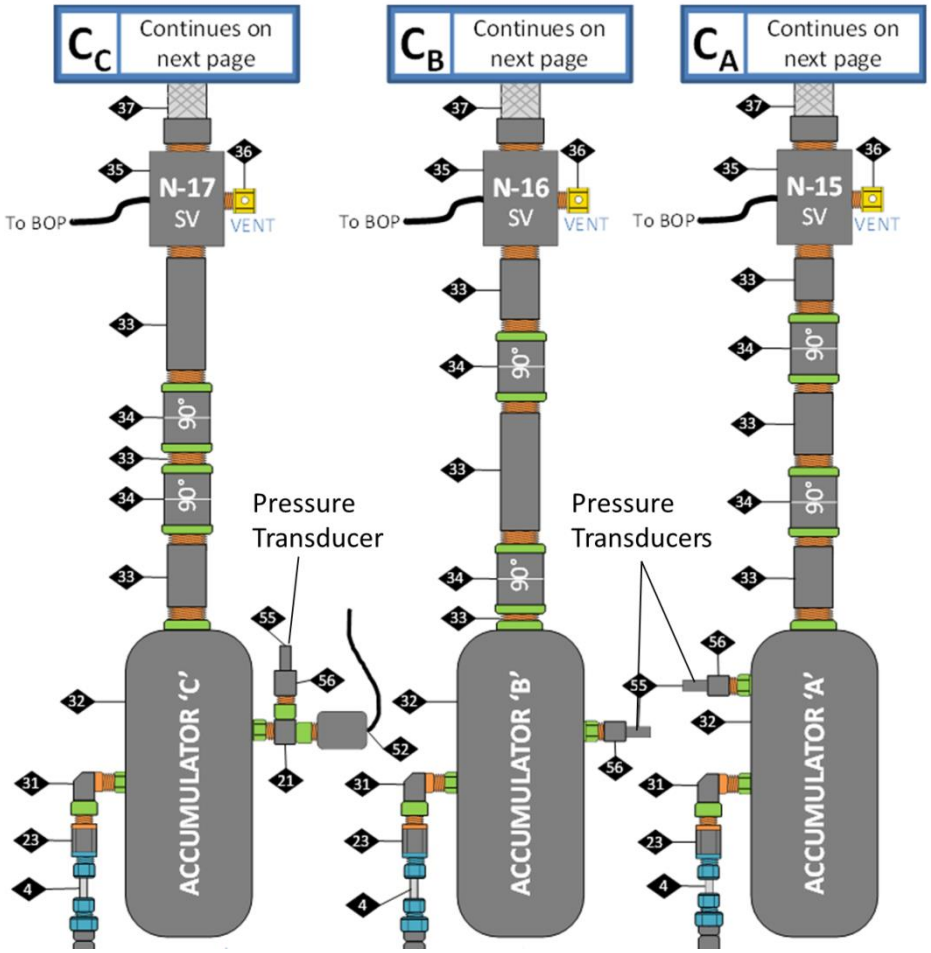

Figure 7. Pressure Transducer Location Accumulator

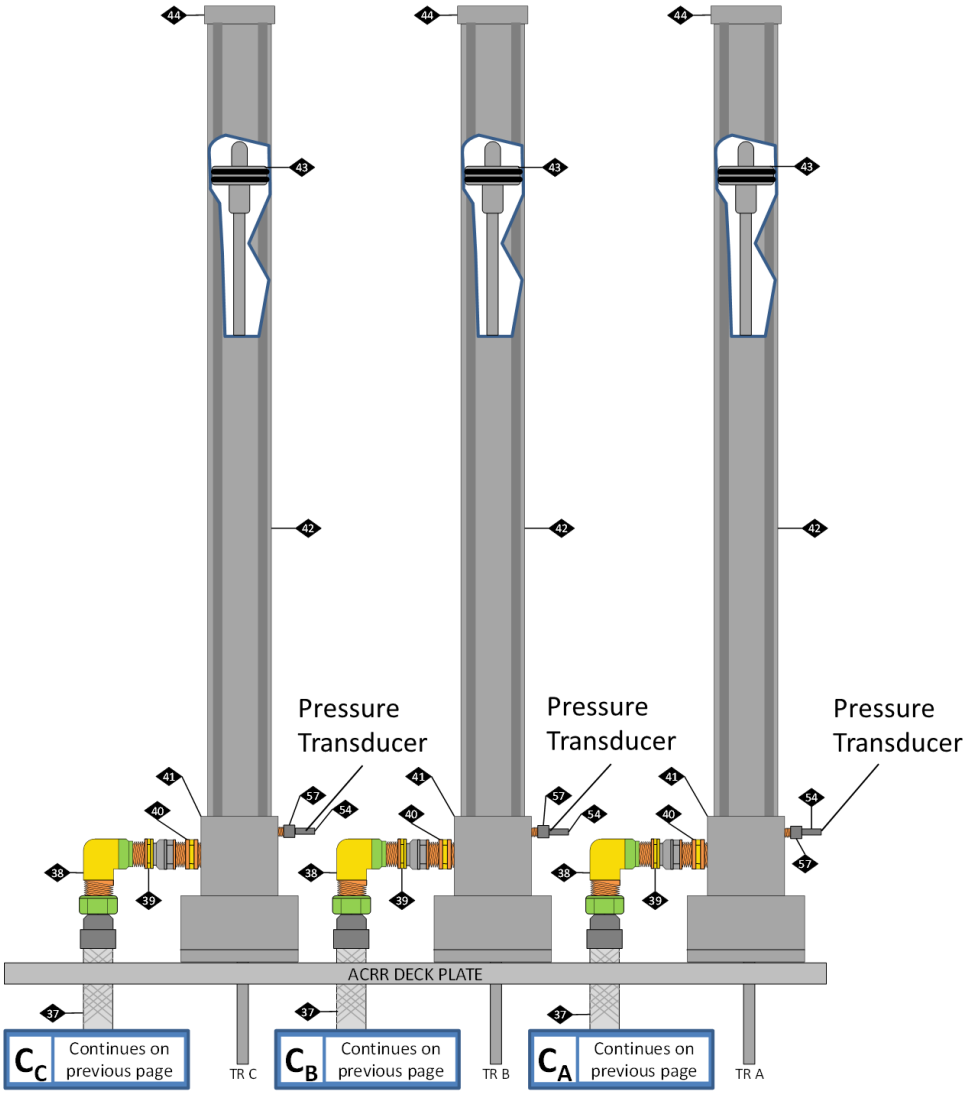

Figure 8. Pressure Transducer Location Manifold Block

Processing of Data

Raw Data

The output from the raw data is a set of time versus voltage data (measured in mV). The data is then run through the calibration curves (each transducer has a slightly different equation for calibration) to make it usable. A sample plot of the data is shown in Figure 9.

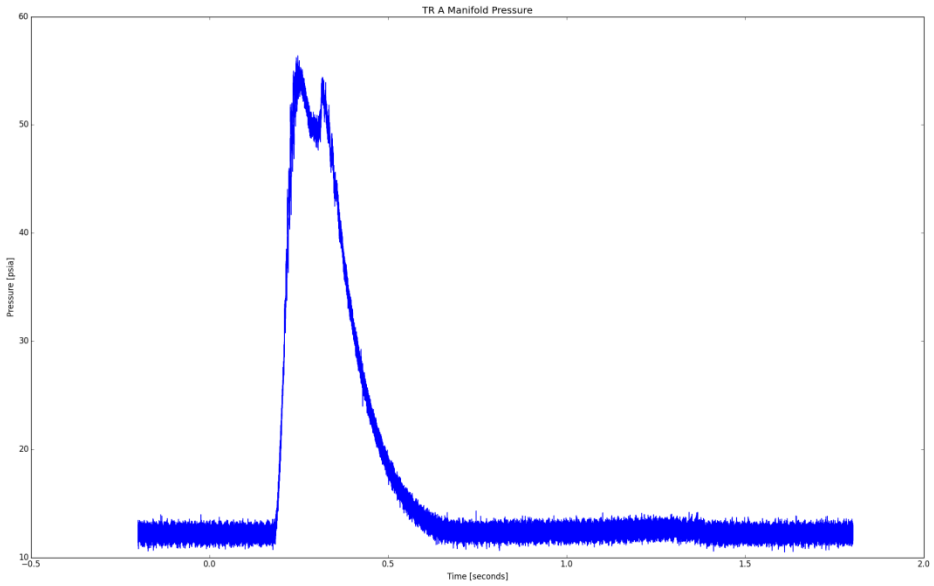

Figure 9. Unfiltered TR Manifold Pressure Data

Filtering Method

The data is filtered using a Savitzky-Golay filter. The Savitzky-Golay filter smooths the data using the convolution method in order to increase the signal to noise ratio while keeping the integrity of the signal [5]. The primary advantage of the Savitzky-Golay over other types of filters (e.g. frequency based filters) is that the data does not shift in time. When applying low pass filters as a test, it was noted that the data was shifted in time by as much as a few hundredths of a second, which is unacceptable for this analysis, due to the short duration of the pulse. A sample set of filtered data is shown in Figure 10.

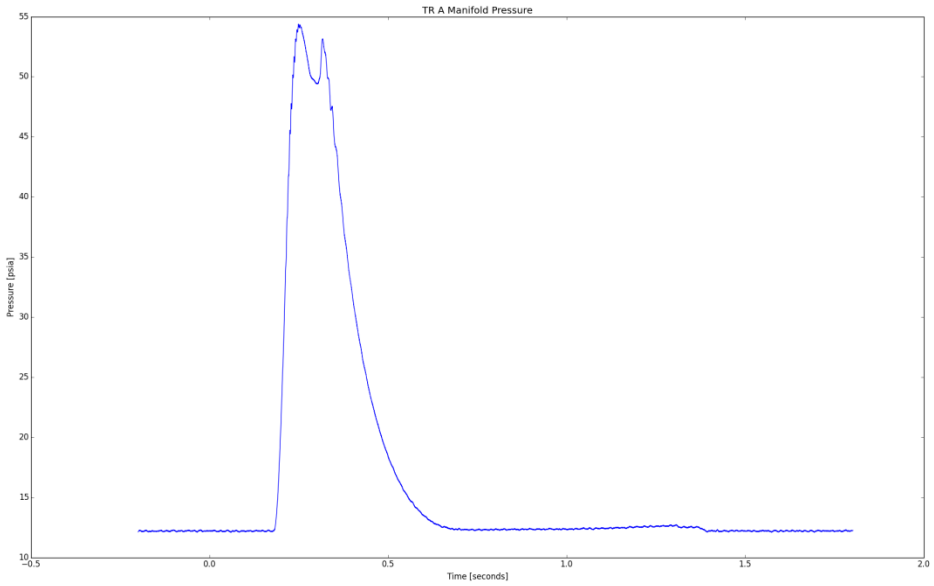

Figure 10. Filtered TR Manifold Pressure Data

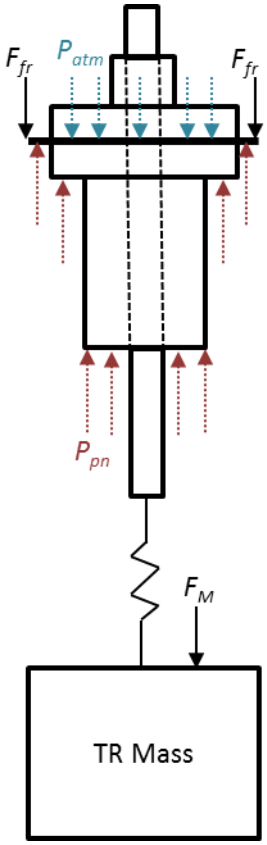

Figure 11. Force Balance on Pneumatic Piston

Force Balance

Pneumatic Force

The pneumatic force F_{pn} (see Figure 11) is calculated from the pressure pushing against the bottom faces of the piston.

$$F_{pn} = \left(P_{pn} - P_{atm}\right) * A_p \tag{1}$$

Where $A_p = 4.604\ in^2$.

Weight

The weight of the transient rod is determined based off of the moving mechanical linkages. The weight of each component is listed in Table 1.

Table 1. TR Weights

Component	Weight [lbs]
Piston	0.9
Piston Rod	3.9
Upper Aluminum Connecting Rod	3.2
Dashpot Rod	0.6
Lower Aluminum Connecting Rod	1.7
Poison Rod	3.8
Total (F_M)	**14.1**

Friction Force

The friction force on the TR is determined by the friction created between the piston seal and the pneumatic cylinder. The specific seal is a Parker 8400 Series U-Cup design made out of carboxylated nitrile. Since very little public testing has been done on this material, Parker was contacted in order to determine an idea for the friction force [6]. The rule of thumb given for friction force is as follows

$$F_{fr} \approx \pi D_{bore} F_c \tag{2}$$

Where $F_c = 1.5\ lbs\ of\ force\ per\ inch\ of\ circumference$ and $D_{bore} = 2.5\ inches$.

$$F_{fr} = \pi(2.5\ in)\left(1.5\frac{lbf}{in}\right) \approx 12\ lbf \tag{3}$$

To find the net force, use the following equation:

$$F_{net} = F_{pn} - F_{fr} - F_M \tag{4}$$

Displacement Algorithm

The general algorithm for calculating displacement is shown in Figure 12. Depending on the location of the piston along its path, the kinematics might change slightly.

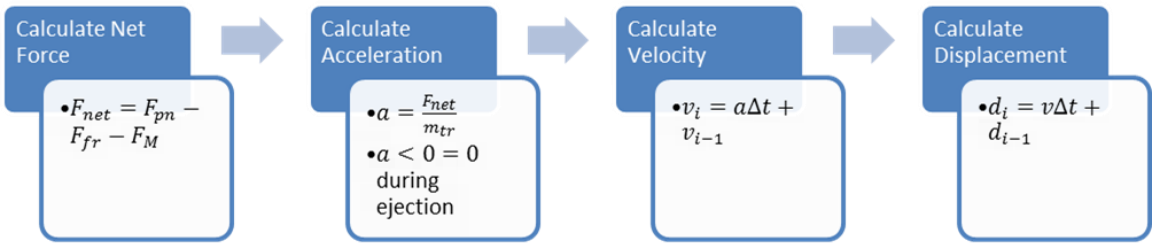

Figure 12. Displacement Algorithm

Rod Unit Definition

In order to define the position of the piston along its travel, Rod Units were created. A Rod Unit (RU) is defined as 0.1 mm. The path of travel for the piston (as shown in Figure 13) starts at 0 RU without the pedestal or at 4370 RU with the pedestal. About two-thirds of the way through the travel (roughly 7800 RU), the dashpot piston enters the dashpot and begins its deceleration to stop upward motion. The full travel of the piston stops when the piston reaches 9000 RU.

At each of the four points mentioned (except for 0 RU), there is a limit switch located on the outside of the cylinder. These limit switches are activated by the magnet on the piston assembly and measure the nominal time at which the piston passes by. PDN 1 (Piston Down) corresponds to 4370 RU, Fire T to 7800 RU, and PUP (Piston Up) to 9000 RU.

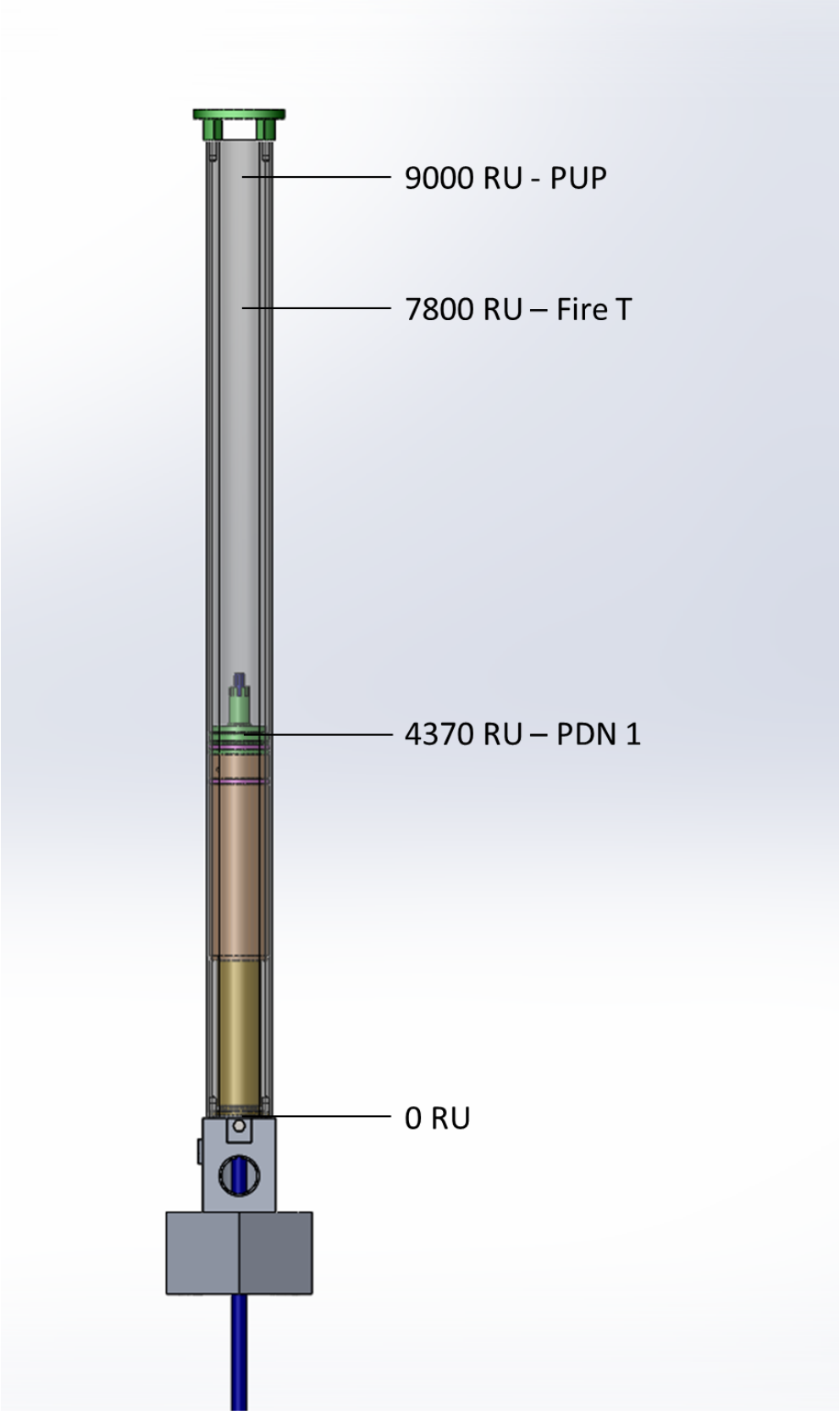

Figure 13. Piston-Cylinder Assembly with Various Rod Unit Locations and Limit Switch Names

Dashpot Deceleration

The TR starts decelerating rapidly once the dashpot piston enters the dashpot (roughly correlated with the pneumatic piston passing the Fire T limit switch). A visual representation of the dashpot piston and dashpot is shown in Figure 14. The TR is assumed to decelerate at a constant rate over the total travel in the dashpot (5.9 inches). This also assumes that the velocity of the TR is 0 when the dashpot piston reaches its end of travel. Ideally, the dashpot is designed such that the dashpot piston motion stops before reaching a hard stop. The dashpot piston can stop due to a physical impact if the water inside the dashpot is forced completely out by the end of full travel. There is a small groove cut into the dashpot (directly below the green adapter in Figure 14) that is the hard upper stop for the dashpot piston in case the hydro-lock brake concept does not work as designed.

An equation for constant deceleration can be derived using basic kinematics. The acceleration is shown below:

$$a = -\frac{v_i^2}{2d} \tag{5}$$

Where v_i is the speed of the TR entering the dashpot, and d is the distance traveled in the dashpot (5.9 inches). This equation can also be used to estimate the slowing of the TR when the piston enters the air cushion (lower stop) with adjusted initial velocities and travel distances.

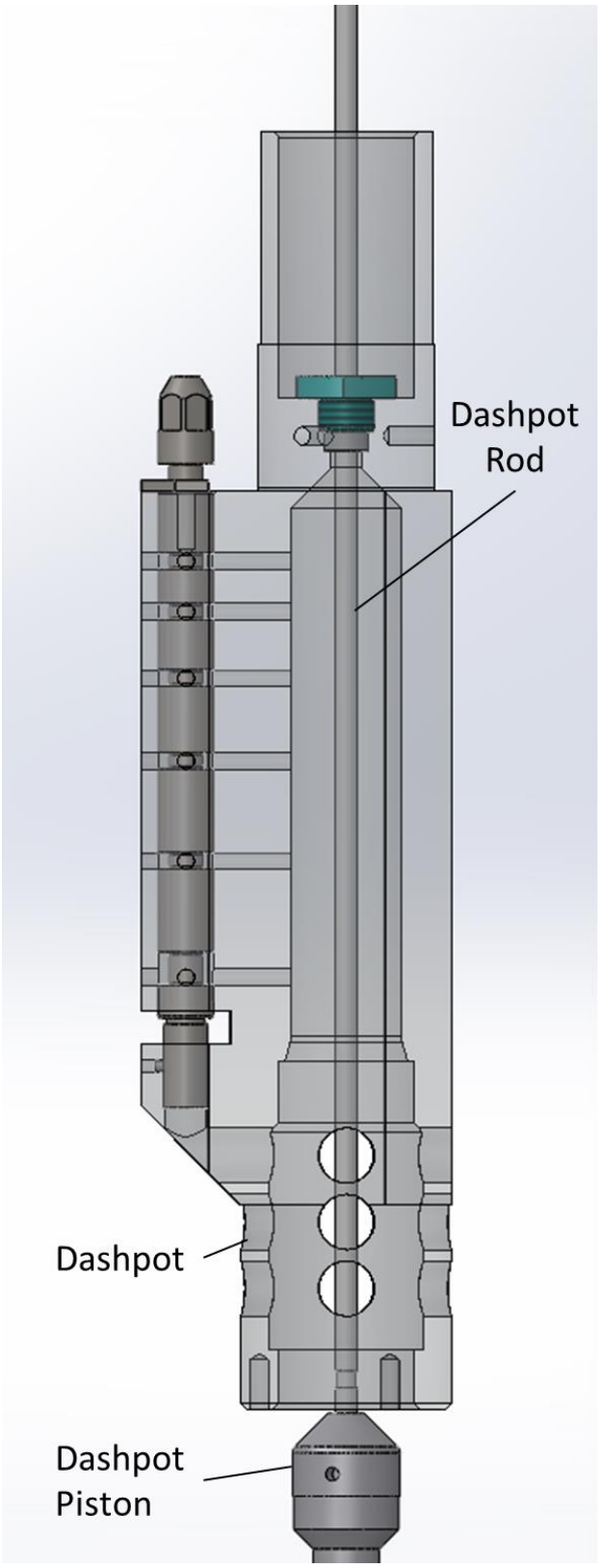

Figure 14. Dashpot Piston Entering Dashpot

Results

Sample Results

The pulse used to generate the plots below is pulse 11616. It has parameters of $1.657 reactivity addition, 5299 RU TR starting height, and a 0.25 second RHU time.

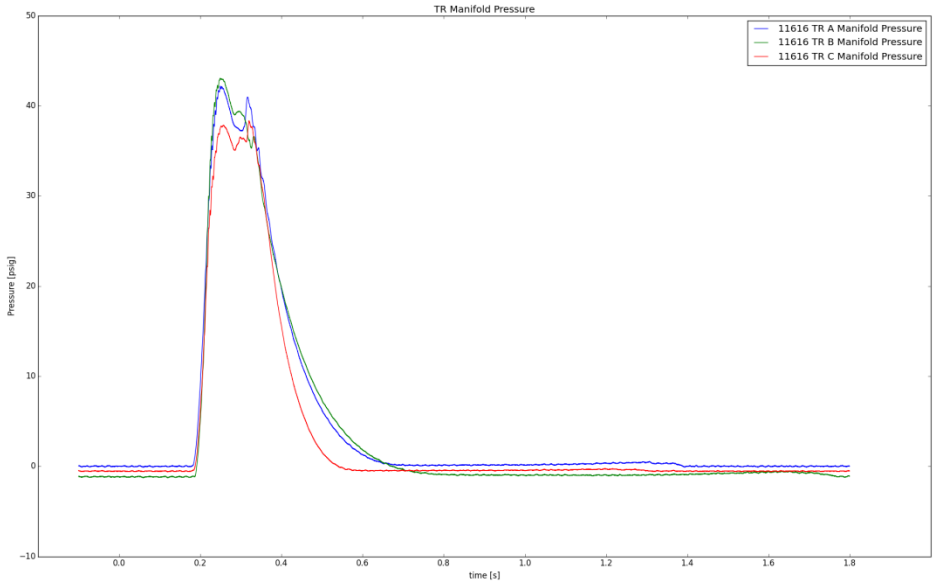

Figure 15. TR Manifold Pressures for a Typical Pulse

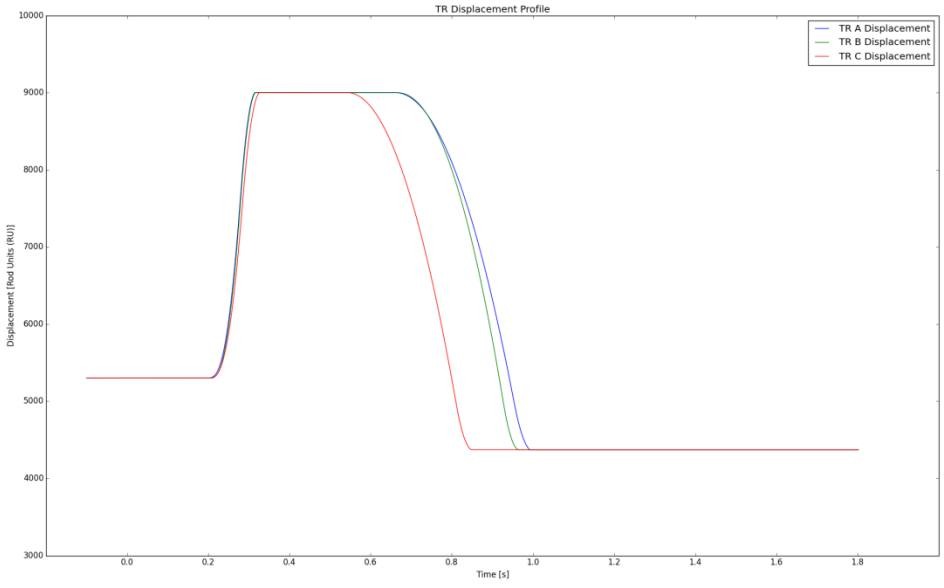

Figure 16. TR Displacements for a Typical Pulse

Trends

There are a few general trends to be aware of after looking at Figure 15 and Figure 16.

- TR B has the highest peak pressure of all three rods (~ 7 psig difference between B and C).
- All three TRs have the same general shape during the peak and plateau sections. This shape is consistent throughout all pulse cases currently available.
- TR A has a higher ending pressure than B or C (~0.35 psig; see Figure 16 after 0.8 seconds).
- Because of the lower peak pressure, TR C starts to fall earlier than A or B. It should also be noted that a bleed hole was drilled in the vent of TR C to decrease the fall time, which correlates to a quicker drop-off in pressure.
- Because of the higher ending pressure for TR A, it takes the longest to reach the full-down position.

Displacement Timing

The displacement profiles are generated using a Python script that implements the displacement algorithm in Figure 12 to calculate the majority of the displacement. However, there are two locations where the algorithm changes: deceleration at both the upper and lower stops. These changes occur starting at roughly 7800 RUs on the rod ejection and roughly 5000 RUs on the rod drop. The effect of the decelerations causes the displacement profiles to flatten out as they approach the full-up and full-down positions respectively.

Rod Hold-Up (RHU) time as shown in Figure 17 is defined as the time at which the signal to close the solenoid valve is sent. Sample values for RHU times in this study are 0.25, 0.40 and 0.70 seconds. What's important to note about RHU time is that it does not directly interface with the piston, but does affect piston motion by setting the time at which the pressure starts to evacuate from the TR pneumatic system.

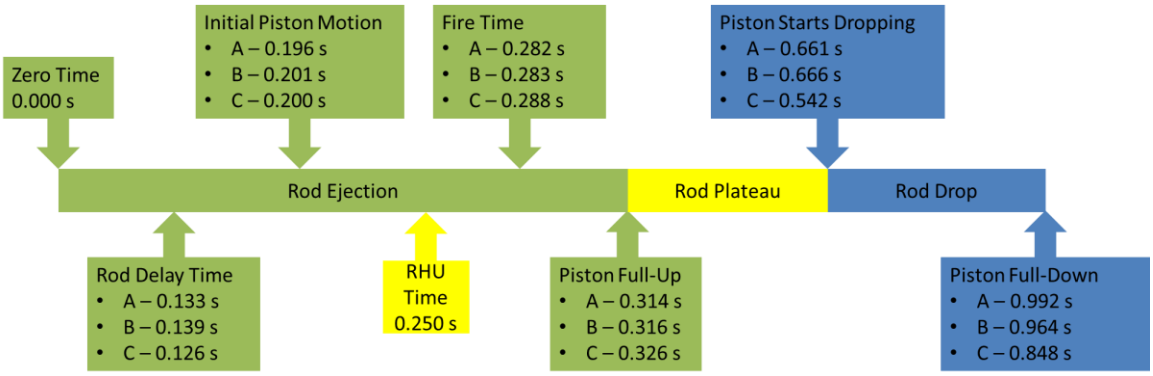

Figure 17. Timing Sequence for a Typical 0.250 Second RHU Pulse

Figure 17 is based off of a 0.25 second RHU, $1.657 reactivity insertion pulse with the TR bank starting position at 5299 RU. A few notes about Figure 17 are listed below:

- Friction is included on the piston seal on the way up is ~12 lbf, and there is no friction on the way down. The friction was "removed" in order to accelerate the drop times. Otherwise, the piston for TR A would not have dropped fully before running out of pressure data. This means that the Piston Full-Down times should be ~ 0.5 seconds longer for each rod than what is shown in Figure 17.
- Each color specifies a certain region of the pulse as noted in the central timeline. The RHU times falls in the rod ejection region for pulses with RHU times shorter than the piston full-up time. There is no correlation between RHU time and piston full-up time; they are independent of each other.
- Figure 17 corresponds to the displacement profiles from Figure 16.
- The rod ejection region is consistent among all pulses with only slight differences in times due to slightly varying pressures and starting positions. RHU time does not have an effect on rod ejection, only on how long the rods stay in the full-up position and when they start to drop back into the core.
- RHU time directly influences the time at which the rod drop starts. Longer RHU times (e.g. 0.4 and 0.7 seconds) will occur during the rod plateau region after the manifold pressure has started to level off near an equilibrium value.

The surprising fact seen with Figure 17 is that TR A does not have the fastest travel times. In fact, TR B travels the full distance in 3 ms less that TR A. While 3 ms is not a very large difference, it rules out the hypothesis that TR A is failing more often due to

quicker ejection times. What is surprising is how much slower the ejection time of TR C is than A or B. A 10 ms difference between TRs A and B vs TR C is more significant. Understandably, this is due to a lower peaking pressure distribution; however, it is seen throughout every pressure data set gathered. Further study (placing potentiometers and accelerometers on the piston) to understand the timing difference is planned for mid-2016.

Comparison with Operator Data

In order to verify that the model in Figure 17 is roughly accurate, the calculated displacement times from Figure 17 were compared with actual operator data. The only two data points that correspond to the figure that are recorded are the Rod Delay Time and Fire Time. Since the Rod Delay Time is set based off of operator estimates, the only way to calibrate the model is using the Fire Time. The comparisons are made in Table 2.

Table 2. TR Fire Times for a 5300 RU Starting Position

TR	Measured [s]	Calculated [s]
A	0.281	0.282
B	0.282	0.283
C	0.285	0.288

There is a very good comparison between the measured and calculated fire times validating the previous calculation method.

Uncertainties

Even though the data in Table 2 matches well, there are still uncertainties in both the Operator data and the calculation method that must be addressed.

Within the operator data, the fire time is measured using a proximity sensor on the outside of the pneumatic cylinder. The proximity sensor is set to trigger when the magnet on the piston passes by the sensor, thereby registering the location and sending the time to the control room for display. However, because the signal has to travel a significant distance and pass through several components, there is a delay in the signal display. The

delay of the whole process (registering, travel and display of the signal) has been estimated to be less than 10 ms [7].

Within the calculation method, the timing is directly driven by one main assumption: the value of piston friction in the cylinder. Since the piston seal is made of a unique material, there is very little published data on friction factors. Also, the friction is assumed to be constant throughout (using a rule of thumb used by Parker [6]) instead of the typical static versus kinetic friction. Changing the value of the friction force drastically affects motion since the friction force is a component of the force balance, influencing the rest of the kinematic parameters appropriately. The only way to know the exact friction values is to measure them directly. The friction factor can change the timing by tens of ms in either direction.

Other assumptions that play lesser effects on the timing include the data filtering method, the exact mass of the TRs, and the geometry of the piston. Each method introduces uncertainties on the order of ms, but the uncertainties are not directly calculated since the friction assumption has higher uncertainties.

Because of the high uncertainty from the assumptions, it was decided that a full statistical comparison of operator and calculated values for fire times is unneeded and unnecessary. For this study, the fact that they are close is sufficient enough.

TR Ejection Limit

An important limit set by the safety requirements of the ACRR is TR ejection time. The limit was initially set by measuring the displacement of the TRs from the pedestal (located at 40.7 cm at the time of measurement) to the dashpot and extrapolating the motion in the dashpot as constant deceleration from the dashpot entrance velocity. From the previous measurements, the withdrawal times ranged from 70 ms for a $1.00 pulse to 88 ms for a $3.50 pulse [8]. Since pulsing with a pedestal can only reach ~ $3.50 in reactivity addition, the $4.25 max pulse was extrapolated to take 80 ms (adding conservatism as well). This 80 ms limit has been implemented to extend to every pulse, regardless of size.

What is not clear about the previous definition is what the 80 ms limit stands for. Does it mean for reactivity insertion time or total motion of the TRs? Looking at Figure 18, it should only be defined for total reactivity insertion since the measurements show it

takes 100 ms to travel ~35 cm from the pedestal, which, coincidentally, corresponds well with the entrance of the TR into the dashpot. The entrance of the dashpot also corresponds well with the effective height of the fuel region within the core (see Figure 19). The dashpot represents the last 5.9 inches (~15 cm), putting the entrance of the dashpot near 75 cm. Even though the effects of reactivity do not turn off as soon as the poison rod leaves the fuel region, the effects do start to taper off significantly. From the previous TR bank reactivity worth curve, the worth drops to 0 at roughly 77 cm [8].

The results from the calculated displacement profile as compared to the TR ejection limit are discussed later on in Chapter 5. Since the displacement profile cannot accurately predict reactivity addition, clarifying the results will be discussed in the context of Razorback, which does take into account the reactor kinetics in relation to the TR motion.

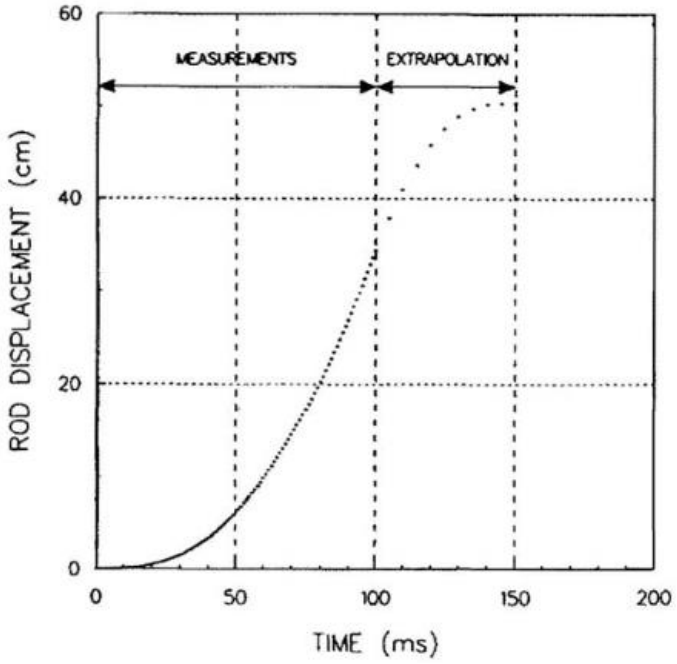

Figure 18. Previously Understood Definition of TR Motion for a Pulse from Pedestal

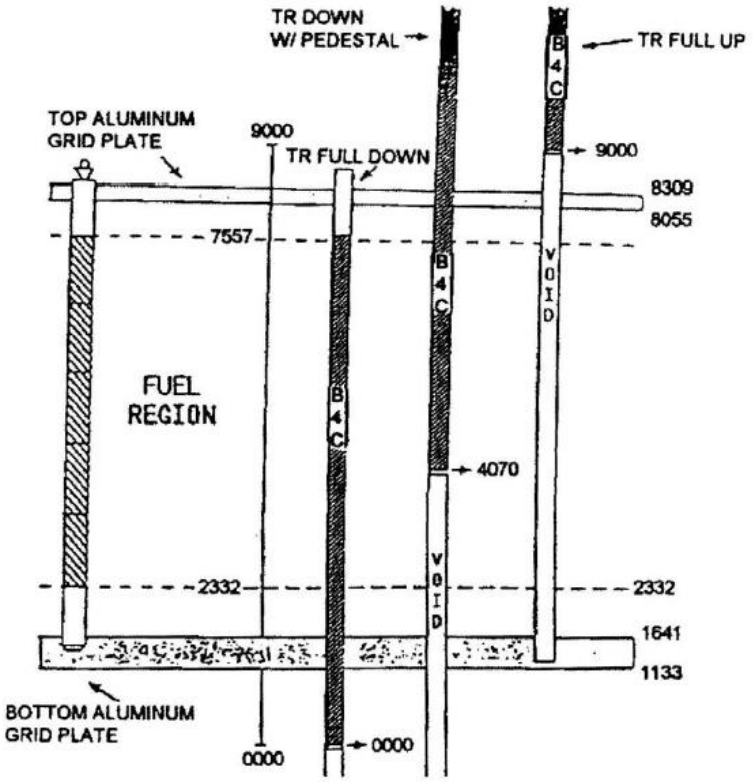

Figure 19. Location of Fuel Region and Various TR Positions in Terms of Rod Units

Discussion

Analyzing the pressure data comprised the largest portion of this thesis. The pressure data is the only viable source available to connect theory of how the TRs should work versus how they work in reality. Because of this, the resulting TR motion will be used to study other phenomenon in the reactor including:

- Using the TR velocity profile as an input into Razorback to study reactor kinetics
- Predicting velocity and acceleration of a broken transient rod as it impacts the dust cap

In terms of predicting why TR A might be failing more often than B or C, this data is inconclusive. It does; however, provide a couple leads for further study, which include:

- Why is TR A failing more often yet TR B actually takes less time to travel in the cylinder? Is there a correlation between travel time and TR failure?

- Does the shape of the pressure data around peak pressure for each of the TRs (shown in Figure 32) have any meaning? Does the oscillation of pressure imply there was an impact in the dashpot?
- TR A has a higher ending pressure (after the TRs have dropped back to the pedestal) than TRs B or C. Could that imply a slower fall time and more stress on the system?
- How accurate is the assumption of deceleration in the dashpot? Does it come to a smooth stop or is there an impact at the end of travel?

All of these questions could potentially lead to the reason why TR A is failing more often. The only way to solve these questions is with more and different types of information. Potentiometer, accelerometer, and strain gauges could be used to measure motion and stress values on certain components (respectively). Luckily, this instrumentation is planned for installation later in 2016, and should help solve the mystery of the failing TR.

CHAPTER 4
ANALYTICAL DERIVATION OF FLOW IN TR PNEUMATIC SYSTEM

Problem Statement

The purpose of this analysis is to analyze the flow of nitrogen through the TR pneumatic system in order to develop a motion profile of the piston during the pulse and be able to predict the pressure distributions inside both the cylinder and accumulators. The predicted pressure distributions will be validated against pressure transducer data, while the motion profile will be compared to proximity switch data. By predicting the motion of the piston, pulse timing will be determined and provided to the engineers/operators for verification. The motion profile will provide an acceleration distribution to be used in Razorback to more accurately predict reactivity insertion into the system.

Problem Definition

The analysis for the TR pneumatic system is split into two sections: accumulator to solenoid valve and solenoid valve to cylinder (see Figure 20 and Figure 21).

Accumulator to Valve

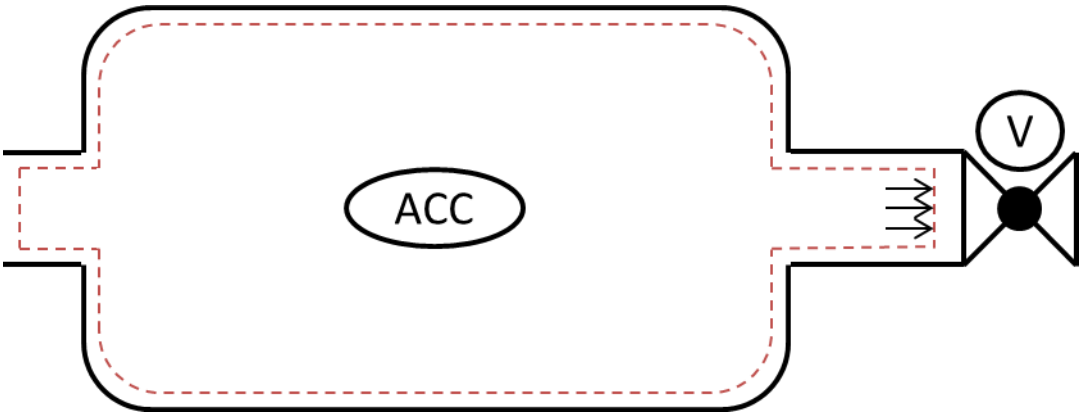

Figure 20. Geometric Representation of the Accumulator to Valve System

Boundary Conditions

- Temperature: Ambient = 294 K (70 F)
- Pressure: 533 kPa (77.2 psia)

Assumptions

- Piping up to accumulator provides insignificant amount of volume during the duration of the pulse; therefore, can be ignored.
- Volume between the accumulator and valve is small meaning the accumulator-valve system can be modeled as a single control volume.
- Solenoid valve is considered to have negligible inner volume.
- Losses and geometry factors within the solenoid valve are taken into consideration when calculating mass flow rate (see Appendix B).

Valve to Cylinder

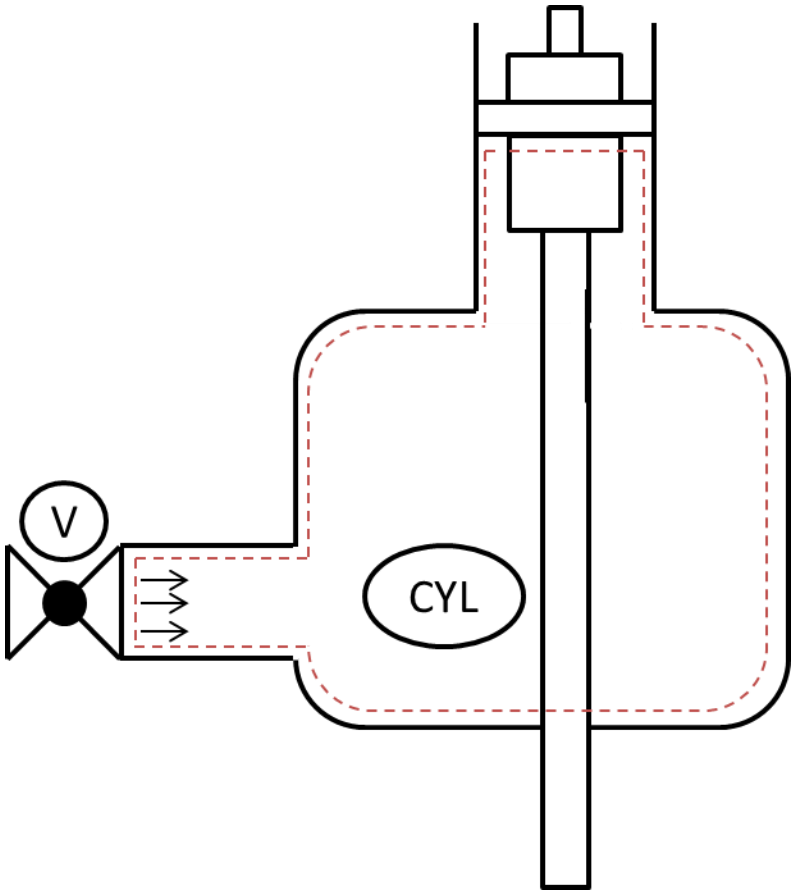

Figure 21. Geometric Representation of the Valve to Cylinder System

Boundary Conditions

- Temperature: Ambient = 294 K (70 F)
- Pressure: Atmosphere = 84.1 kPa (12.2 psia)

Assumptions

- Solenoid valve is considered to have negligible inner volume.
- System volume is static up to initial piston motion and dynamic once the piston starts moving.

Solenoid Valve

The solenoid valve in use by each TR is a Parker Hannifin Model H2001NC12501 1.25" NPTF Three-Way "Hustler" valve. The specification sheet for the H2000 series valve is located in Appendix A. This valve is a globe-type valve that operates with an internal piston moving vertically to allow for flow from port to cylinder or cylinder to exhaust. The manufacturer drawings of the solenoid valve are in Figure 22. Nitrogen enters Port P from the accumulator and exits at Port A as it moves up towards the cylinder. Port E is the exhaust port. The valve is normally closed meaning that in the de-energized state Port A is open to Port E, while Port P is blocked by the internal piston. When the valve energizes, the piston unseats from the Port P position allowing flow from Port P to Port A. Note that the valve doesn't have to be fully open for flow to exit the valve. When the valve closes, nitrogen can flow back through the valve through Port A and exhausts through Port E.

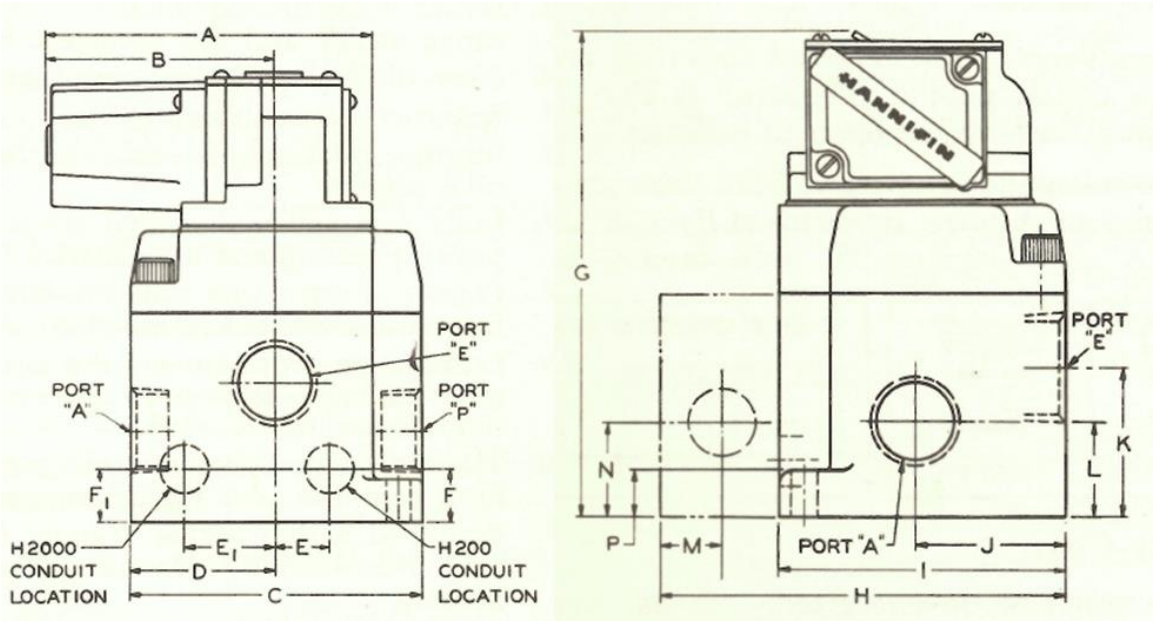

Figure 22. Front and Side Views (Respectively) of Solenoid Valve Drawings

Methodology

The methodology contains three major sections: analytical derivations, calculation algorithm, and TR timing.

Analytical Derivations

The analytical derivations are the application of thermodynamic mass and energy balances to the specific problem definitions as listed above. The two derivations vary significantly due to different conditions and assumptions; however, they both use the foundational approach that is described in [9]. The full derivations can be found in Appendix B.

Calculation Algorithm

A high level overview of how the calculation algorithm uses mass and energy balances is as follows:

1. Define given parameters (temperature, pressure, etc.)
2. Calculate flow parameters (mass flow rate, etc.)
3. Calculate new accumulator parameters
4. Calculate net force on piston
    a. Calculate piston displacement if $F_{net} > 0$
5. Calculate new cylinder parameters
6. Repeats steps 2-5 until pulse is over

Understandably with the pulse timing, the previous algorithm is a little more complicated. Some other notes include recalculating piston acceleration once the piston enters the dashpot, holding up the piston after it has reached the top until the pressure drops enough to cause the piston to fall, and switching the direction of flow (and mass flow rate) to allow the piston to fall.

Transient Rod Timing

In order to accurately model a pulse, the timing of how the TR fires and drops must be understood. However, while comparing the timing sequence provided by ACRR operators to experimental measurements (more on this in the results section), there

happened to be significant discrepancies between the two. Here both the operator perspective and data perspectives will be explained.

Operator Perspective

Figure 23 shows the transient rod timing sequence as observed by the operator and the components that the firing sequence goes through. To note, the words to the right of the cylinder represent the proximity sensors installed on the cylinder to sense the piston location. The five important time ranges during a pulse are

- Fire Delay Time
- Signal Delay Time
- Piston Ejection/Stroke Time
- Rod Hold-Up (RHU) time
- Rod Drop Time

The countdown timer, which is set by a logic controller to two minutes in order for people in and around the reactor to know when the reactor is about to pulse, starts the pulse timing sequence. Once the countdown timer reaches 0, the zero timer starts and then cycles through the fire delay time for each transient rod. Fire delay time is set by the operators at certain times for each TR. The purpose of the fire delay time is to set each TR's timing sequence such that all three reach the FireT limit switch simultaneously. Once the fire delay time is reached, the logic controller for each TR sends an electronic signal to the solenoid valve. The time it takes for the signal to reach the valve from the controller is estimated at 30 ms, but that number has not been confirmed with any verifiable accuracy. Once the signal reaches the valve, the valve, which operates as a globe valve, actuates a solenoid inside causing a piston inside the flow volume to un-seat allowing nitrogen from the accumulator to start flowing into the cylinder. However, the process of actuating the piston inside the valve also takes time, which is called the valve opening time. The value for valve opening time is widely unknown, but a similar valve from the same manufacturer is said to open in roughly 40 ms [6]. During this 40 ms, the nitrogen starts to flow according to a linear opening profile (since the valve exhibits characteristics of a globe valve), meaning that the flow coefficient of the valve is linearly inhibited during the time it takes the valve to open [10]. From the operator's perspective,

the valve opening time is built into the signal delay time and the beginning of the piston stroke.

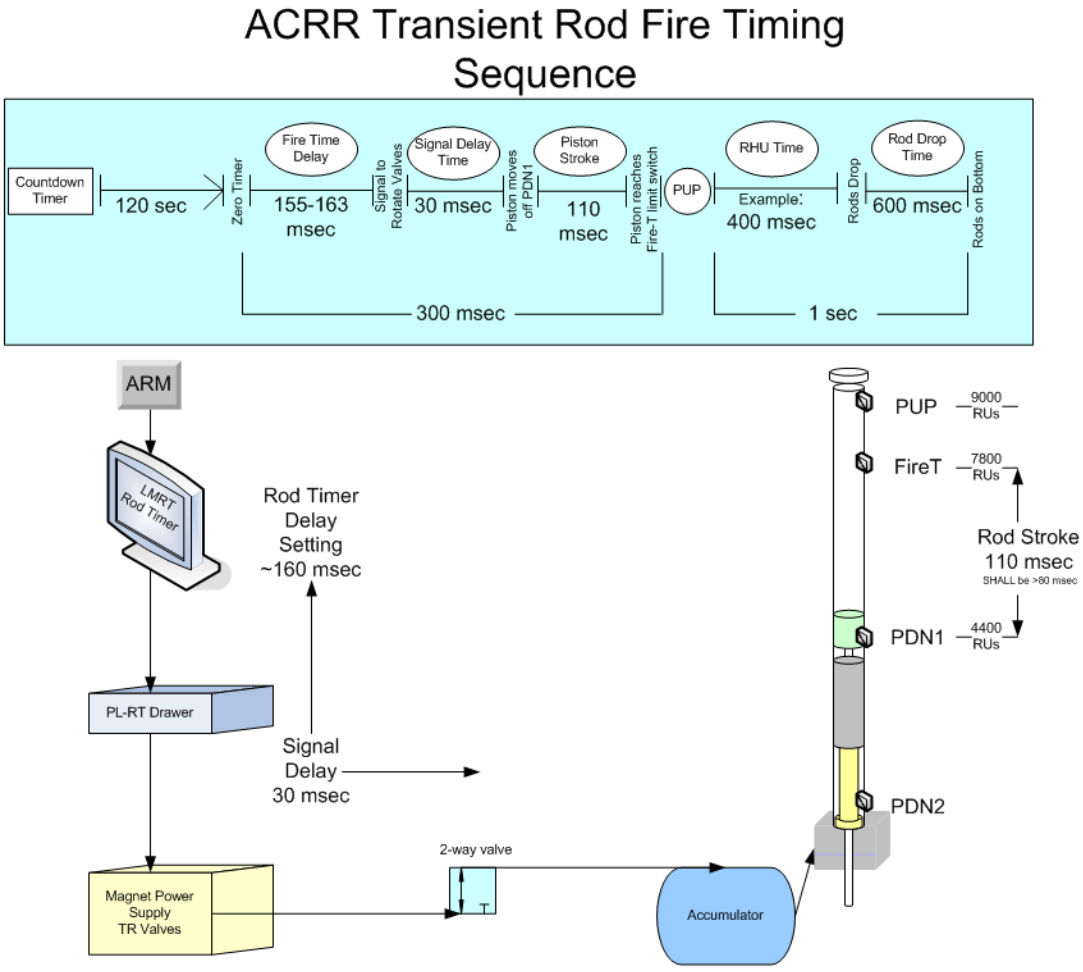

Figure 23. Diagram of Transient Rod Timing Sequence as Predicted by the Operators

Once the valve is fully open, the nitrogen flows uninhibited from the accumulator to the valve. The flow causes the piston to move rapidly up the cylinder. After the piston hits the full up position (measured by a magnet passing by a magnetically operated limit switch on the outside of the cylinder), the RHU time starts. The rod then stays in the full-up position for the duration of the RHU time. Once the RHU time is exhausted, the valve is signaled to close and allow the cylinder to exhaust to atmosphere. Another cycle of signal delay time and valve closing time (assumed to be the same as valve opening time) starts off the rod drop time portion. After the piston has dropped back to the pedestal, the pulse is finished.

Data Perspective

The operator and data perspective on TR timing differ primarily in RHU time. After thoroughly analyzing the data and pinpointing the locations along the pressure distributions where certain characteristics occur, the RHU time can be backed out as starting at the zero timer rather than after the piston hits the piston up limit switch. This phenomenon is especially noticeable with a 0.250s RHU time, in which the valve is signaled to close before the piston reaches the full up position. Figure 24 shows a visual representation of RHU discrepancy, along with a couple other additions, such as dislodging the valve opening time from the signal delay time and piston stroke, and further separation of piston motion. The method to discovering the discrepancies and separations is explained later on in the results section.

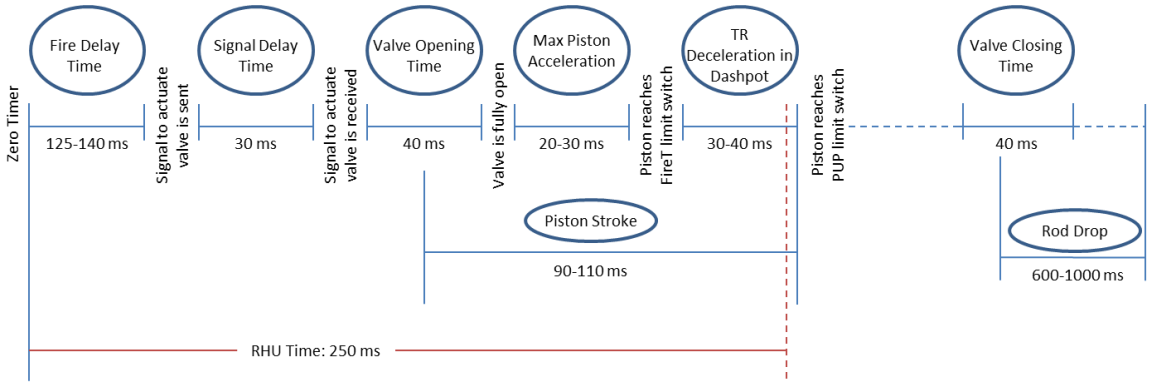

Figure 24. TR Timing Diagram Concluded from Experimental Data 0.250 s RHU Time Only

Results and Findings

Two sets of flow results will be presented in this section: experimental pressure transducer results and analytical coding results. The two will be compared to explain discrepancies and nuances. The following pressure distributions and displacement profiles only correspond to the case of 0.250 second RHU times. Longer RHU times (0.40 seconds) were found to be difficult to analyze due to an unforeseen inconsistency which is explained in detail in the Rod Hold-Up Anomaly section.

Pressure Distributions

Experimental Data

The data in Figure 25 was taken from Endevco 8530B pressure transducers mounted on the accumulator and cylinder manifold blocks for all three TRs. The specific example above is only for TR A, but the other two rods exhibit similar results for the pulse. Notable timing of certain events is summarized in Table 3.

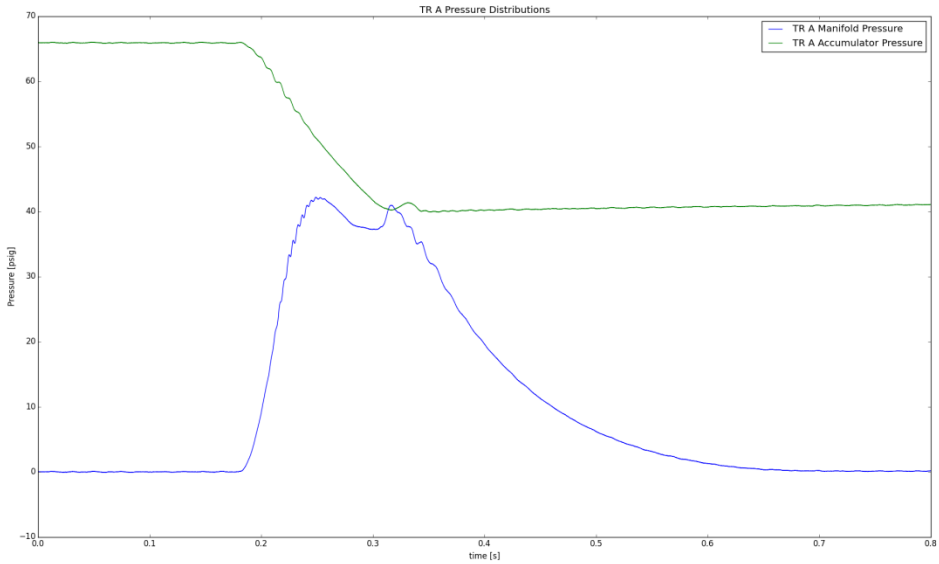

Figure 25. Pressure (Gauge) Distributions for both the Accumulator and Manifold during a Typical Pulse

A few notable events are derived from Table 3. First of all, there are many delays that occur before the piston even starts to move (roughly around .180s). Other than the set delay (Fire Time), there is a roughly 10 ms delay from sending the signal from the Log Master Rod Timer (LMRT) through the Pulse Logic Rod Timer to the Magnetic Power Supply (MPS) ending at the solenoid valve. The MPS, which contains three magnetic power relays, has a maximum delay of roughly 10 ms due to the mechanical actuation of the three magnetic relays.

The flow delay time, explained in greater detail in the Assumption Justifications section, accounts for a roughly 7 ms delay on rod ejection; however, during the rod drop, the flow delay time is increased to roughly 10 ms due to a decreased pressure drop (which results in a smaller mass flow rate and flow velocity).

Table 3. TR Timing for Experimental Pressure Data

Event	Duration	Elapsed Time	Significance
Zero Time	0.000s	0.000s	Transient rods are primed for ejection
Fire Time Delay	0.133s (for A, differs for B and C)	0.133s	Signal is generated to actuate valve
Signal Delay Time	0.010s	0.143s	Time for the signal to reach the valve
Valve Opening Time	0.040s	0.183s	Time for valve to actuate (Note that fluid starts flowing through valve before it is fully open)
Flow Delay Time	0.007s	0.190s	Time for nitrogen to travel from valve to cylinder
Rod Hold Up (RHU) time	0.250s (from Zero Time)	0.250s	Signal to close valve is generated
Piston Full Up	~0.70-0.90s (from first piston motion)	~0.260s	Piston hits full up position
Signal Delay Time	0.010s	0.260s	Signal reaches valve to close it
Valve Fully Closed	0.040s	0.300s	Nitrogen vents out of the cylinder through the valve
Flow Delay Time	~0.010s	0.310s	Manifold pressure starts dropping

Analytical Data

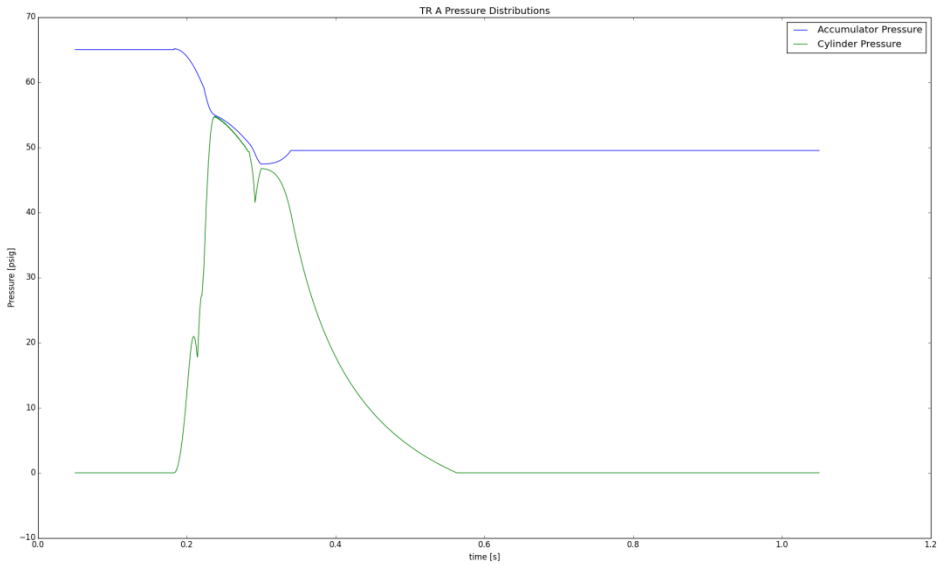

Figure 26. Analytical Pressure Distributions of TR A for both the Accumulator and Cylinder

Figure 26 shows the pressure distributions as generated from the coding of the analytical solution. The most distinct differences can be seen between the peaks in the cylinder data, and also the higher pressure readings as compared to the experimental data. The major and minor differences are stated and explained in the list below:

- The small hump in the cylinder distribution at about .21 sec is due to the volume expansion from the movement of the piston in the cylinder being greater than the increase in mass of the system.
- The deceleration of the piston in the dashpot is assumed to work as follows: as the mushroom cap enters, the velocity of the piston decreases by ~ 10 m/s per time step. What happens from this is that the piston velocity (which is ~ 40 m/s as it enters the dashpot) decreases very significantly in a short amount of time and then fluctuates between positive and negative for the next .100s or so. The result from this is a jagged, but relatively flat pressure distribution (from .23 sec to .28s) and an oscillating displacement profile during the same period (explained in more detail in the next section).

- The justification for the choice in deceleration profiles is due to the fit of the pressure graph as compared to the experimental data.
- As can be seen from Figure 27, the calculated versus experimental accumulator pressures do not align too well. This is due to the algorithm used to calculate the mass flow rate. As the pressures are closer in magnitude, the mass flow rate drops significantly causing less mass to flow from the accumulator. This keeps the accumulator pressure artificially high.

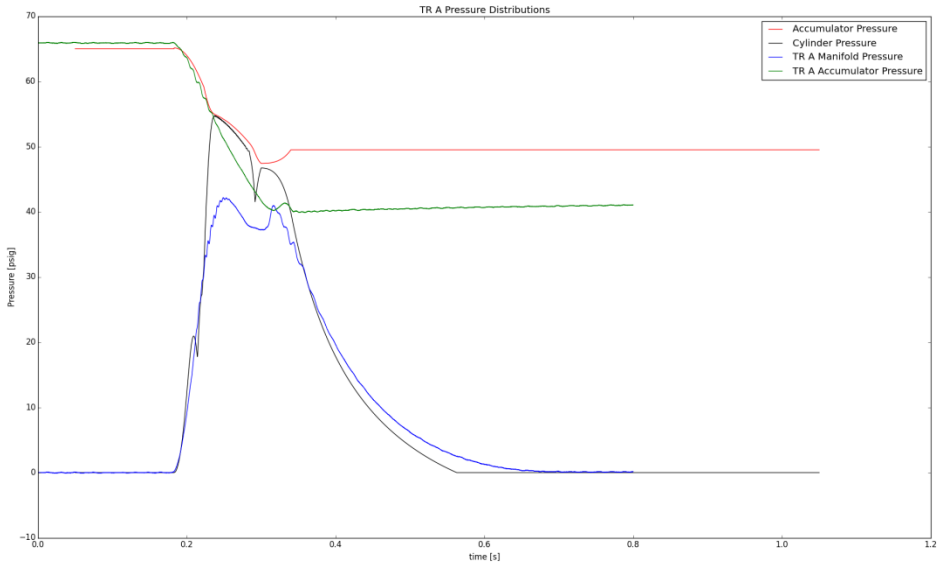

Figure 27. Overlay of Analytical and Experimental Pressure Distributions for a Typical Pulse

Table 4 explains the TR timing sequence implemented in the coding of the analytical solution; as well as notable events during the pulse.

Table 4. TR Timing for Analytical Pressure Data

Event	Duration	Time	Significance
Zero Time	0.000s	0.000s	Transient rods are primed for ejection
Fire Time Delay	0.133s (for A, differs for B and C)	0.133s	Signal is generated to actuate valve
Signal Delay Time	0.010s	0.143s	Time for the signal to reach the valve
Valve Opening Time	0.040s	0.183s	Time for valve to actuate (Note that fluid starts flowing through valve before it is fully open)
Jagged Edge in Rise (Volume Expansion)	~ 0.010s	~0.210s	Pressure drops due to expansion of volume in the cylinder
Rod Hold Up (RHU) time	0.250s (from Zero Time)	0.250s	Signal to close valve is generated
Signal Delay Time	0.010s	0.260s	Signal reaches valve to close it
Piston Full Up	~0.90-0.110s from first piston motion	~0.290s	Piston hits full up position
Valve Fully Closed	0.040s	0.300s	Nitrogen starts venting out of the cylinder

Displacement Profiles

Note that the following displacement profiles only include the rise of this piston.

Experimental Data

The displacement of the piston in the experimental data (shown in Figure 28) assumes one major piece of data: the piston moves smoothly based on the pressure distribution. This, in reality, is not true due to massive deceleration in the dashpot. Dashpot deceleration has currently not been estimated for this data set, but will be soon. The time for full piston motion is ~ 90 ms, but this will likely change with dashpot deceleration.

Analytical Data

There are massive discrepancies between the experimental and analytical data set for motion profiles. This is due solely to the assumption of dashpot deceleration. Since the deceleration assumed in the code model is based on decreasing velocity, there are sections of negative and flat motion. From what is thought about the piston motion, this case is not true; however, some insight can be gleaned from this data. The deceleration in the dashpot is based solely on the concept of a hydro-lock brake, which works by forcing dashpot motion into a decreasing volumetric flow region as a function of time, bringing a piston (mushroom cap in this case) to an abrupt stop once the volume cannot be compressed any further. Since this system uses the hydro-lock brake, the motion in the dashpot is highly uncertain. It is highly likely that the piston will slow at varying rates of speed due to fluctuating deceleration values (likely non-constant). The rise and drop lead to mechanical vibration and stress in the TR components, and the drop could lead to the TR components transitioning from tension to compression (vibration). In terms of the motion distribution in Figure 29, it is unlikely that the flat portion is completely accurate; nevertheless, this is what the code outputs.

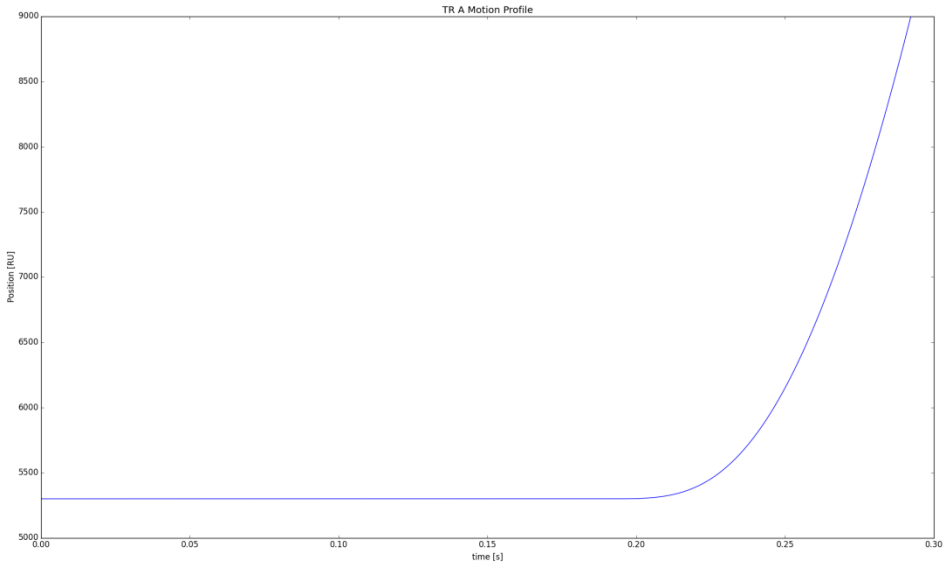

Figure 28. Motion of the Piston in TR A during a Typical Pulse

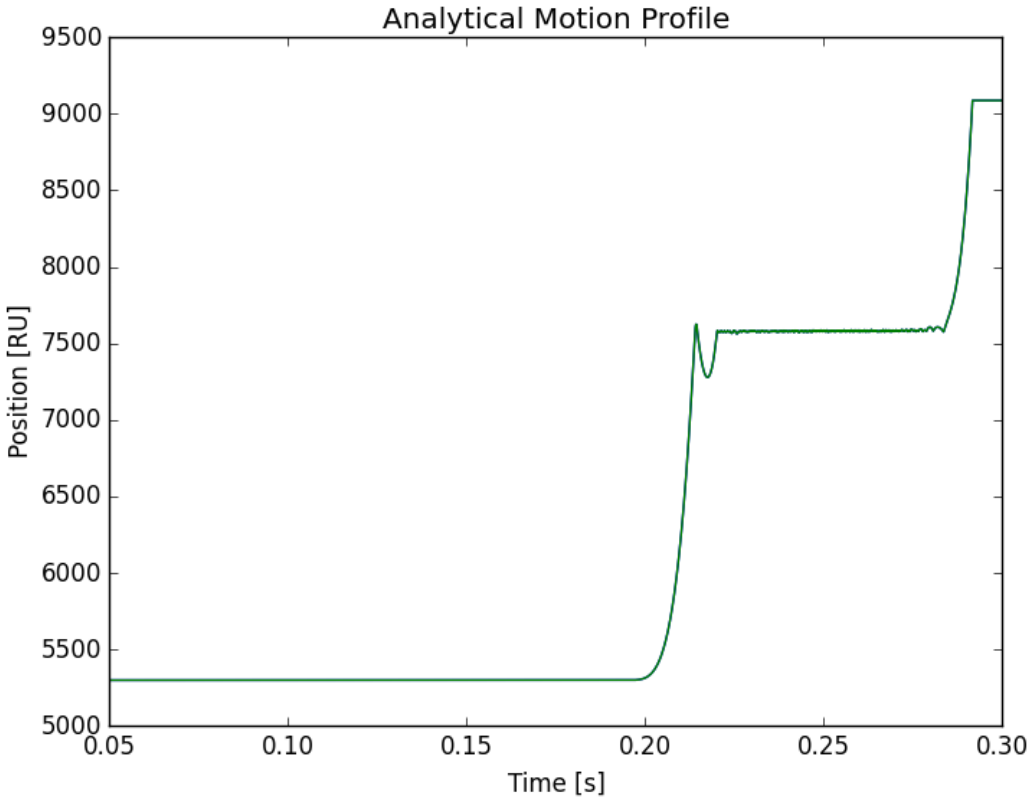

Figure 29. Motion of the Piston Derived from Analytical Data

When comparing the data from Figure 30, one notices that the rise time for both is nearly identical. This timing should be expected; however, is not completely accurate due to the inclusion (and assumption) of dashpot acceleration in the analytical model, and the exclusion of dashpot acceleration in the experimental data.

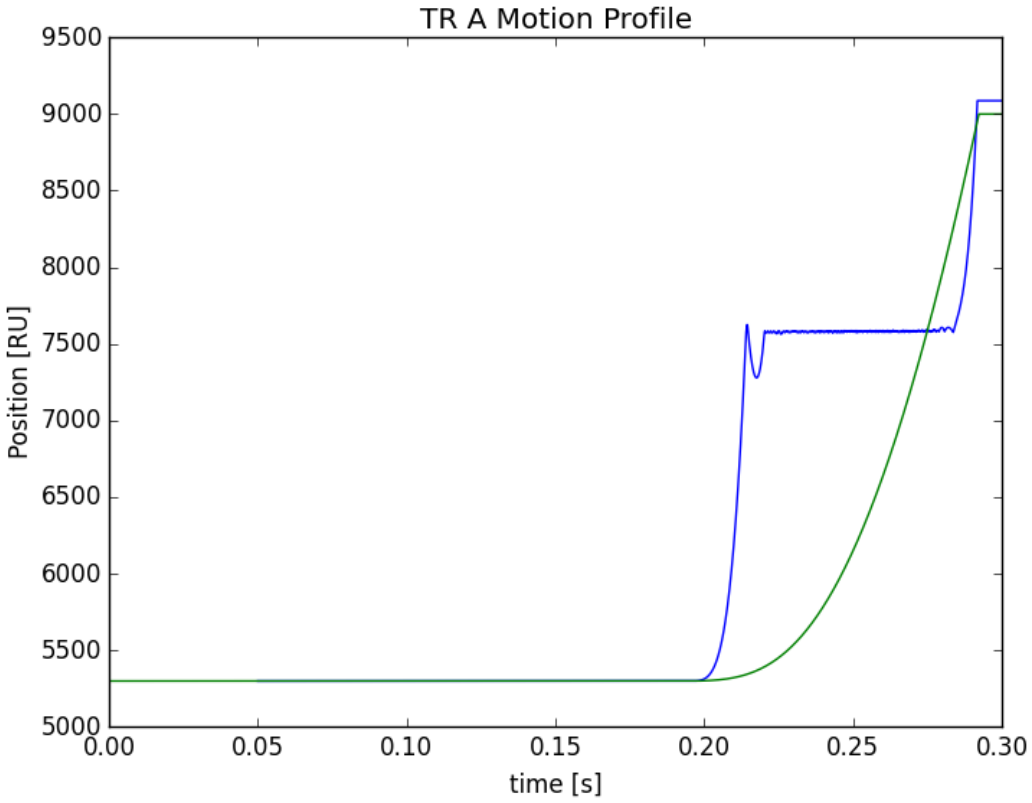

Figure 30. Comparison of Analytical (Blue) and Experimental (Green) Piston Displacements

Rod Hold-Up Anomaly

It should be stated that the foundation of the results discussed in the previous section is based on a 0.25 second rod hold-up (RHU) time pulse. To restate, the RHU time starts at the beginning of the pulse, and once reached, signals for the solenoid valve in the TR pneumatic system to close and start the process of dropping the rods back into the core. In all the available data, there are only instances of three distinct RHU times: 0.25, 0.40 and 0.70 seconds. When trying to extend the analysis to longer RHU times, an odd trend in the data revealed itself. The time at which the manifold pressure distributions drop off for longer RHU times is wildly inconsistent.

Figure 31 shows a set of six 0.25 second RHU pulses, all starting from the same position and being completed in succession (over three days). Between the six pulses, the pressure starts dropping at roughly the same time (~0.32 seconds). This is the consistency expected from the ACRR in terms of pulse repeatability.

However, when comparing a similar set of 0.40 second RHU pulses (Figure 32), the times when pressure starts dropping varies wildly. The pressure drops range from 0.49-0.70 seconds. In terms of repeatability, this is curious and should not be accepted. In reality, there are no dire adverse effects to come from varying pressure drop times. Minor effects include holding the TR in the full-up position for a longer period of time which may lead to higher mechanical stresses and a higher energy deposition in the core. Also, this variation could likely imply that there are issues with the electrical equipment responsible for generating the pulse.

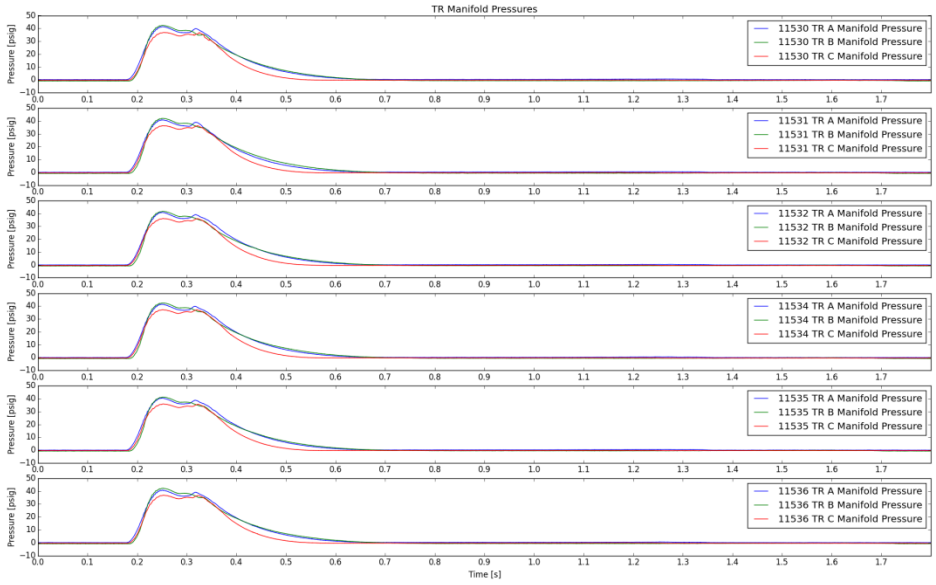

Figure 31. Set of 0.25 second RHU Pulses

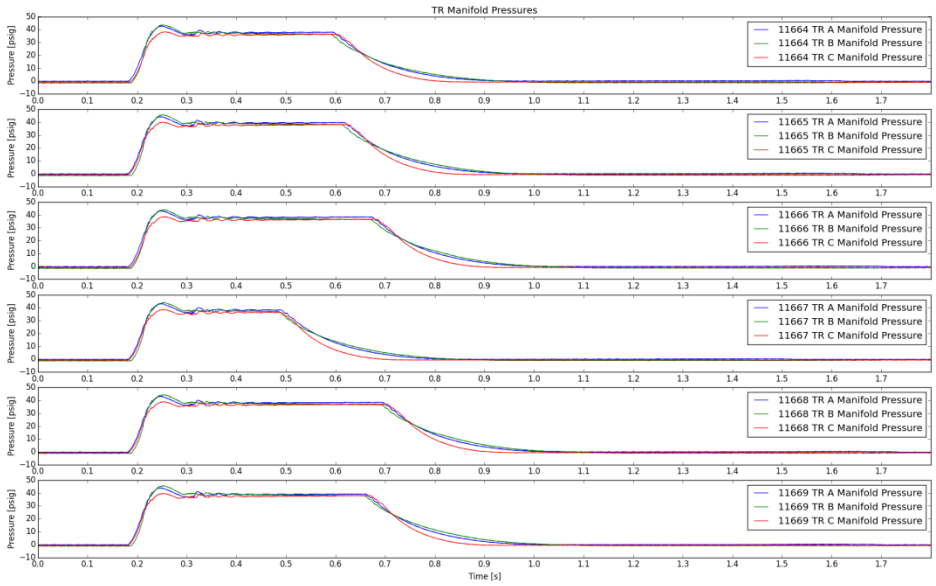

Figure 32. Set of 0.40 second RHU Pulses

Pulse Sequence

In order to propose any problems with electrical equipment, the sequence through which the pulse is generated must be understood. Figure 33 provides a very concise, yet detailed explanation of how the pulsing logic of the ACRR is completed. The central portion of the figure details the circuits and switches that must be activated in order for the signal to be sent. Above the circuits are the specific electrical components that each switch lies within.

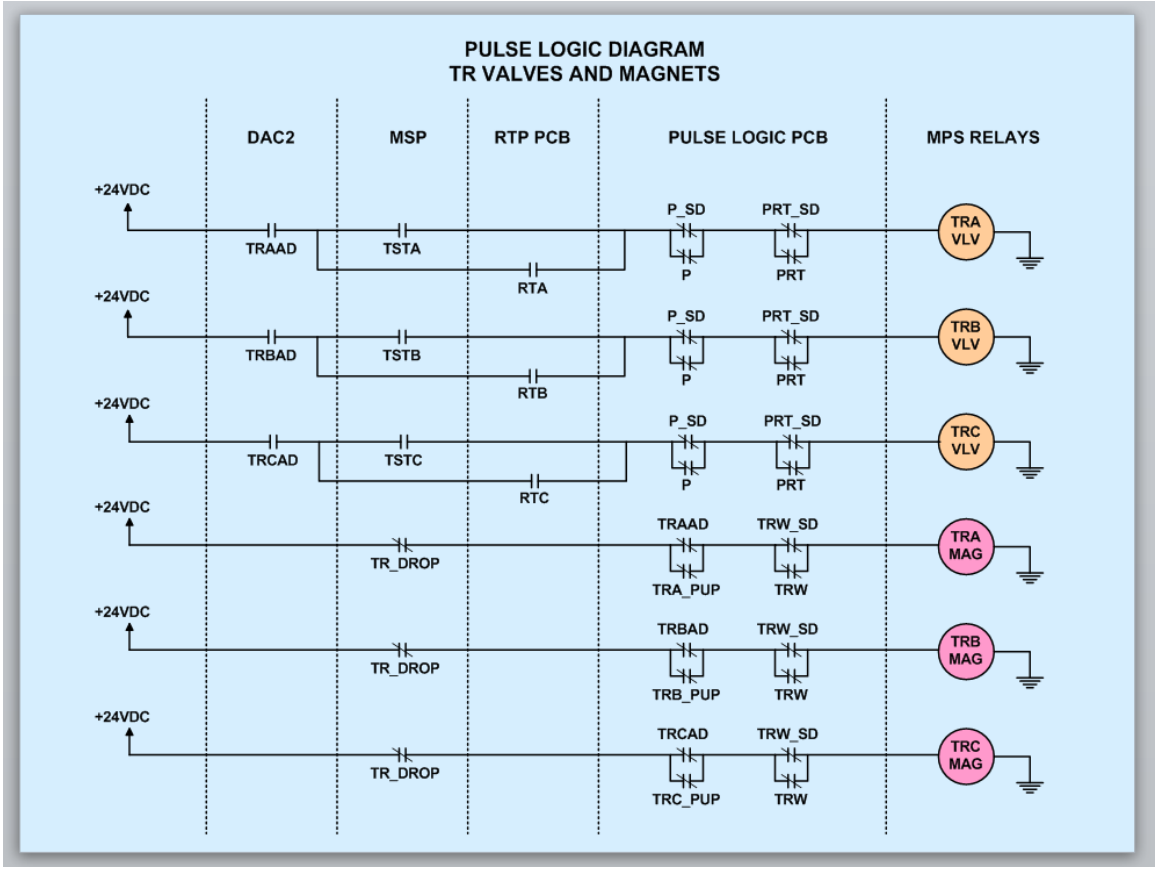

Figure 33. Pulse Logic Diagram [11]

When preparing a pulse, the order of activating the switches in Figure 33 is as follows:

1. Set the Rod Timer (connecting the RTA/B/C switch)
2. Start the Master Countdown Timer (not shown)
3. Choose either Pulse (P) or Pulse Reduced Tail (PRT) mode
4. Arm the rods (connecting the TRA/B/CAD switch)

Once the TRs have been armed and the Master Countdown Timer has reached zero, the circuit completes and the signal is allowed to flow through to the magnet power supply where signal to open the valves is issued [12].

Once the pulse has hit the set RHU time, the pulse (or PRT depending on the mode selected) shutdown signal is generated in the Pulse Logic Printed Circuit Board (PL-PCB) causing the circuit to become open and stop sending the signal to the valves. Consequently, the valves close and lead to the drop-off of pressure in the cylinder.

Notes about RHU Anomaly

The most likely components to be causing this anomaly are either the PL-PCB or the 6602 Counter/Timer Cards (not shown in Figure 33). The PL-PCB is the integral component of the pulsing sequence as it is the part where all of the signals are conglomerated and then three separate signals are sent out to each of the TR valves. The 6602 Counter/Timer Cards, which input into the PL-PCB, are the components that generate the timing signals for the all pulsing.

Without actual testing, it is unclear as to what is causing the RHU anomaly. Fortunately for the ACRR, another project is currently underway to upgrade all electrical components that control the reactivity control system (RCS). While this anomaly may not present a critical issue to operations (it has gone unnoticed until now), this will most definitely something that is tested with the install of the new system to verify pulse repeatability.

Conclusions

Of all the information presented in this chapter, there are two main takeaways:

1. Delays in the pneumatic and control systems were identified and quantified.
2. The RHU anomaly was studied in the context of the pulse sequence to determine possible failure points.

By defining the delays in the TR timing, pneumatic operation of the TR system is better understood. The pneumatic delays will help in the understanding of rod displacement and timing by defining better when the motion of the piston actually begins. The discovery of the RHU anomaly allowed the author to bring it to the attention of the operators and engineers such that it can be avoided in the future.

CHAPTER 5
RAZORBACK RESULTS

Purpose

This chapter ties the motion of the TRs to the nuclear effects within the ACRR. The facilitator to understand this connection is the coupled thermal hydraulic – point kinetics code Razorback being developed at Sandia by Darren Talley [13]. In this chapter, a parametric study to measure reactivity addition, system reactivity, dynamic reactivity, and pulse timing will be completed as they relate to TR starting position and accumulator set pressure. Differences between TRs A, B, C and constant acceleration motion will also be noted when possible.

Background

Brief Overview of Razorback

Even though it is not analyzed in this study, it should be noted that Razorback uses the point reactor kinetics equations with eight delayed neutron precursor groups to calculate the neutronics parameters [13]. The specific sections of interest to this study include the reactivity control systems and reactivity feedback solution methods.

Reactivity Control Systems

Reactivity (defined as the deviation of core multiplication $=\frac{k(t)-1}{k(t)}$) is added into Razorback via the TR differential worth curve of the form

$$\frac{d\rho}{dz} = Asin^2[B(z - z_0) + C] \tag{6}$$

Where A is a coefficient correlated to the total TR bank worth. The coefficients A, B, C and z_0 are determined from TR bank worth operations computed from fits of MCNP data for TR bank differential worth (derived from TR bank integral worth). Sample plots for TR bank integral and differential worth are shown in Figure 34 [14]. The coefficients used for the pulse simulations in this study are 0.135676, 0.046212, 0.569848, and 25 for A, B, C, and z_0 respectively [15].

The TR differential rod worth curve is only valid over a certain range of positions. After looking at the MCNP data, it was determined that the effective range of Equation 18 is from 25-85 cm (2500-8500 RU). The importance with this condition is that all reactivity is predicted to be inserted 5 cm from full travel of the rods. Starting pulse height is also affected by the calculation range in that pulses starting below 25 cm do not start adding reactivity until they reach 25 cm in height.

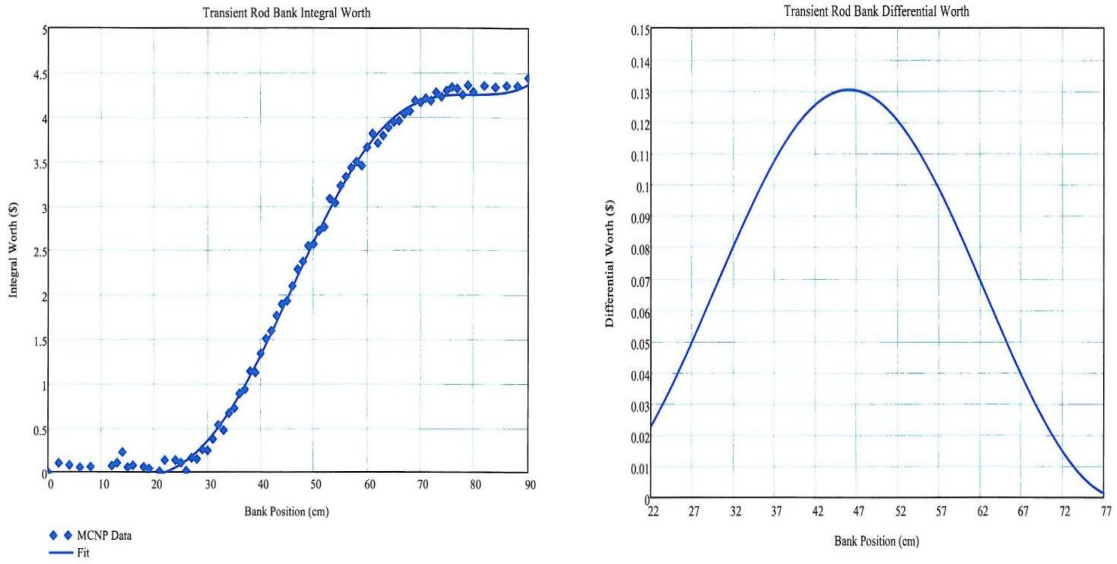

Figure 34. Sample fit of TR Bank Integral (left) and Differential (right) Worth from MCNP Data

Reactivity Feedback

To determine the reactivity feedback, Razorback uses five different drivers for the feedback. These five factors include:

- Fuel temperature
- Fuel expansion
- Cladding expansion
- Coolant density
- Coolant temperature

The equations for how each component is used to calculate the feedback can be found in [13]. For the studies presented in this chapter, the feedback in the fuel due to temperature has the most significant effect on causing the phenomenon known as dynamic reactivity.

Transient Rod Motion

Currently, Razorback uses a constant pressure (and thereby constant acceleration) method to calculate the velocity and displacement of the TRs, which is used to determine the reactivity addition with equation 6 (see page 49). The major issue with how this method calculates motion is that the constant pressure used is the set pressure of the accumulators, nearly 20 psig higher than the peak values measured in the manifold block (close to where the piston sits). An ideal solution to this problem would be to develop an acceleration curve that would fit all sets of pressure data and TR starting position. However, an alternative method would be to generate a velocity profile based on each set of pressure data and input that directly as TR velocity (even though it requires the pressure data for generation).

Methodology

Transient Rod Motion

Using a set of discrete velocity points for the TRs was determined to be the best method for two main reasons:

1. The implementation in Razorback relied on changing only a couple of code snippets instead of making significant changes to a couple subroutines.
2. The position-based assumption of dashpot deceleration (see page 20) can be isolated to only the function used to manipulate the pressure distribution and piston kinematics rather than having to implement it in Razorback. This would have included changing the velocity and acceleration of the rods based on the position of the TRs within Razorback instead of having a set of velocity points pre-calculated (likely resulting in increased run-times).

To run Razorback with the TR velocity profile, the velocity points must be saved (from the Python manipulation function) to a text file, which is read in by Razorback when the accumulator pressure is set to a negative value. From there, a linear interpolation function between velocity points was added in the case that the time step in Razorback did not align with the time step in the text file.

Another slight change made within the Razorback input file was to increase the scram delay time, which is the time after the RHU time when the TRs start to fall. It was originally set to 0.005 seconds, causing the TRs to start falling back into the core with a 0.250 second RHU time, since the rods have not yet reached the top for any pulse by 0.255 seconds. The new scram delay time is set at 0.5 seconds, which is sufficient enough for the cases in this study.

Another note to make about the constant acceleration versus velocity profile is that the constant acceleration will immediately start increasing velocity with no build-up time whatsoever. The velocity profile, however, is the prediction of the whole velocity of the actual TR motion from Zero Time to end, which implies that the TRs don't start motion until the pressure has built up enough the cause the net force to be positive upwards. This effect is side-stepped by adding the extra time to the initial delay for the constant acceleration case. The delay ends up being 0.203 seconds. With the added delay, the motion is roughly comparable (within roughly 5-10 ms).

Five Pulse Case Study

In order to test the effects of starting position, a set of five different pulses have been chosen for comparison. The pulses range from ~$1.15 to $3.00 in added reactivity, and from 4370-5700 RU starting position. The velocity profiles for each rod (A, B, C) are also compared against the constant acceleration assumption.

Pressure Comparison

Razorback uses the accumulator pressure as its input meaning that only one input has to be changed. For a velocity profile; however, a distribution of pressures is needed. This leads to a problem since all of the pressure transducer data corresponds directly to a 65 psig accumulator set pressure. Unfortunately, pressure data was not able to be obtained for other accumulator set pressures. Because of this, an assumption for how the pressure distribution under the piston would behave has been developed.

<u>Pressure Distribution Generation</u>

Firstly, there are a few assumptions that had to be made in order for a pressure distribution to be created. The assumptions are:

- All pressure distributions start increasing at 0.185 seconds from Zero Time.
- Inflection point of pressure distribution is also at roughly the same time for each pressure (0.233 seconds from Zero Time, as measured by the 65 psig case).
- The inflection point is defined as 90% of peak pressure.
- All set pressures peak at roughly the same time (0.250 seconds from Zero Time, as measured by the 65 psig case).
- Pressure equilibrium is achieved at 0.400 seconds from Zero Time.
- The curve is fit piecewise: starting time to time of peak pressure is fit with a second-order polynomial and the times corresponding to the peak and equilibrium pressures are fit linearly.
- Pressures outside of the starting time and equilibrium time are 0. This assumption is valid beyond 0.400 seconds since the piston has already reached full travel by this time.
- Peak pressures are estimated for each set pressure using a mass and energy balance as documented in Appendix A.

The sequence of events used to create the pressure distributions and corresponding velocity points for Razorback is:

1. Estimate peak pressure using mass and energy balance.
2. Plot all four points and create fits.
3. Generate pressure distribution from the fits.
4. Calculate force, acceleration, velocity, and displacement from pressure distribution.
5. Iterate on constant acceleration value in the dashpot until the velocity at 9000 RU is as close to zero as possible.
6. Convert velocity to cm/s and export to text file.
7. Run Razorback.

Results

Five Pulse Case Study

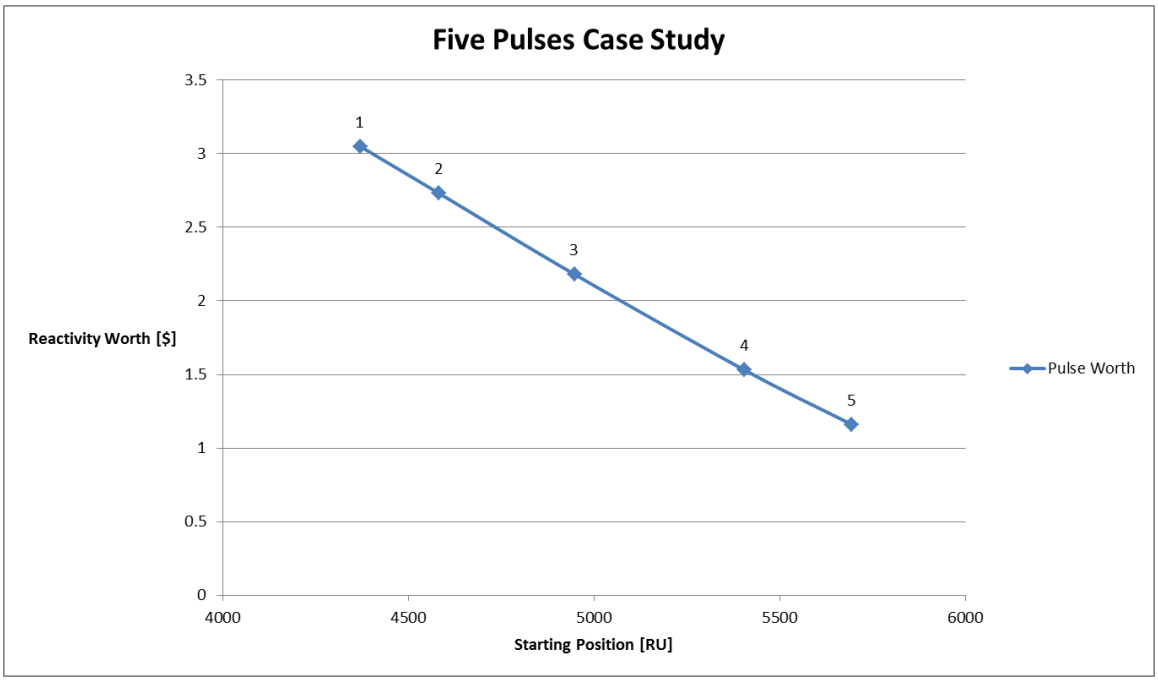

Figure 35. Reactivity Worth Dependence on Starting Position for each of the Five Pulses Studied. Note the numbers above each point are labels corresponding to the pulse in Table 5.

Table 5. Description of Pulse Parameters for Each of the Five Pulses Studied

Label	Pulse #	Pulse Worth ($)	Starting Position [RU]
1	11513	3.05	4370
2	11500	2.73	4583
3	11493	2.18	4948
4	11555	1.53	5406
5	11554	1.16	5695

The five pulses for this study were chosen solely based off the range of pulses exemplified in the pressure data. They range from the largest pulse available (label 1, a pulse from the pedestal) to the smallest pulse available (label 5). Note the reactivity pulse worth values are taken from Razorback (based on a $4.45 TR bank worth) rather than from the experimentally measured worth due to the consistency within Razorback for calculating reactivity addition.

This set of five pulses will show how the reactivity parameters and pulse timing are related to the starting position of the TR bank.

Reactivity Concerns

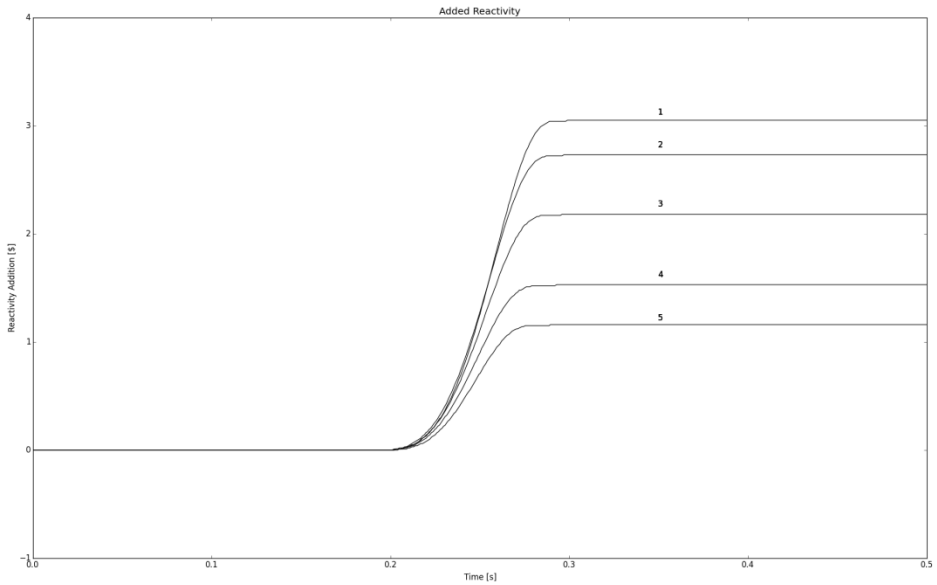

Figure 36. Reactivity Addition Curve of TR A for Each of the Five Pulses Studied (number corresponds to label in Table 5)

Reactivity addition, calculated based off equation 6 (see page 49) and TR motion, is added very smoothly for each pulse. Pulses 2-5 have very similar curve shapes with just slightly varying rates of addition. Something interesting of note is that Pulse 1 actually adds reactivity at a slower rate in the beginning than Pulse 2, even though the total reactivity addition is higher for pulse 1. This is caused by the shape of the differential worth curve (see Figure 36), which peaks around the 46 cm mark (roughly where Pulse 2 starts).

While added reactivity is an important measure for pulse determination, it is based off a set motion and reasonably consistent throughout all pulses. System reactivity, defined in equation 7, is a different story.

$$System\ Reactivity = Reactivity\ Added + Total\ Reactivity\ Feedback \quad (7)$$

The reactivity feedback is highly dependent on temperature, implying that a larger reactivity insertion will lead to diverging system reactivity (as seen in Figure 37).

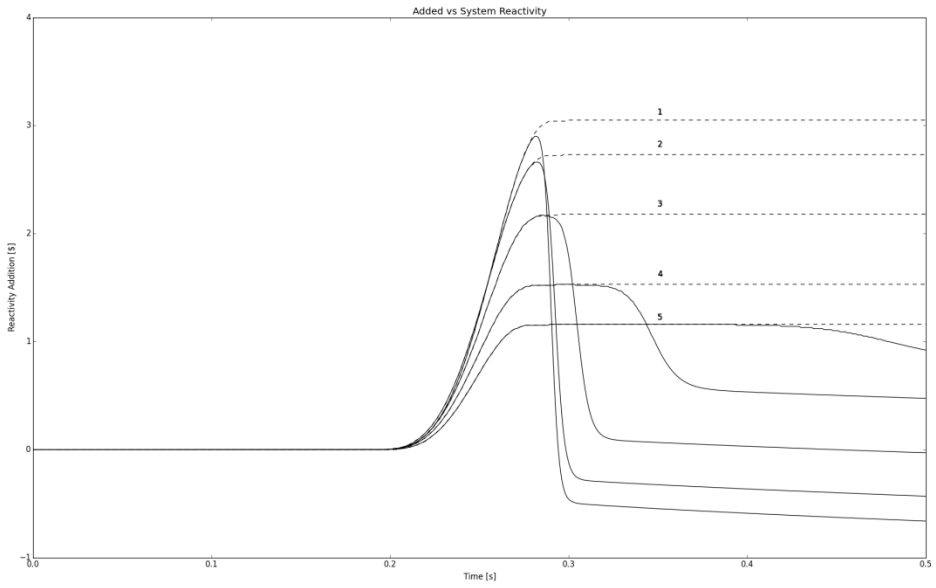

Figure 37. System Reactivity Overlaid on Total Reactivity Addition for TR A of Each Pulse

Interestingly, system reactivity does not drop off during rod motion for pulses below the $2.00 range. Only when the total reactivity insertion reaches closer to $3.00 does reactivity begin to affect the maximum system reactivity achieved. As expected, larger pulses lead to more rapid heating in the fuel which results in more reactivity feedback. It is possible that faster reactivity insertion times could allow for the full added reactivity to be inserted, and this hypothesis is studied later in this chapter by measuring the effects of changing accumulator set pressure. Since pulse 1 is the largest pulse that the ACRR is capable of in its current state, any estimate to generate a quicker pulse would not be realistic. The only feasible way to increase the speed of the pulse, other than raising the starting position of the TR bank, would be to increase the accumulator pressure anyway.

Pulse Timing

As referenced in the TR Ejection Limit section, each pulse has two distinct times to be aware of: reactivity addition (shown in Figure 38) and rod travel times (shown in Figure 39). The difference between the two is that reactivity addition stops at 85 cm in the cylinder, whereas rod travel time extends to the full 90 cm. The difference in time between the two is attributed to the deceleration in the dashpot, which takes longer time for shorter pulses (due to lower velocities entering the dashpot). Shorter pulses take longer to stop due to lower dashpot entrance velocities meaning the constant deceleration term calculated is lower. Even though the shorter travel pulses take longer in the last 5 cm of travel, it is only by roughly 5-10 ms.

In terms of setting a timing limit for rod motion, it should clearly be based on the reactivity addition time rather than rod travel time. Rod travel time is more important for the study of the TRs since a shorter time difference between the two times leads to larger forces experienced in the dashpot which extend to the rest of the TR mechanical linkages.

From Figure 38, TR B is shown to have the quickest travel of all three rods. This is not surprising due to a higher peak pressure seen in TR B data versus A or C (as mentioned in the Discussion of TR motion). Note the data for pulse 1 from TR C is suspect due to pressure transducer dropouts; therefore, it has been excluded from the plots. Also, the constant acceleration times are expected to be quicker because the TR velocity is modeled after smooth motion (build-up included) instead of having instantaneous acceleration.

The previous estimate of effective withdrawal times (70 ms for a $1 pulse to 88 ms for a $3.50 pulse) corroborates highly with the Razorback results. Razorback predicts only slightly longer times for larger pulses (~ 88 ms for a $3.05 pulse), but the important difference between the predicted range and calculated range is that each TR has a slightly different range. TR B may be slightly under the limit while TR C is over the limit. As a safety limit, 80 ms is not an unreasonable estimate, even though it could likely be extended. However, further testing and simulation would be needed to see how shorter reactivity addition times affect other parameters such as fuel temperature and coolant temperature before any new limits could be set in place.

Another limit to setting any new limits is operator instrumentation. As of currently, there are only proximity sensors at the limits of travel (manifold, pedestal and top of cylinder) and the fire time sensor. This implies that the operators would be able to back out full motion and timing for a pulse on the pedestal or manifold but nowhere in between.

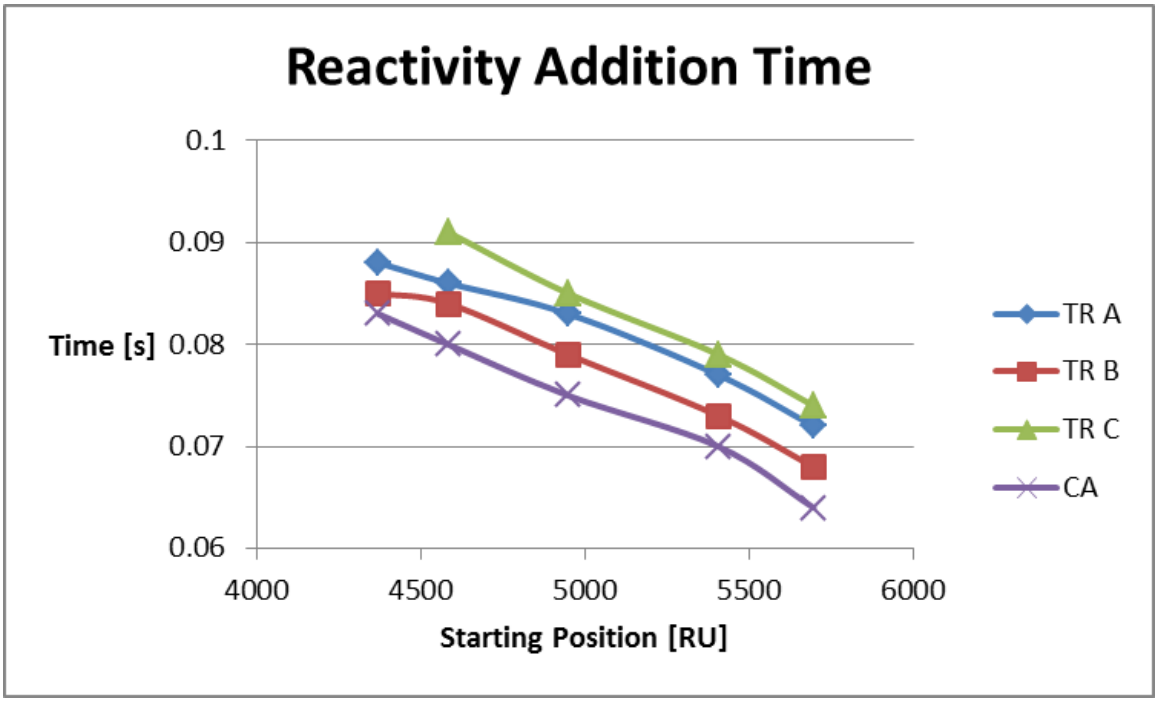

Figure 38. Difference in Reactivity Addition Time between Constant Acceleration (CA) Assumption and Velocity Profile Inputs for each TR

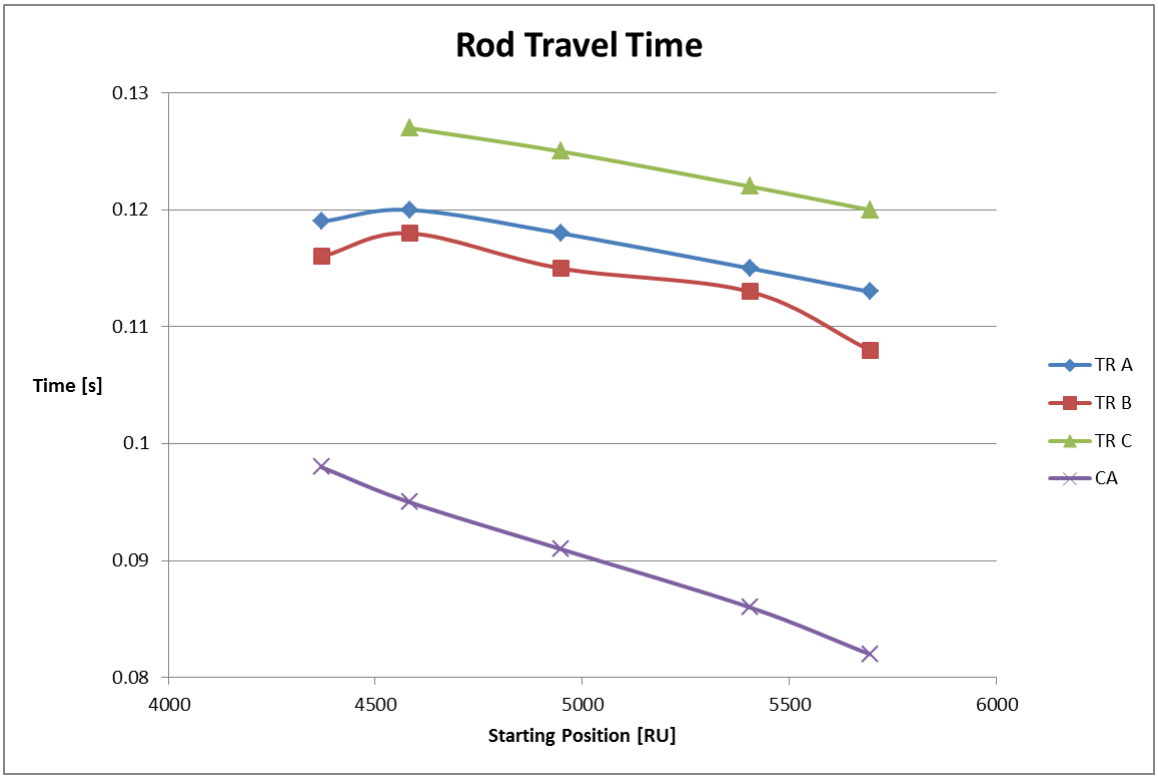

Figure 39. Difference in Rod Travel Time between Constant Acceleration (CA) Assumption and Velocity Profile Inputs for each TR

Pressure Variation

The set pressures tested were from 15 psig to 125 psig in increments of 10 psig. The 15 psig limit was chosen since 5 psig is not enough to cause a pulse. The upper 125 psig limit is derived from the relief valve set pressures, which would cause a 125 psig pressure if the regulator were to fail. Pressure distributions and TR kinematics were derived using the method in the Pressure Distribution Generation section.

Reactivity Concerns

The pulse used to test varying pressure is a max pulse from pedestal which corresponds to a $3.05 reactivity addition. As the set pressure is increased, the time it takes for the total reactivity addition decreases. Meaning in Figure 40, the leftmost curve corresponds to the highest set pressure, and the rightmost curve represents the lowest set pressure. The time for total reactivity addition ranges from 188 ms for a 15 psig set pressure to 69 ms for a 125 psig set pressure. These results are expected as changing the set pressure implies higher or lower pressure forces on the piston resulting in shorter

travel times for pressures higher than 65 psig and longer travel times for pressures lower than 65 psig.

When looking at Figure 41, it becomes clear that the lower the set pressure leads to a higher dynamic reactivity effect in the ACRR. The dynamic reactivity amount (difference in max system reactivity and max total reactivity added) ranges from 63 cents for a 15 psig set pressure to 3 cents for a 125 psig set pressure. To keep the dynamic reactivity within 10 percent of the reactivity addition (30 cents), a set pressure of at least 35 psig is needed, whereas a dynamic reactivity within 5 percent (15 cents) requires at least a 65 psig set pressure. What is surprising is that no matter how fast the reactivity is inserted, the reactivity feedback will still have an effect on the reactivity addition. Supposedly, one could use higher set pressures and reactivity insertion times to achieve a full reactivity insertion, but none of those options are practical as the system is not capable of safely operating above 125 psig set pressure.

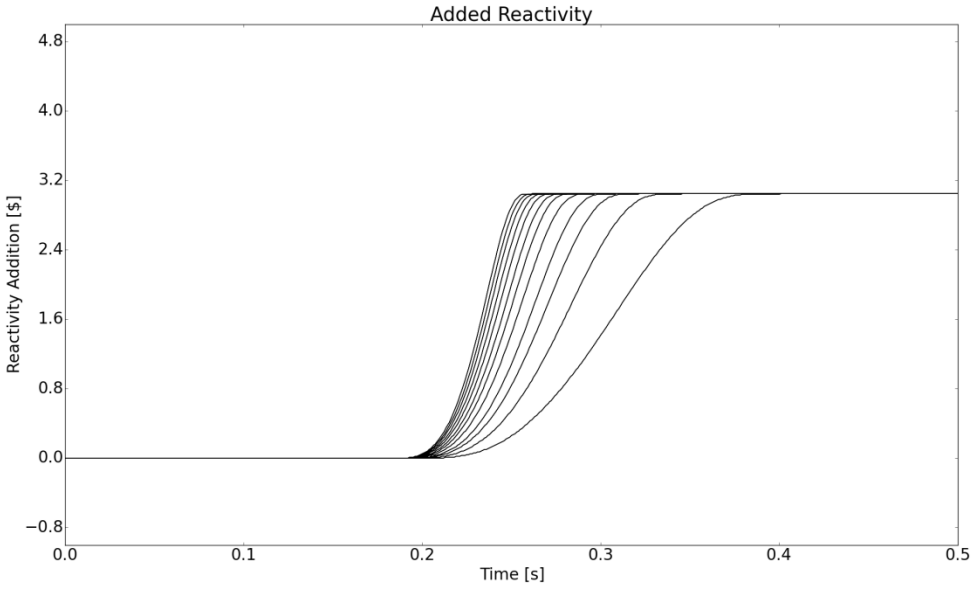

Figure 40. Added Reactivity Curves for Estimated Pressure Profiles (In order from lowest pressure to highest pressure)

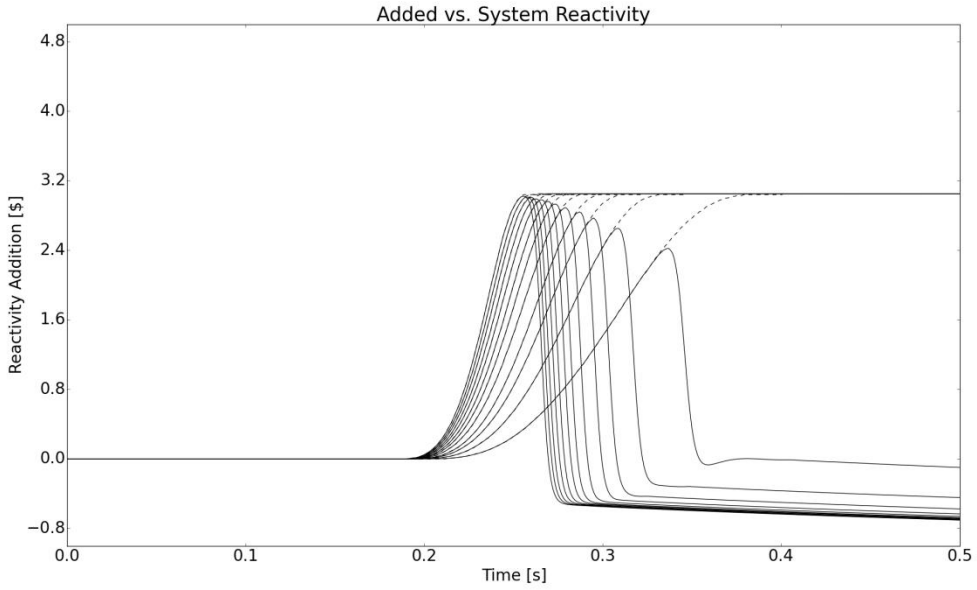

Figure 41. System Reactivity Curves Overlaid on Reactivity Addition Curves (dotted) for Estimated Pressure Profile

Pulse Timing

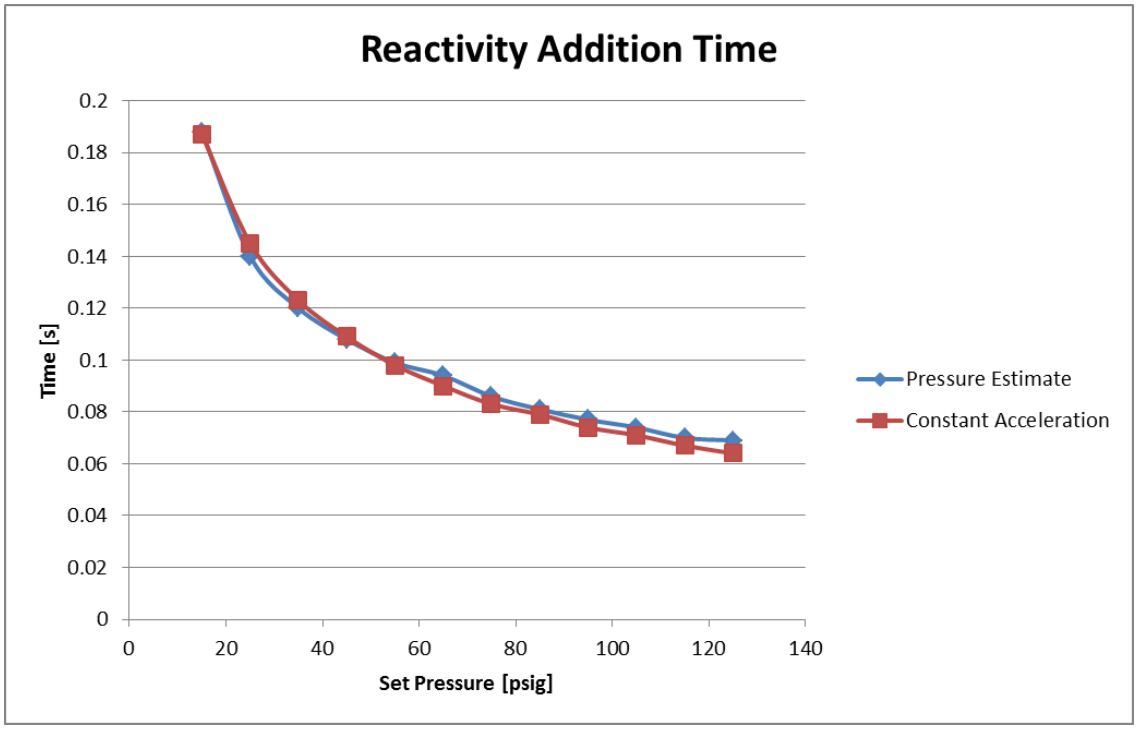

Figure 42. Comparison of Estimated Pressure Profile to Constant Acceleration Assumption in regards to Time for Complete Reactivity Addition

Reactivity addition time compares very well (in Figure 42) between the two pressure estimates. As mentioned before, the time for total reactivity addition ranges from 188 ms for a 15 psig set pressure to 69 ms for a 125 psig set pressure. It would be expected for the estimated pressure profile to have a slightly longer reactivity addition time due to an expected build up time; however, the quadratic fit between the start and peak pressures sort of negates the time addition. In hindsight, adding a second inflection point between the start and peak pressures would have improved the pressure fit (could be fit using a cubic polynomial or spline curve instead of quadratic) and likely delivered on the expected longer reactivity addition time. Regardless of the fit type, having the two sets of data closely match each other shows that the assumptions made when fitting the pressure data are reasonable.

The reasoning as to why the estimated pressure profile rod travel times are significantly longer is due to the dashpot deceleration included in the pressure estimation method. The constant acceleration is programmed such that the rods do not slow down before reaching the extent of piston travel. A value of 0.02-0.03 seconds for this slowing is not unreasonable. By taking out the dashpot slowing, Figure 42 and Figure 43 would look very similar.

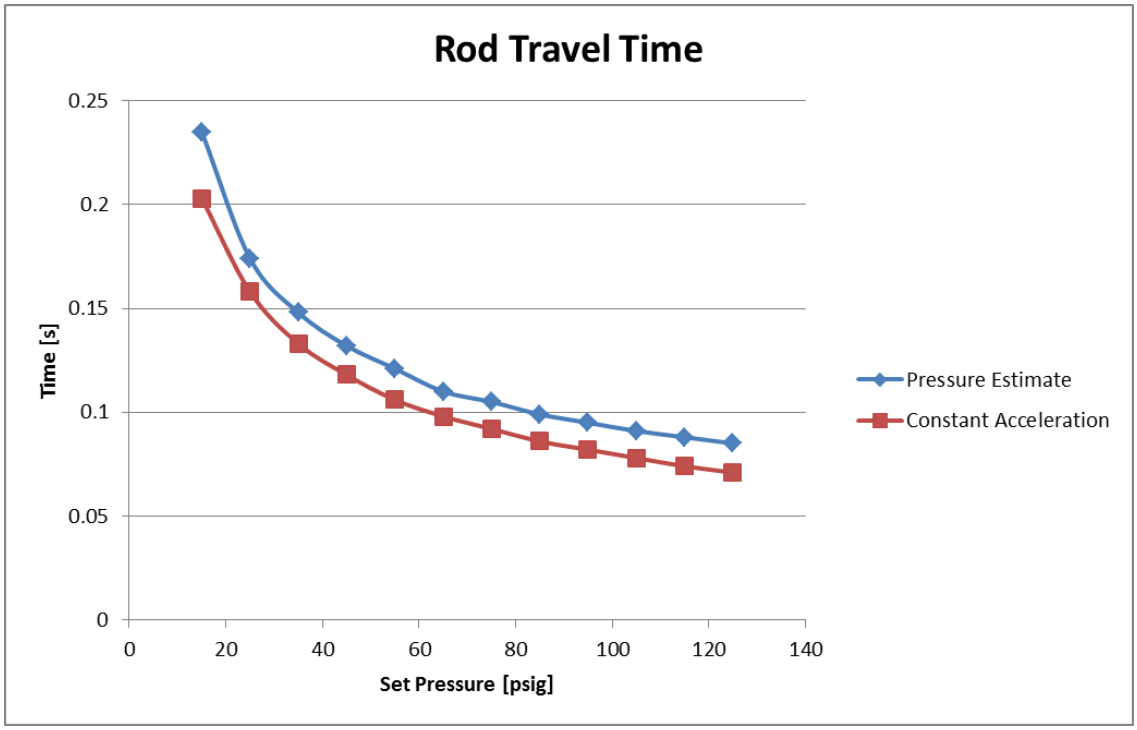

Figure 43. Comparison of Rod Travel Time for Constant Acceleration and Pressure Estimation Methods

Discussion

The important takeaways from the study of TR motion on reactivity insertion in the ACRR are:

- Each TR has a different reactivity rate addition into the ACRR.
- The time in which it takes to insert reactivity plays a significant role in the amount of system reactivity achieved by the pulse.

Since TR B is moving quicker than A or C, it inserts reactivity into the core slightly faster than TR A. TR C, on the other hand, takes significantly longer due to longer ejection times. Once more information is known on the exact positioning of the TRs during a pulse (from potentiometers or accelerometers), Razorback can be modified to split the TR worth into single rods and add them together instead of treating all three together. This could drastically improve the prediction of reactivity insertion and system reactivity seen during a pulse.

Interestingly, using the 65 psig set pressure, a pulse from the pedestal takes roughly 90 ms to insert all $3.05 of reactivity. In terms of safety analysis, to say that a roughly $3.00 pulse can insert all the reactivity in 80 ms, the set pressure would need to

be raised to roughly 85 psig. Or in other terms, the reactivity addition limit could be increased to 90 ms for a roughly $3.00 pulse. The 80 ms time limit likely adds in a 10 ms buffer as a factor of safety, but once more precision is involved with the measurement of rod timing; there is no reason why the factor of safety cannot be decreased to say 5 ms or less.

Another possible use for this data is for use in analyzing whether the set pressure can be lowered. There are evident advantages from lowering the accumulator set pressure such as less mechanical stress on the TR mechanical linkages and lowered pressure safety concerns. However, as seen with Figure 41, in order to keep the system reactivity within 5 percent of the expected total reactivity insertion, 65 psig is needed. Depending on what the experimenters are trying to achieve, it might be possible to lower the set pressure, but an improved method of predicting total reactivity insertion into the system would need to be developed.

CHAPTER 6
DUST CAP FAILURE ANALYSIS

Purpose

The following study applies results derived from the previous study completed in Chapter 3 to determine loading forces on the aluminum cylinder dust cap due to pulsing with a broken transient rod. This study is an input into a Corrective Action which the ACCR TR Pneumatic System Design Study must address.

Background

This analysis was prompted by the most recent 13-8 PH rod mechanical linkage failure in which subsequent pneumatic TR operations (in maintenance mode) were performed with the broken rod. The undiagnosed condition resulted in the piston rod striking the dust cap multiple times causing it to shear at the edges and dislodge from its installed location. A visual of the dust cap – cylinder model is located in Figure 44 for reference. Note about the figure, the cylinder has been cut at ~ 2 inches from the top for ease of study; the cylinder is actually ~ 90 cm in height.

The TR was broken at the top threads of the dashpot rod, thus removing the upper stop to TR motion. The new upper stop was now the dust cap, which is designed to keep debris out of the pneumatic cylinder, not take multiple impacts from the piston rod. The dust cap can most likely withstand one impact just fine, albeit causing plastic deformation to the cap itself. However, multiple strikes will most certainly cause a failure. This hypothesis is sought to be corroborated with this study.

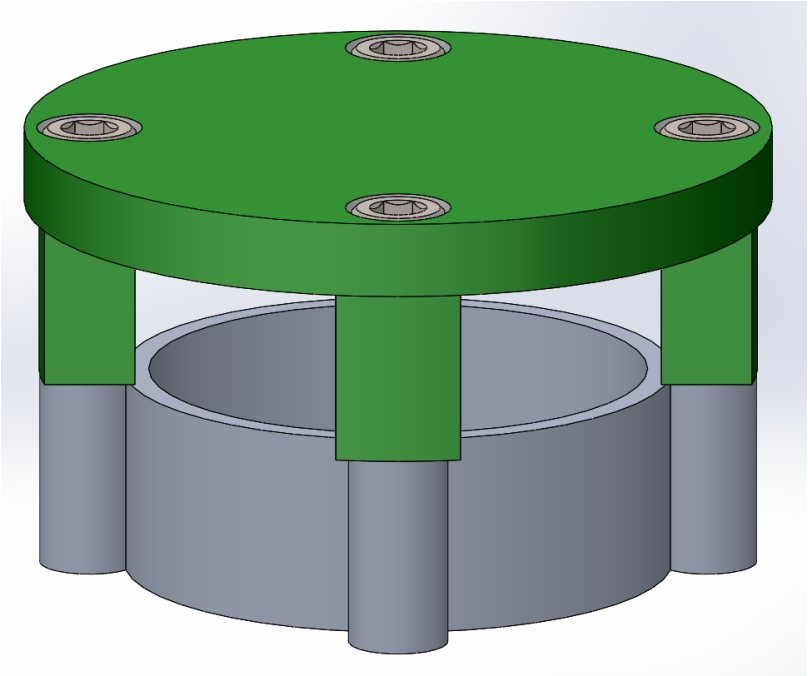

Figure 44. Model of Dust Cap - Cylinder Assembly

Methodology

The general approach to this study is:

1. Determine the methods in which the dust cap- cylinder assembly might fail
2. Calculate an approximate loading force on the dust cap due to the broken TR
3. Complete a baseline hand-calculation with circular aluminum plate to approximate stresses
4. Generate SolidWorks FEA analysis with the loading force as a boundary condition
5. Complete parametric study on loading force with respect to estimated impact time
6. Compare SolidWorks results to approximate failure stresses for each component
7. Estimate force range for yielding of material

Failure Methods

Using knowledge from mechanic of materials, this problem can be thought of in terms of analyzing the behavior of solid materials when exposed to large impact loading forces. This problem, when simplified to its foundational pieces, can be compared to a simple beam or plate failure calculation. In this type of calculation, one would analyze the material's geometry and fixtures combined with the loading to determine parameters such as displacement, shear, and moments. With these parameters, stress and strain

would then be used to determine the most appropriate failure theory to apply to the given problem.

As with most beam or plate problems, the most common failure is due to bending stresses. Bending stresses are a combination of shear, tensile, and compressive stresses of which dominate at specific locations. Near the location of loading, tensile and compressive stresses will have the largest influence due to maximum displacements and moments. The shear is most likely to occur at the edges and near connections.
The Max Normal Stress Theory (Mises Failure) and Max Shear Stress Theory (Tresca Failure) both come into play here [16]. These two failure methods allow the splitting of the bending stresses for analysis separately. SolidWorks uses both methods to predict tensile and shear failure respectively.

Since the dust cap does not fail on the first impact, it is safe to say that the cause of failure is more likely to be answered with a fatigue analysis rather than a single impact. Also, since this model must be simplified to solve by hand, the typical fatigue studies would be difficult to complete. This study is intended to gauge the results after a single impact due to uncertainty and complexity of computationally modeling a pre-deformed model.

In order to determine the stresses on the dust cap, cylinder and bolt the loading force on the dust cap is required. The rest of this section identifies certain proposed methods of failure for this assembly and calculates the estimated force required for failure. These forces are then used as inputs for both the analytical and computational solutions.

Three different failure methods thought to have caused the dust cap failure. They include: shear failure of the bolt extrusion on the dust cap, shear failure of the internal threads of the aluminum cylinder (stripping of the threads) or the tensile failure of the socket head cap screws bolting the dust cap and cylinder together.

Method 1: Shear Failure of Aluminum Extrusion on Dust Cap

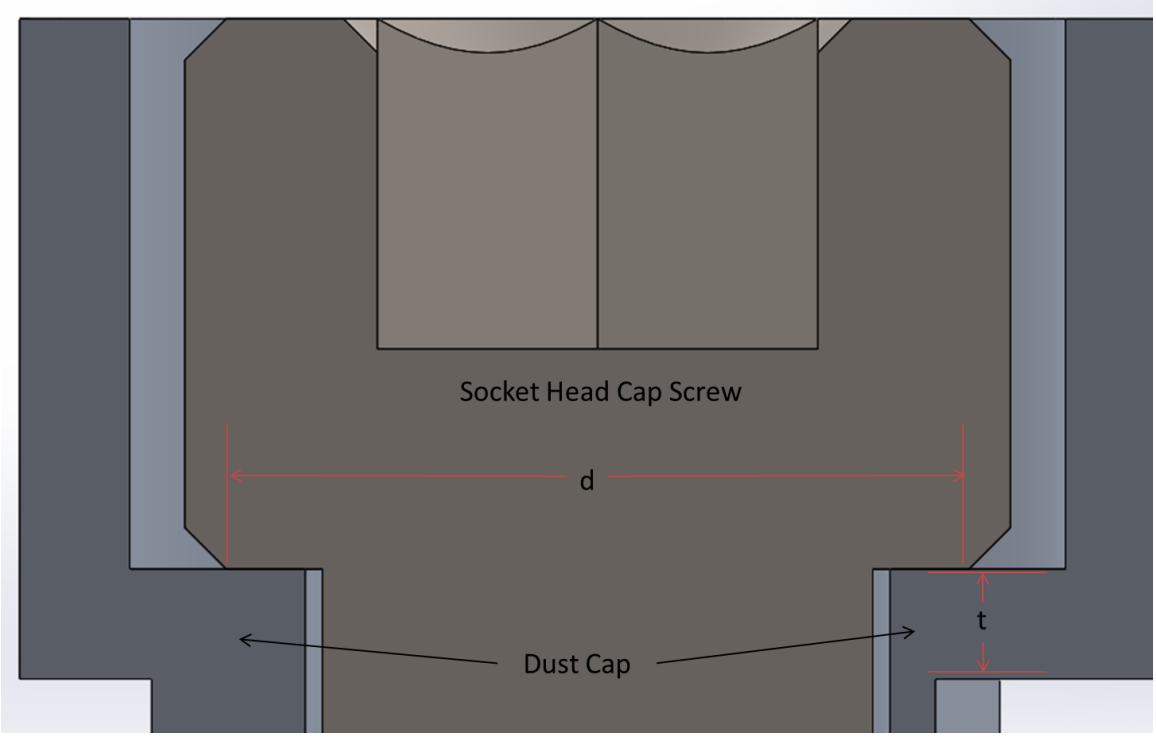

Figure 45. Cross Section of Connection between Bolt and Dust Cap

Explanation of Failure

In this method, the dust cap will fail via a shearing force transversely by ripping the tab of the dust cap (bottom of Figure 45) off of the top plate.

Given Information

- d = 0.4233 in.
- t = 0.060 in.
- Dust cap is made of 6061-T6 Aluminum plate with shear stress τ = 27 ksi

Equations

$$Shear\ Stress = \tau = \frac{F}{A} \tag{8}$$

$$A = \frac{\pi dt}{2} \tag{9}$$

Solution

$$F = \tau A = 27000 \frac{lbf}{in^2} * \frac{\pi * 0.4233" * 0.060"}{2} = \mathbf{1122\ lbf} \quad (10)$$

Method 2: Shear Failure of Internal Threads of Cylinder

Explanation of Failure

In this method, the bore of the threads in the aluminum cylinder will fail via axial shear. This method, in the mind of the author, is the most likely method of failure due to the threaded connection and difference in material strengths between the bolt and cylinder.

Assumptions

- First 6 threads (conservatively) of bolt/cylinder take 100% of loading
- Bolt is a 5/16" – 18 thread per inch (TPI) socket head cap screw with class 2 threads
- Formula for area came from [17]

Given Information

- L = length of thread engagement = 0.333 in.
- $D_{s,min}$ = minimum major diameter of the external threads = 0.3206 in.
- $E_{n,max}$ = max pitch diameter of internal thread = 0.2817 in.
- n = threads per inch (TPI) of bolt = 18
- Shear failure of extruded 6061-T6 aluminum = τ = 24 ksi

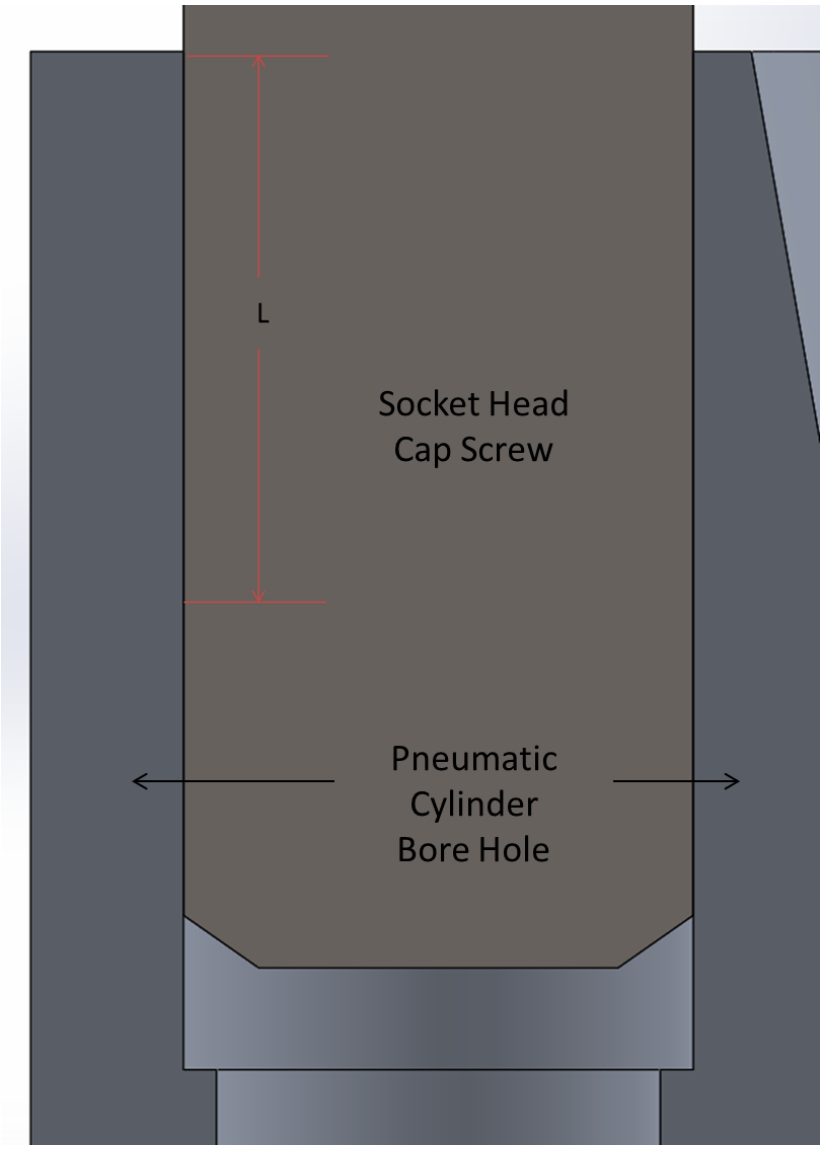

Figure 46. Cross Section of Bolt in Cylinder

Equations

$$Shear\ Stress = \tau = \frac{F}{A} \tag{11}$$

$$A = \pi L D_{s,min}\left[\frac{1}{2n} + 05.7735\left(D_{s,min} - E_{n,max}\right)\right] \tag{12}$$

Solution

$$A = \pi(0.333\ in)(0.3206\ \text{in})[\frac{1}{2(18\ \text{in}^{-1})} + 0.57735(0.3206\ \text{in-}0.2817\ \text{in})] \\ = 0.2273\ in^2 \quad (13)$$

$$F = \tau A = 24000\frac{lbf}{in^2} * 0.2273\ in^2 = \mathbf{5454\ lbf} \quad (14)$$

Method 3: Failure of Bolt in Tension

Explanation of Failure Method

This method considers the bolt to be the cause of the failure in that it will fail in tension due to the axial loading applied to the dust cap.

Assumptions

- Bolt is made of alloy steel with an ultimate tensile strength (UTS) of 190 ksi and yield strength of 150 ksi.

Given Information

- d_s = diameter of bolt shank minus the thread width = 0.2452 in.
- n = threads per inch of bolt = 18

Equations

$$Tensile\ Stress = \sigma = \frac{\mathrm{F}}{\mathrm{A}} \quad (15)$$

$$A = \frac{\pi}{4}\left(d - \frac{0.9743}{n}\right)^2 \quad (16)$$

Solution

$$F = \sigma A = 190000\frac{lbf}{in^2} * \frac{\pi}{4}\left(0.2452\ in - \frac{0.9743}{18\ in^{-1}}\right)^2 = \mathbf{5488\ lbf} \quad (17)$$

Loading Force

The impact force on the dust cap is determined by using the impulse principle in that the force is equivalent to the change in momentum over the change in time of the collision. The momentum of the TR as it hits the dust cap is found using the mass of the TR and its velocity at impact. Each impact force will also be analyzed based on the likelihood of the impact time, since the impact time and impact force are very highly dependent on each other.

Assumptions

- Force is applied as an impact loading at the center of the dust cap distributed throughout the area of the piston rod.
- Pulse occurs with a TR broken at the upper threads of the dashpot rod.
- The TR is broken before the pulse and not during.
- Ending velocity (v_f) is 0.
- Parametric study applied to impact time to determine rough yield limits.

Given Conditions

- Mass of broken TR is 8.018 lbm or 0.2492 slugs.
- Velocity at impact (~9300 RUs) is 40 ft/s (as calculated from the pressure data).
- Acceleration at impact is ~ 615 ft/s^2 (as calculated from the pressure data).

Equations

$$F = \frac{dp}{dt} = \frac{m(v_i - v_f)}{\Delta t} \tag{18}$$

Solution

$$F = \frac{0.2492\ slugs\left(\frac{40ft}{s} - \frac{0ft}{s}\right)}{0.001s} = 9968\ lbf \tag{19}$$

Four cases were tested and the resultant forces (in ascending order) are shown below in Table 6.

Table 6. Impact Forces Calculated Based off Impact Times

Impact Time [s]	Impact Force [lbf]	Notes
0.0652	153	F=ma
0.0050	1996	5 ms impact time
0.0022	4488	Method 1 force used
0.0010	9986	1 ms impact time

Analytical Solution

Description

The dust cap model is simplified to a simple circular, solid plate simply supported at the edges. The 6061-T6 aluminum plate is 3.75 inches in diameter and 0.375 inches thick. Loading is applied uniformly over a small circular central area. The equations and calculations are found in Appendix C.

Results

The maximum displacement, radial moment and stress values were calculated for each of the four loading cases and are shown in Table 7.

Table 7. Maximum Values calculated for each loading force in Table 6.

Loading (lbf)	Displacement (in)	Moment (lbf-in)	Stress (ksi)
153	0.000588	44.8	1.91
1996	0.00767	585	24.9
4488	0.0172	1310	56.1
9986	0.0384	2920	125

Along with the maximum values, a distribution of the displacement was plotted and overlaid on the non-deformed dust cap geometry (shown in Figure 47) for comparison.

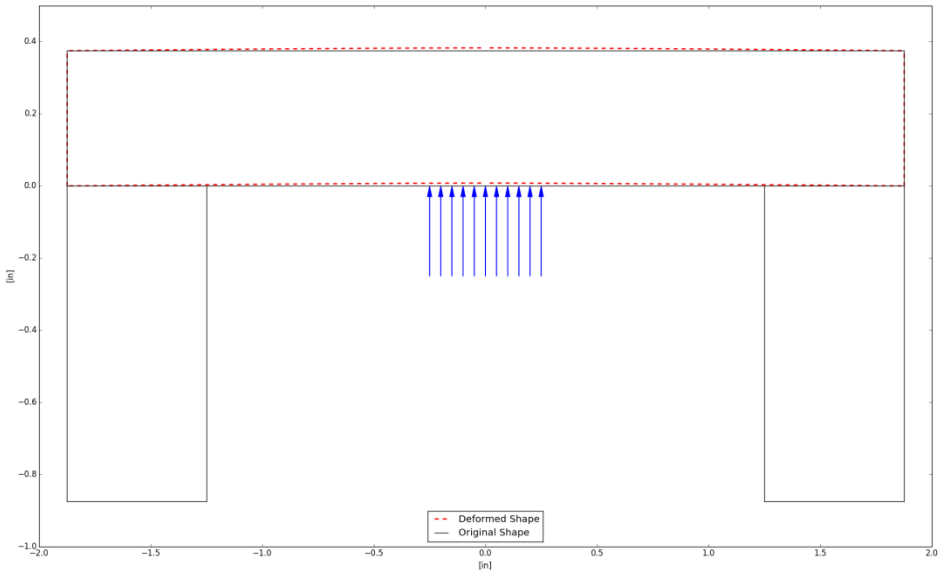

Figure 47. Deformed plate (to scale) from 1996 lbf loading case of dust cap shown in relation to non-deformed dust cap (loading forces shown as blue arrows)

Even though the deformed result does not take into effect the tabs, it can still be used to gauge whether the SolidWorks comparisons are on the right track. Seeing stress values close to the yield point of the aluminum (35 ksi) hints at a yielding limit between two and four thousand pounds.

SolidWorks Comparisons

In order to check whether the theoretical and analytical calculations make sense, a SolidWorks model of the full dust cap, cylinder and bolts was created for simulation. The model is shown in Figure 44.

Setup

The model is set up that the dust cap sits flush on top of the cylinder (also known as coincident). This is the same case for the bolt in the recessed hole of the dust cap. The bore of the dust cap is of slightly larger diameter leaving a 0.02 inch annular gap. The bolt fits tightly within the cylinder bore.

The study type used is a linear static simulation with the impact force applied to the small diameter of the piston rod at the center of the dust cap. The force is set according to each of the cases mentioned in Table 6. There is a no penetration contact

applied between the dust cap and cylinder (meaning that the two components will stay rigid in the face of deformation), otherwise the rest of the components are bonded together. The bottom of the cylinder is fixed as if in concrete. Mesh controls were applied at the connections of the components and to important faces such as the bolt shank and inner dust cap flange face in order to get more accurate results.

Results

The results presented here are intended to be used as a guideline rather than a definitive answer. From the results, an estimated loading force and impact time will be calculated in order to avoid yield and shear stress, and as a result, plastic deformation. Also, max stresses on each of the three components (dust cap, cylinder and bolt) will be compared. SolidWorks also does not handle plastic deformation well and will give unreliable results when applied in this manner. The study presented here is only meant to be used to gauge the results from a single strike. Since the impact is thought to cause plastic deformation, the results will likely cause an asymmetrical geometry, which then leads to an asymmetrical loading on the subsequent impacts.

SolidWorks Stress Profiles

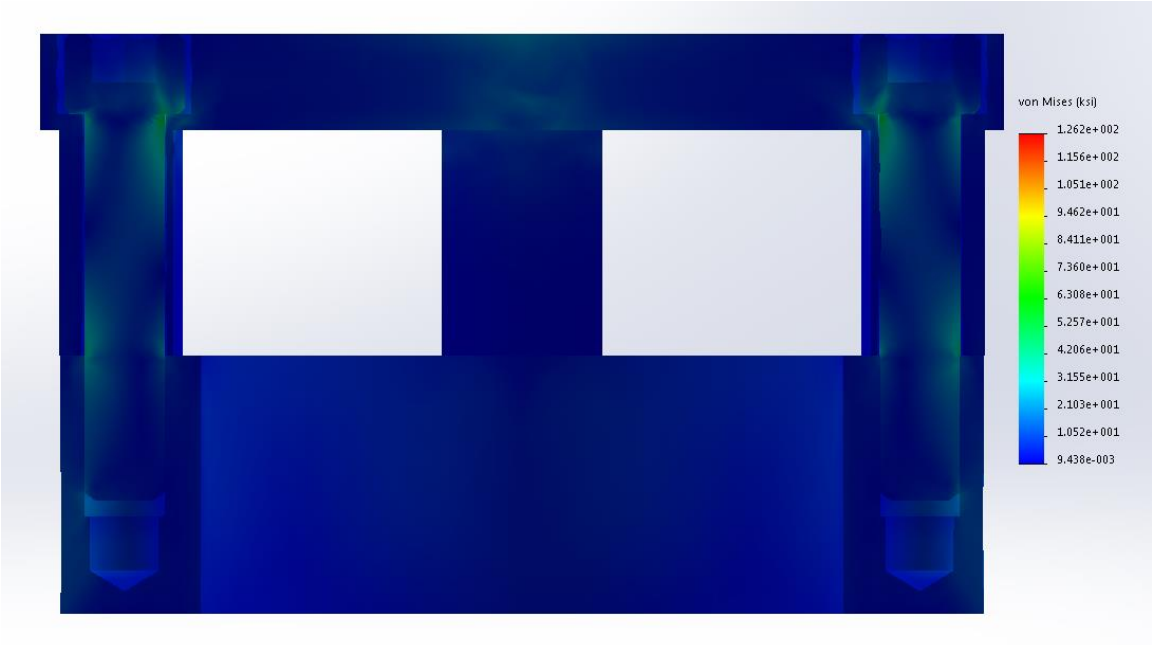

Figure 48. Typical Von Mises Stress Plot for Full Model

Highlighted in Figure 48 (light green areas), the high Von Mises stress points are where the bolt and dust cap contact, as well as, the bolt and top edge of the cylinder. These locations are designed to resist deformation causing them to show large stresses. The numerical results to the stress plots are shown in Table 8.

There are a few things about Table 8 that need more explanation. Firstly, these values are the max stress values as seen on each component for each case. Secondly, the shear stress values are only measured in terms of Tau XY, which represents the shear stress trying to shear the dust cap transversely at the connections. Tau XY also had the highest values of all the shear stresses measured by SolidWorks.

In terms of failure prediction, two types of failure are predicted: yield and shear. The limits for the dust cap and cylinder are from [18] and the bolt is from [19]. The component expected to yield first is the dust cap, as shown by the red highlighted column. The yield or failure limits were calculated by using linear interpolation between the values in each column as stress scales linearly with force.

Table 8. Von Mises and Shear Stress Results for SolidWorks Model with Failure Prediction Modes

Full Model - Stress Values				**Failure Prediction**			
Von Mises Stress		*Units [ksi]*		*Von Mises Stress*		*Type: Yield*	
Case [lbf]	**Dust Cap**	**Cylinder**	**Bolt**	**Notes**	**Dust Cap**	**Cylinder**	**Bolt**
153	1.76	0.86	2.58	Limit	**35**	35	150
1996	22.8	11.2	33.5	Unit	**ksi**	ksi	ksi
4488	53.6	24.1	96.8	Prediction [lbf]	**2983**	6764	7024
9980	120	50.4	212	Impact Time [ms]	**3.34**	1.47	1.42
Shear Stress (Tau XY)		*Units [ksi]*		*Shear Stress*		*Type: Shear*	
Case [lbf]	**Dust Cap**	**Cylinder**	**Bolt**	**Notes**	**Dust Cap**	**Cylinder**	**Bolt**
153	0.88	0.25	0.54	Limit	**27**	24	150
1996	11.39	3.18	6.97	Unit	**ksi**	ksi	ksi
4488	18.93	6.29	35.64	Prediction [lbf]	**6357**	10000+	10000+
9980	42.64	14.59	58.88	Impact Time [ms]	**1.57**	< 1	< 1

Discussion

After reviewing the results, it becomes quite clear that the dust cap will hit its yield point before either the cylinder or bolt does. Using 35 ksi as the yield/failure point for the dust cap in tension, the full model estimates a maximum impact loading force of **2983 lbf**. This impact force corresponds to an impact time of **3.34 ms**, which seems reasonable for a full impact of aluminum on aluminum at high speed.

The analytical solution predicts yield (using the same 35 ksi limit) at **2803 lbf**. Adding in the extra support from the bolts and cylinder should cause an increase in the allowed loading which is seen. At the very least the yield of both solution methods are comparable to make the SolidWorks results more believable.

A complete failure after one impact would be caused by a stress higher than the 42 ksi ultimate tensile strength of the aluminum. The 42 ksi limit is hit at 3362 ksi and 3550 ksi for the analytical and SolidWorks results respectively. From these limits, a range of loading forces to cause failure in pure tension would be between **2983 lbf and 3550 lbf** (based on the SolidWorks results).

In shear, the dust cap would also fail first, but with a larger required force than would be required in tension. In shear, the dust cap is predicted to fail at roughly 6357 lbf with a corresponding impact time of 1.57 ms.

In reality, the dust cap likely failed as a combination of both shear and tension. It is also likely that the first few impacts weakened the threaded connection of the bolt in the cylinder to produce failure at much lower forces than would be required on first impact. Pictured in Figure 49 is the actual failed dust cap. It is seen that the dust cap did not fail symmetrically but on one half of the dust cap. The analysis corroborates that the failure occurred at the connection between the top plate of the dust cap and the aluminum extrusions designed to guide the bolt. Multiple impacts can be seen by the numerous indentions in the center of the dust cap. From Figure 49, it is seen that the loading is not always perfectly symmetric, but the impact location is shallower on the side of the attached tabs. This fact implies a loosening of the bolted connection on the side of the failure. While it is near impossible to predict the exact mode of failure for the dust cap using SolidWorks or analytically, this exercise provided confirmation that the mode of failure would be expected upon multiple strikes to the dust cap.

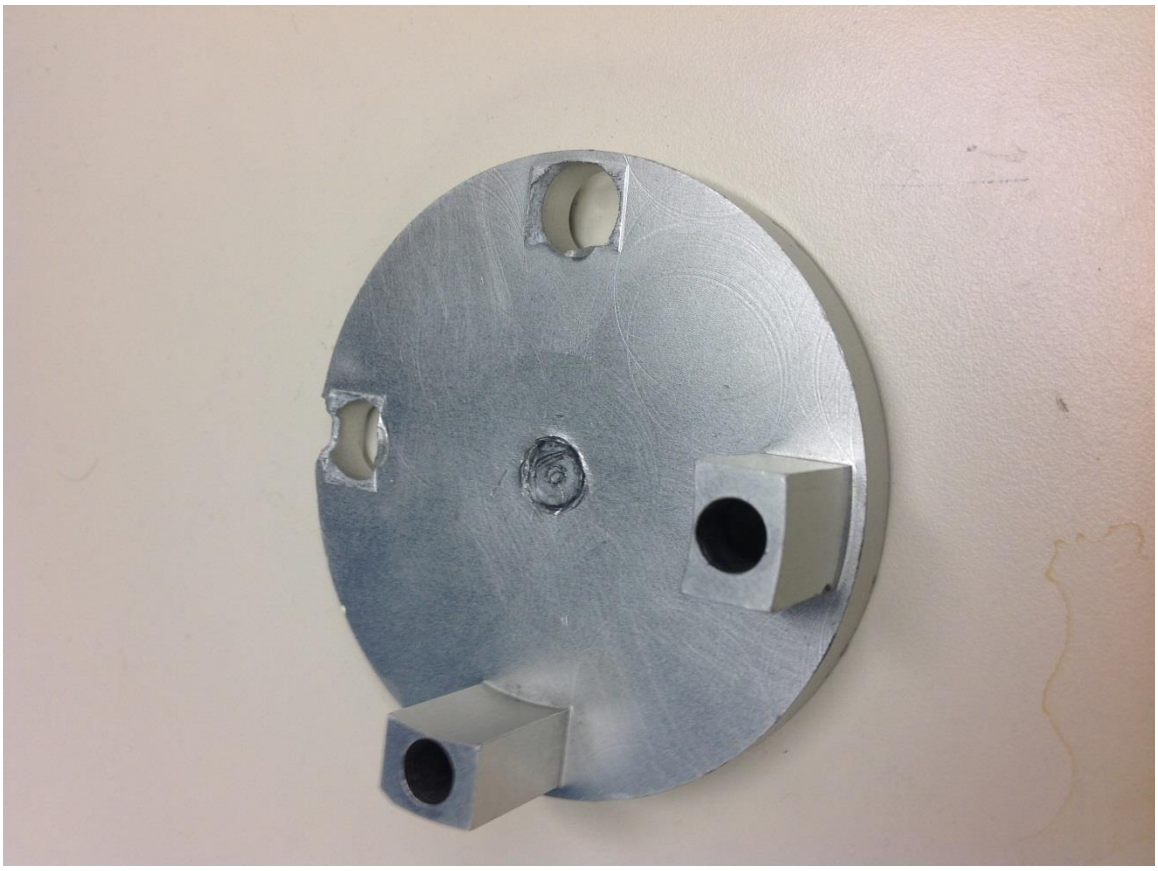

Figure 49. Broken Dust Cap

Future study to further narrow the failure method would be to apply a fatigue analysis to the SolidWorks results. The fatigue analysis would be able to simulate multiple impacts at various time intervals.

CHAPTER 7
DISCUSSION

This study investigated how the TR pneumatic system affects TR motion, timing and reactivity insertion into the ACRR. The completion of this study provides a better foundational understanding of the connection between the components of the whole TR system and how they work together to power the ACRR during pulsed operations.

Summary of Findings

Given pressure distributions at two locations on the TR pneumatic system, a profile for TR motions was generated for varying starting positions. The motion profile was validated with the operationally-measured Fire Times to a relatively close certainty. Using the motion profiles, a previously set limit for TR motion was further explored and clarified. However, the conclusions generated with this study are still simply hypotheses until more data can be gathered for verification.

By starting with the first-order principles, the pressure distributions in the TR pneumatic system were replicated with some verifiability. Except for motion in the dashpot, TR motion during a pulse aligned well based solely off of mass and energy balances with what is experimentally measured. Most importantly, the analytical approach provided a clearer understanding of the delays associated in TR timing.

Both motion profiles and estimated pressure distributions were varied to examine how reactivity within the ACRR would respond. It was determined that the previous work in setting the limit for TR motion that the timing of reactivity addition was both clarified and corroborated to an extent, with larger pulses deviating on the more conservative side. Dynamic reactivity proved to be present with even higher consequences for slower TR motion and lower accumulator set pressure.

Lastly, discrete points along the TR motion profile were used to study the impact of the TRs on the dust cap. The resulting loading estimate closely models the actual failure method even though further simulation is needed to for a fatigue analysis.

Future Work

A plentitude of future work is planned to relate this study to the rest of the work needed to be done on the project. Firstly, as mentioned previously, accelerometers and potentiometers are scheduled for installation on the piston to garner more accurate motion profiles. Also, strain gauges are also going to be installed on the dashpot rod to measure the loading forces seen during operation.

In line with the measurement of mechanical stresses, a 3D model has been created to analyze high stress points on the TR mechanical linkages. The motion profile will be used as an input into SolidWorks to simulate mechanical stresses on each component, with the dashpot, dashpot rod and poison sections being of high interest.

Also, a test stand (mock-up of the ACRR with all three TRs to scale) is in the process of being built in order to test proposed changes to system performance without having to install directly on ACRR. Combining knowledge of the current system with re-designs of certain components will allow the ACRR to become more reliable and perform more efficiently in the future.

APPENDIX A: SOLENOID VALVE SPEC SHEETS

PARKER HANNIFIN
AIR CONTROL VALVES

CATALOG 0635
FILE A84.2

series
H200 and H2000
3-way "HUSTLER"


Series H200 With Junction Box


Series H200 Without Junction Box

SPECIFICATIONS

1. A base mounted, plug-in valve that can be serviced or converted from normally closed to normally open without disturbing the piping or wiring.
2. Valve can be converted from normally closed to normally open by simply changing the cartridge assembly.
3. Nylon encapsulated plug-in coil available in a wide range of AC and DC voltages.
4. *Shur-Shift* chamber ensures positive shift.
5. External pilot exhaust.
6. Internal pilot supply—may be converted to external pilot supply.
7. Both pilot and main valve are poppet type, ensuring positive sealing and insensitivity to foreign material.
8. Poppet construction will provide millions of trouble free cycles without lubrication.
9. Lubrication requirements are not critical, which permits the valve to operate dry or with heavy, light or intermittent oil delivery.
10. The short piston poppet stroke provides speed and uniform response, plus high flow capacity.
11. Equipped with Locking Manual Override–(Available with Non-Locking Manual Override–Add M1A to Model).
12. Built to J.I.C. Specifications.
13. Compact—takes less space than other three-way valves.
14. Response Time and Flow Capacities (Cv) are related in the table below.

USES

1. Brake and clutch actuation.
2. Single-acting cylinders.
3. In pairs to operate double-acting cylinders for high speeds, positioning or inching.
4. Selection of two different pressures or pressure sources.

- 3-WAY (AND 2-WAY) 2-POSITION
- SOLENOID ACTUATED — MAINTAINED CONTACT
- PILOT OPERATED — INTERNAL PRESSURE RETURNED
- PISTON POPPET
- 1/2", 3/4", 1", 1-1/4" NPTF TAPPED SIDE PORTS Alternate Porting Available (See "How to Order")
- PRESSURES — 15 TO 150 PSI AIR
- 115/120 AND 230 VOLT, 50/60 CYCLE CONTINUOUSLY RATED SOLENOIDS STANDARD — 7.7 Watts (0.24 Amps Inrush, 0.14 Amp Holding on 115-120/50-60 Cycle). Other AC and DC Solenoids Available

HOW IT WORKS

Normally Closed

With the solenoid de-energized, internal pressure raises the piston poppet. Pressure at Port "P" is blocked and Port "A" is open to exhaust Port "E".

When the solenoid is energized, pilot pressure drives the piston poppet down. Pressure at Port "P" is open to Port "A", exhaust Port "E" is blocked.

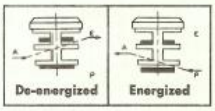

Normally Open

With the solenoid de-energized, internal pressure raises the piston poppet. Pressure at Port "P" is open to Port "A", exhaust Port "E" is blocked.

When the solenoid is energized, pilot pressure drives the piston poppet down. Pressure at Port "P" is blocked and Port "A" is open to exhaust Port "E".

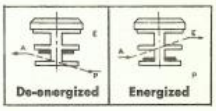

Response Times and Capacity Coefficients

Valve Series	Valve Size	Response Time (Seconds) 12 Cubic In. Chamber Fill	Exh.	100 Cubic In. Chamber Fill	Exh.	Capacity Coefficients(Cv)† Flow Directions P to A	A to E
H200	½" NC	.025	.036	.066	.090	6.28	9.21
	½" NO	.031	.052	.073	.120	6.46	8.32
	¾" NC	.025	.029	.060	.088	7.89	9.39
	¾" NO	.031	.036	.063	.100	8.25	8.48
Valve Series	**Valve Size**	**100 Cubic In. Chamber Fill**	**Exh.**	**500 Cubic In. Chamber Fill**	**Exh.**	**Flow Directions P to A**	**A to E**
H2000	¾" NC	.069	.087	.200	.221	10.66	17.06
	¾" NO	.080	.093	.203	.256	10.99	14.71
	1" NC	.067	.078	.173	.190	14.92	19.74
	1" NO	.071	.093	.185	.235	14.92	16.02
	1 ¼" NC	.062	.072	.162	.176	17.24	19.74
	1 ¼" NO	.068	.090	.156	.204	17.24	16.39

†See reverse side for Cv formula.

HOW TO ORDER

Valve Model Numbers

PIPE SIZE -50— 1/2" NPTF -75— 3/4" NPTF -100—1" NPTF -125—1-1/4" NPTF		SERIES H200 Side Ports Tapped*	Bottom O-Ring Ports	Side & Bottom Ports Tapped*	SERIES H2000 Side Ports Tapped ♦	Bottom O-Ring Ports	Side & Bottom Ports Tapped
3-Way Normally Closed	Without Junction Box	H201NC-50 -75	H203NC-75	H205NC-50	H2001NC-100 -125	H2003NC-125	H2005NC-75 -100
	With Junction Box	H202NC-50 -75	H204NC-75	H206NC-50	H2002NC-100 -125	H2004NC-125	H2006NC-75 -100
3-Way Normally Open	Without Junction Box	H201NO-50 -75	H203NO-75	H205NO-50	H2001NO-100 -125	H2003NO-125	H2005NO-75 -100
	With Junction Box	H202NO-50 -75	H204NO-75	H206NO-50	H2002NO-100 -125	H2004NO-125	H2006NO-75 -100

*Available with 3/8" porting. ♦Available with 3/4" porting. Specify solenoid voltage and cycles.

Installation, Operation and Maintenance Instruction Form V-249 packed with every valve shipped.

PARKER HANNIFIN

PNEUMATIC DIVISION
PARKER HANNIFIN CORPORATION
OTSEGO, MICHIGAN

17

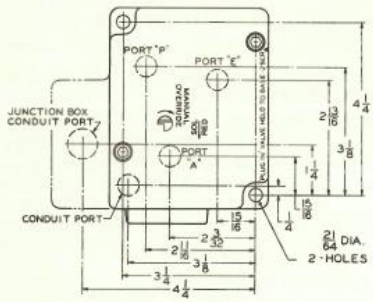

TOP VIEW H2000 SERIES
Port Locations of Bottom – Ported Models Shown Dotted.

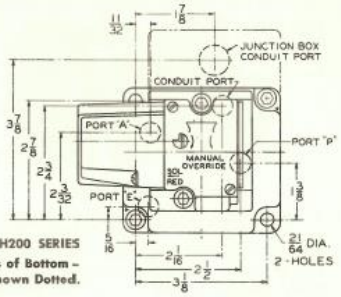

TOP VIEW H200 SERIES
Port Locations of Bottom – Ported Models Shown Dotted.

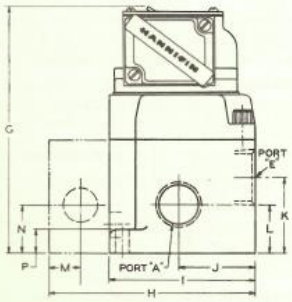

SIDE VIEW H200 AND H2000 SERIES

- These valves will operate mounted in any position.
- Red electrical wires in junction box lead to Solenoid Red.
- Valves without junction boxes are supplied with 6' leads. Valves with junction boxes have 9" leads with attached terminals.
- Filtered and lubricated air recommended for maximum valve life and minimum maintenance.

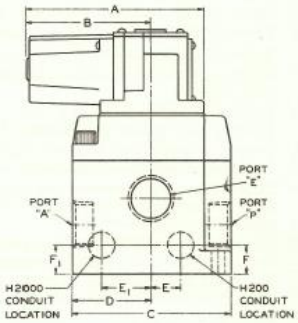

FRONT VIEW H200 AND H2000 SERIES

VALVE DIMENSIONS

VALVE SERIES	PIPE SIZE	A	B	C	D	E	E_1	F	F_1	G	H	I	J	K	L	M	N	P
H200	½" ¾"	4¼	2 21/32	3¾	1⅞	1 1/16	—	1 3/16	—	5⅞	4 15/16	3½	1 13/16	1 13/16	1 3/16	¾	1⅛	5/16
H2000	¾" 1" 1¼"	4¼	2 21/32	4⅞	2 5/16	—	1¾	—	1 3/16	7 5/16	5 3/16	3⅞	2 1/16	1¾	1¾	¾	1⅛	5/16

PORT DIMENSIONS

	SIDE PORTS				SIDE & BOTTOM PORTED			BOTTOM O-RING PORTS			
SERIES	H200		H2000		H200	H2000		H200—¾"		H2000—1¼"	
VALVE SIZE	½"	¾"	1"	1¼"	½"	¾"	1"	COUNTER-BORED HOLE	O-RING GROOVE	COUNTER-BORED HOLE	O-RING GROOVE
PORT P*	½"	¾"	1"	1¼"	½"	¾"	1"	45/64"	1 1/16"	1 5/32"	1 5/16"
PORT A*	½"	¾"	1"	1¼"	½"	¾"	1"	43/64"	1 1/16"	1 5/32"	1 5/16"
PORT E*	1"	1"	1½"	1½"	½"	1"	1"	45/64"	1 1/16"	1 5/32"	1 5/16"
CONDUIT PORT†	½"	½"	½"	½"	½"	½"	½"	½"	¾"	½"	¾"
JUNCTION BOX† CONDUIT PORT	½"	½"	½"	½"	½"	½"	½"	47/64"	1 1/16"	47/64"	1 1/16"

* Pipe Threads are NPTF † Conduit Threads are NPSM

C_v—Capacity Coefficients—(sometimes called Flow Factors). Each flow path through the valve has its own C_v value. All C_v ratings for each valve cataloged on this page are listed on the front side of this sheet.

$$C_v = \frac{Q}{22.67}\sqrt{\frac{GT}{(P_1-P_2)P_2}}$$

Q = Flow in Standard Cubic Feet per minute (14.7 PSIA at 60°F.)
P_1 = Inlet Absolute Pressure (gauge pressure +14.7)
P_2 = Outlet Absolute Pressure (gauge pressure +14.7)
Note: P_2 must be greater than .53 x P_1
G = Specific Gravity of flowing medium (Air, G=1)
T = Absolute Temperature of Air (460+°F.)

APPENDIX B: ANALYTICAL SOLUTION DERIVATIONS

Analytical Derivations

The analytical derivations are the application of thermodynamic energy balances to the specific problem definitions as listed above. The two derivations vary greatly due to differing conditions and assumptions; however, they both use the foundational approach that is described in [9]. Here they are in full detail.

Nomenclature

$CV =$ control volume

$m_{cv} = m =$ control volume mass

$\dot{m}_v =$ mass flow rate through valve

$\dot{m}_k =$ mass flow rates in and out of the control volume

$m_i =$ mass in CV at time t_i

$m_{i-1} =$ mass in CV at time t_{i-1}

$\Delta t = t_i - t_{i-1}$

$E_{cv} =$ control volume energy

$\dot{W}_s =$ rate of shaft work

$P_0 =$ atmospheric pressure

$V =$ volume of control volume

$\dot{Q}_0 =$ heat transfer rate with atmosphere

$\dot{Q}_k =$ heat transfer rate with other components

$h_k =$ enthalpy of fluid at each orifice

$v_k =$ velocity of fluid at each orifice

$g =$ gravitational constant

$z_k =$ height of each orifice

$h_v =$ enthalpy of fluid in the valve

$V_v =$ velocity of fluid through the valve

$u_{cv} = u =$ internal energy of control volume

$T_i =$ Temperature in CV at time t_i

$T_{i-1} =$ Temperature of fluid in CV at time t_{i-1}

C_v = constant volume specific heat constant of the fluid

P_i = pressure in CV at time t_i

ρ_i = density of fluid in CV at time t_i

R = specific gas constant

F_{net} = net force on piston

P_g = gauge pressure in CV

A_{piston} = surface area of bottom face of piston

F_{fr} = friction force on piston seal

F_M = weight of TR components

P_{pn} = pneumatic pressure on A_{piston}; same as P_i

D_{cyl} = diameter of cylinder

dV = incremental control volume in cylinder

a_i = acceleration of piston at time t_i

v_i = velocity of piston at time t_i

d_i = displacement of piston at time t_i

Accumulator to Valve

Assumptions

- Adiabatic
- Ideal gas law applies
- No shaft work
- No inlet, one outlet
- Negligible potential and kinetic energy effects
- Constant volume

Mass Balance

$$\frac{dm_{cv}}{dt} = \sum_k \dot{m}_k \tag{20}$$

After applying the third assumption, (1) simplifies to

$$\frac{dm_{cv}}{dt} = -\dot{m}_v \tag{21}$$

Where $\dot{m}_v$ is the mass flow rate through the valve.

Using finite difference in time, m_i can be represented as follows

$$m_i = m_{i-1} - \dot{m}_v \Delta t \tag{22}$$

Energy Balance

$$\frac{dE_{cv}}{dt} = -\dot{W}_s - P_0 \frac{dV}{dt} + \dot{Q}_0 + \sum_k \dot{Q}_k + \sum_k \dot{m}_k \left(h_k + \frac{v_k^2}{2} + g z_k \right) \tag{23}$$

After applying the assumptions, (23) simplifies to

$$\frac{dE_{cv}}{dt} = -\dot{m}_v h_v \tag{24}$$

Where

$$E_{cv} \equiv U_{cv} = m_{cv} u_{cv} = mu \tag{25}$$

Simplifying the left hand side,

$$\frac{dE_{cv}}{dt} = \frac{d(mu)}{dt} = m\frac{du}{dt} + u\frac{dm}{dt} = m\frac{du}{dt} - u\dot{m}_v \tag{26}$$

Recombining (24) and (26) yields

$$m\frac{du}{dt} - u\dot{m}_v = -\dot{m}_v h_v \tag{27}$$

Apply the finite difference method to (27) which defines the following variables as

$$m = m_{avg} = \frac{m_{i-1} + m_i}{2} \tag{28}$$

$$u = u_{avg} = \frac{u_{i-1} + u_i}{2} \tag{29}$$

$$\frac{du}{dt} = \frac{\Delta u}{\Delta t} = \frac{u_i - u_{i-1}}{\Delta t} \tag{30}$$

Multiply (27) by Δt along with some algebraic simplification yields the following equation for u_i

$$u_i = \frac{u_{i-1}(m_{i-1} + m_i + \dot{m}_v \Delta t) - 2\dot{m}_v h_v \Delta t}{m_{i-1} + m_i + \dot{m}_v \Delta t} \tag{31}$$

Utilizing the First Law of Thermodynamics to relate internal energy and temperature, T_i is represented by the following equation

$$T_i = \frac{u_i + u_{i-1}}{C_v} + T_{i-1} \tag{32}$$

The pressure is calculated using the Ideal Gas Law below

$$P_i = \rho_i R T_i \tag{33}$$

Where R is the specific gas constant and

$$\rho_i = \frac{m_i}{V} \tag{34}$$

Equations (22) and (31-34) are the basis to calculating the parameters for code implementation of the accumulator to valve system.

Valve to Cylinder

Assumptions

- Adiabatic
- No shaft work, significant piston work
- One inlet, no outlet during rod withdrawal
- One outlet, no inlet during rod drop
- Negligible potential and kinetic energy effects
- Non-constant volume
- Ideal gas law applies

Mass Balance

$$\frac{dm_{cv}}{dt} = \sum_k \dot{m}_k \tag{35}$$

After applying assumption three, (35) simplifies to

$$\frac{dm_{cv}}{dt} = \dot{m}_v \tag{36}$$

Using finite difference, m_i can be represented as follows

$$m_i = m_{i-1} + \dot{m}_v \Delta t \tag{37}$$

Energy Balance

After simplifying (23) with the assumptions for the Valve-Cylinder system and applying the simplification in (38), the energy balance reduces to

$$m\frac{du}{dt} + \dot{m}_v u + P_0\frac{dV}{dt} = \dot{m}_v h_v \tag{38}$$

Where P_0 refers to atmospheric pressure.

Applying the finite difference equations in (28-30) to (38) and solving for u_i

$$u_i = \frac{2\dot{m}_v \Delta t h_v - 2P_0 dV + u_{i-1}(m_{i-1} + m_i - \dot{m}_v \Delta t)}{m_{i-1} + m_i + \dot{m}_v \Delta t} \tag{39}$$

Note from (39) that when the piston is not moving, $dV = 0$; however, during piston motion dV is non-zero and significant.

Force Balance

In order to solve for dV, a force balance must be completed on the piston. Figure 50 shows all of the forces acting on the piston during the pulse. Note that F_{fr} changes directions when the piston is falling.

$$F_{net} = P_g A_{piston} - F_{fr} - F_M \tag{40}$$

Equation (40) represents the sum of the forces on the piston where

$$F_M = 14.234\ lbf \tag{41}$$

$$Gauge\ Pressure = P_g = P_{pn} - P_0 \tag{42}$$

$$F_{fr} = \pi D_{cyl}\left(1.5\frac{lbf}{in.}\right); D_{cyl} = 2.5\ in. \tag{43}$$

$$A_{piston} = 4.604\ in^2 \tag{44}$$

Equation (43) comes from the rule of thumb that Parker uses to calculate friction force on the specific piston seal being used in the grooves of the piston [6]. The specific model of the piston seal is an 8400 series U-cup piston seal of 2.5" diameter made out of carboxlated nitrile. Since there is very little published friction data on carboxylated nitrile, the rule of thumb calculation from Parker will suffice.

The energy balance in [9] assumes that the piston is simply connected to the control volume via the rigid structure; however, in order to correlate the change in volume to the force balance, the following relation was used

$$dV = A_{piston}dx \tag{45}$$

Equation (45) applies since the piston area stays constant throughout the duration of the pulse.

In terms of applying the finite difference method to calculating dV, the net force is calculated as follows;

$$F_{net,i} = \left(P_{cyl,i-1} - P_0\right)A_{piston} - F_{fr} - F_M \tag{46}$$

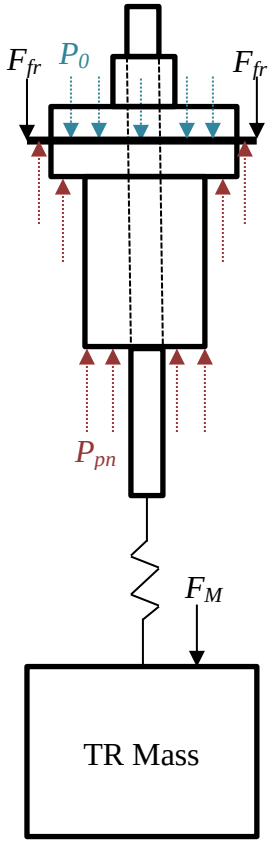

Figure 50. Free Body Diagram on Piston

Piston Kinematics

$F_{net,i}$ is used to calculate the new acceleration as shown in equation (46).

$$a_i = \frac{F_{net,i}}{m_{tr}} + a_{i-1} \tag{47}$$

$$v_i = a_i\Delta t + v_{i-1} \tag{48}$$

$$d_i = v_i\Delta t + d_{i-1} \tag{49}$$

$$dV_i = (d_i - d_{i-1})A_{piston} \tag{50}$$

Velocity and displacement of the piston are calculated from equations (48-49) respectively. The dV calculated in (50) is used to determine the internal energy from equation (31). Temperature, pressure, and density are then calculated in the cylinder using (32-34) respectively.

Assumption Justifications

Nitrogen Supply into Accumulator

There are two sources of nitrogen that will flow into the accumulator during the pulse: nitrogen that has built up in the ~97 feet of .375 in tubing between the accumulator and the pressure regulator and any nitrogen that will flow through the regulator from the nitrogen bottles into the ~97 feet of tubing.

Due to the significant length of tubing that leads into the accumulator, there will be a lengthy delay for the flow passing through the regulator to reach the accumulator. Assuming that the max speed of nitrogen is the same as what is going through the valve (not likely to be this high since the pressure drop across the valve is at least 4 times greater than what would be seen between the piping and accumulator), the flow delay can be calculated as follows:

$$flow\ delay = \frac{flow\ length}{flow\ speed} \tag{51}$$

Where $flow\ length = 97\ feet = 1164\ in$, and $flow\ speed = 73\frac{m}{s} = 2874\frac{in}{s}$.

$$flow\ delay = \frac{1164\ in}{2874\frac{in}{s}} = 0.405\ s \tag{52}$$

Since the rod ejection portion of the pulse occurs on the order of 0.100s, any nitrogen that flows through the regulator after the valve has been opened would not make it to the accumulator before the piston reaches the full-up position.

Before the pulse starts, the 97 feet of tubing between the accumulators and regulator is pressurized to 65 psig like the accumulators. Upon firing, the nitrogen rushes to fill the three accumulators as the accumulators lose pressure through the valve. During the duration of the rod ejection (0.100s), the accumulators drop ~15 psig, implying that the piping leading up to the accumulators also drops about 15 psig. In order to find the

amount of mass that enters the accumulators from the piping, the mass of nitrogen in the piping before and after the rod ejection must be compared.

$$mass\ before = Volume * \rho[65\ psig] \tag{53}$$

$$mass\ before = \frac{\pi(.305in)^2}{4} * 1164in * 2.213x10^{-4}\ \frac{lbs}{in^3} = 0.0188\ lbs \tag{54}$$

Where the internal diameter of .375 in. tubing is .305 in. (.035" wall). The densities of nitrogen at 65 psig and 50 psig are $2.213x10^{-4}\ \frac{lbs}{in^3}$ and $1.783x10^{-4}\ \frac{lbs}{in^3}$ respectively.

$$mass\ after = \frac{\pi(.305in)^2}{4} * (1164\ in) * 1.783x10^{-4}\frac{lbs}{in^3} = 0.0152\ lbs \tag{55}$$

The difference in mass between the two states is 0.0036 lbs pressurized at 50 psig. The difference in mass corresponds to a volume of 20.6 in^3. This volume is split between three accumulators, leaving an addition of 6.87 in^3per accumulator.

$$Volume\ Ratio = \frac{6.87\ in^3}{674\ in^3} = 1.02\% \tag{56}$$

The total volume added over the duration of the rod ejection is ~1% of the total volume of the accumulator. Note that this calculation is assumed to be free of losses, which is very unlikely and will drop the total volume addition to <1% per accumulator. Since the total addition from the piping is <1%, it has little effect on the total pressure in the accumulator or cylinder and can be ignored.

For longer RHU times (0.40s and longer), the valve stays open longer, allowing for more flow through the valve and into the accumulators. However, the rod ejection time stays fairly similar, meaning that the only difference is that the valve is open longer after the piston has reached the full-up position. While more nitrogen will flow into the accumulator during this time, it can be neglected due to the fact that the pressure between the cylinder and accumulators is close to equilibrium. The equilibration of the pressure causes the mass flow rate through the valve to drop towards zero, meaning that the flow into the accumulator will stay in the accumulator and not make it into the cylinder. Even for the longer duration of valve open time, the total volume of nitrogen added to the accumulator might reach up to 10% of the total accumulator volume, which considering very little makes it into the cylinder, means that it has little effect on the total system. Thereby, the assumption that the flow into the accumulator can be neglected is valid.

Flow Timing Delay from Valve to Cylinder

Once the nitrogen exits the valve on its way to the piston, there is a small delay in time for the nitrogen flow to reach the bottom of the piston. The nitrogen has to flow roughly 20 inches through one 1.25 in. diameter hose connected by a 1.25 in. 90 degree elbow before it reaches the cylinder manifold block (see Figure 51). The max flow rate of the nitrogen is near the beginning of the pulse when the pressure drop is the greatest. Based on the calculations with reference [6], the max flow speed is roughly 73 m/s or 2874 in/s. The flow delay is calculated as follows:

$$flow\ delay = \frac{flow\ length}{flow\ speed} = \frac{20\ in}{2874\frac{in}{s}} = .00696s \cong 7ms \tag{57}$$

This has a direct influence on the TR timing such that the pressure transducers don't start picking up the increased pressure until roughly 7 ms after the flow starts in the valve.

During the rod drop, the flow delay is greater due to a decreased flow speed which is caused by a smaller drop in pressure. The pressure drop between the cylinder and atmosphere during rod drop starts at a max value of roughly 40 psig and drops to 0 psig (atmosphere). This translates to an increased flow delay of ~3 ms, totaling ~10ms total.

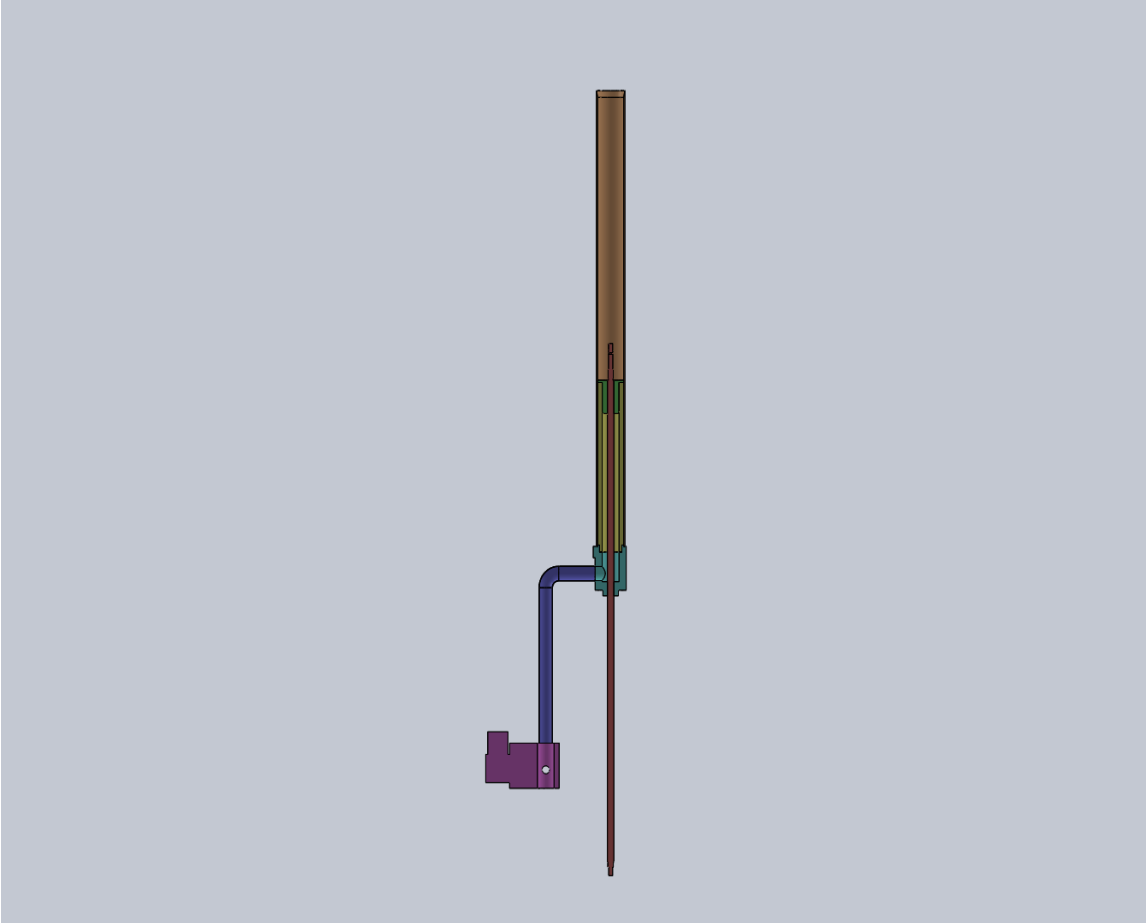

Figure 51. Visual Representation of Valve to Cylinder. The flow starts in the valve (pink) and flows through the piping to the manifold block and ending at the bottom of the piston. The valve and piping geometries are simplified for simulation.

Mass Flow Rate Calculation

Mass flow rate is calculated using ISA-75.01.01-2007, Flow Equations for Sizing Control Valves, published by the International Society of Automation (ISA) [21]. Since the flow through the TR pneumatic system is nitrogen, it is subject to compressible flow effects. The flow through the specific Parker Valve on the TR system can be classified into two categories: choked and non-choked flow. Choked flow occurs when the pressure difference between the two sides of the valve is so great that the mass flow rate is limited by the geometry of the valve. The result of choked flow is that the mass flow rate is only a function of the inlet pressure rather than the pressure difference; thereby, causing the mass flow rate to decrease in a more linear fashion for transient flow. The guidelines for choked vs. non-choked flow, as published by Swagelok (the company that manufactures the majority of parts that make up the TR pneumatic system), states that

flow will be choked when the downstream pressure of the valve is less than half of the upstream pressure [22]. With this in mind, here are the equations used by the analysis to calculate the mass flow rate.

Choked Flow

If $> F_\gamma X_{TP}$,

$$\dot{m} = \frac{0.667 C_v N_6 F_P \sqrt{F_\gamma X_{TP} P_1 \rho_1}}{3600} \qquad \left[\frac{lbm}{s}\right] \tag{58}$$

Where

$$C_v = Flow\ Coefficient = \mathbf{17.5} \tag{59}$$

$$N_6 = constant = \mathbf{63.3} \tag{60}$$

$$F_p = Piping\ Geometry\ Factor = \frac{1}{\sqrt{1 + \frac{\sum \xi}{N_2}\left(\frac{C_i}{d^2}\right)^2}} \tag{61}$$

$$F_\gamma = Specific\ Heat\ Ratio\ Factor = \frac{\gamma}{1.4} = \mathbf{1}\ for\ N_2 \tag{62}$$

$$X_{TP} = \frac{\frac{X_T}{F_p^2}}{1 + \frac{X_T \xi_i}{N_5}\left(\frac{C_i}{d^2}\right)^2} \tag{63}$$

$$X = \frac{P_1 - P_2}{P_1} \tag{64}$$

$$N_2 = 890; N_5 = 1000 \tag{65}$$

$$C_i = 1.3\ C_v \tag{66}$$

And P_1 and ρ_1 are the upstream pressure and density in units of psia and $\frac{lbm}{ft^3}$ respectively. X_{TP} is the pressure differential ratio factor of a control valve with attached fittings at choked flow, while X_T is the same factor without attached fittings. X_T for globe valves with a contoured plug is .72 [21]. ξ is the velocity head loss of a reducer, expander, or other fitting attached to a control valve or trim. The velocity head loss occurs twice at each inlet and exit, as shown below

$$\sum\xi = \xi_1 + \xi_2 + \xi_{B1} + \xi_{B2} \tag{67}$$

Where

$$\xi_1 = 0.5\left[1 - \left(\frac{d}{D_1}\right)^2\right] \rightarrow inlet\ expander \tag{68}$$

$$\xi_2 = 1.0\left[1 - \left(\frac{d}{D_2}\right)^2\right] \rightarrow outlet\ expander \tag{69}$$

$$\xi_{Bi} = 1 - \left(\frac{d}{D_i}\right)^4 \tag{70}$$

d is the nominal pipe diameter of 1.25 inches, and the inner diameter of the piping leading up to and away from the valve is 1.36 inches (D=D_1=D_2=1.36). Plugging in the values for the nominal and inner diameters of the pipes, $\sum\xi = .2304$. C_i is an assumed flow coefficient used for iterative purposes, and if both ends of the valve are the same size (they are), C_i can be used in place of C_v if $C_i \geq \frac{C_v}{F_P}$. Solving for F_p using C_i yields

$$F_P = \frac{1}{\sqrt{1 + \frac{.2304}{890}\left(\frac{1.3 * 17.5}{1.25^2}\right)^2}} = .974 \tag{71}$$

Since $1.3 * 17.5 = 22.75 \geq \frac{17.5}{.974} = 18.0$, F_P stands.

ξ_i from (63) equals the sum of (68) and (70) where $i = 1$. When the values are plugged in, $\xi_i = \xi_1 = .3604$. Solving for X_{TP}

$$X_{TP} = \frac{\frac{0.72}{0.974^2}}{1 + \frac{0.72 * .3604}{1000}\left(\frac{1.3 * 17.5}{1.25^2}\right)^2} = .7202 \tag{72}$$

Simplifying (72) with all of the factors and constants, yields the following equation for mass flow rate

$$\dot{m} = .1696\sqrt{P_1\rho_1} \qquad \left[\frac{lbm}{s}\right] \tag{73}$$

When

$$P_1 - P_2 \geq F_\gamma X_{TP} = .7202 \tag{74}$$

<u>Non-Choked Flow</u>

If $X < F_\gamma X_{TP} = .7202$,

$$\dot{m} = \frac{C_v N_6 F_p Y \sqrt{X P_1 \rho_1}}{3600} \qquad \left[\frac{lbm}{s}\right] \tag{75}$$

Where

$$Y = 1 - \frac{P_1 - P_2}{3 P_1 F_\gamma X_T} \tag{76}$$

APPENDIX C: DUST CAP ANALYTICAL SOLUTION EQUATIONS

The equations to solve this solution are taken from Table 24, Case 16 of Roark's Formulas for Stress and Strain 6th edition [20]. Displacement is calculated with equation 58 below for r>r_0:

$$y = -\frac{W}{16\pi D}\left[\frac{3+\nu}{1+\nu}(a^2 - r^2) - 2r^2 \ln\frac{a}{r}\right] \tag{77}$$

Where r_0 is the radius of the loading force (0.25 inches), ν is Poison's Ratio (0.33 for 6061-T6 Al], a is the radius of the disc (1.875 inches), W is the total applied loading (in lbf) and D is the plate constant represented by:

$$D = \frac{Et^3}{12(1-\nu^2)} \tag{78}$$

Where E is the modulus of elasticity of aluminum (10e6 psi) and t is the thickness of the plate (0.375 inches).

The maximum displacement, located at r=0, is calculated with equation 60:

$$y_{max} = -\frac{Wa^2}{16\pi D}\frac{3+\nu}{1+\nu} \tag{79}$$

The radial moment is calculated using equation 61:

$$M_r = \frac{W}{16\pi}\left[4(1+\nu)\ln\frac{a}{r} + (1-\nu)\left(\frac{a^2 - r^2}{a^2}\right)\frac{r_0^2}{r^2}\right] \tag{80}$$

The maximum radial moment is (at r=0):

$$M_{r,max} = \frac{W}{4\pi}\left[(1+\nu)\ln\frac{a}{r_0} + 1\right] \tag{81}$$

The radial stress can then be calculated based of the radial moment using:

$$\sigma = \frac{6M_r}{t^2} \tag{82}$$

A Python script is used to calculate the previously mentioned parameters. The max displacement, radial moment and stress calculated for W = 1996 lbf are 0.00767 inches, 584 lbf-in and 24.9 ksi respectively.

Figure 52 shows the dust cap with and without deformation.

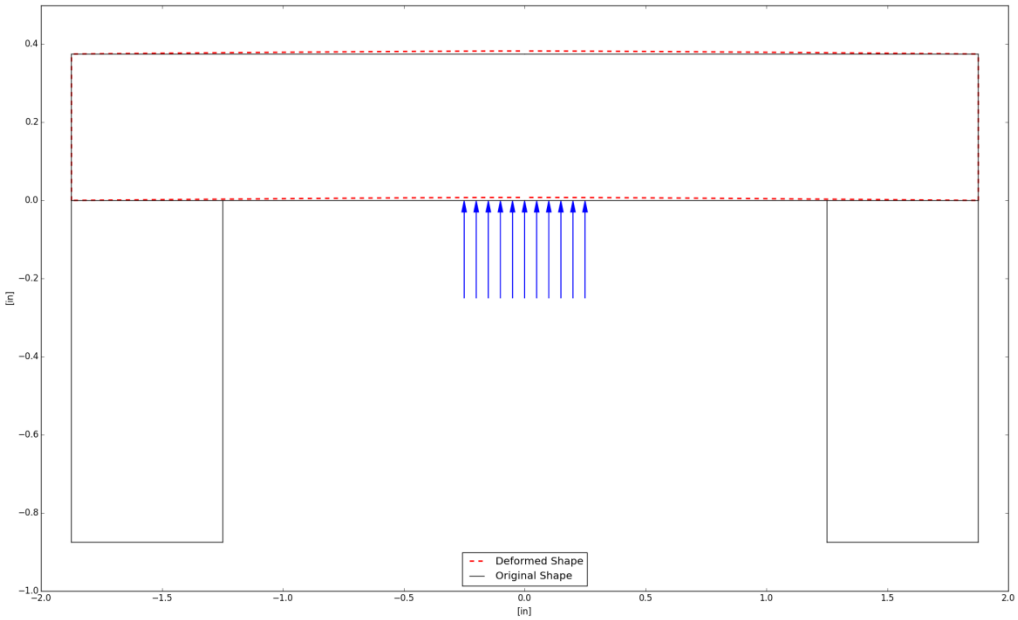

Figure 52. Deformed dust cap to scale according to equation 58

REFERENCES

1. Parma, E. J., et al., “Radiation Characterization Summary: ACRR Central Cavity Free-Field Environment with the 32-inch Pedestal at the Core Centerline,” SAND2015-6483, Sandia National Laboratories, November 2015.

2. Subaiya, P. V., “TA-V, Nuclear Safety Basis & Sandia Labs,” SAND2014-16125PE, Sandia National Laboratories, 2014.

3. Internal SNL Presentation, Lippert, L. L., “Transient Rod Issues Lessons Learned,” Sandia National Laboratories, February 2009.

4. DePriest, K. R., Trinh, T. Q., et al., “Reactor Pulse Repeatability Studies at the Annular Core Research Reactor,” SAND2011-3482C, Sandia National Laboratories, 2011.

5. Savitzky, Abraham, and M.J E. Golay. "Smoothing and Differentiation of Data by Simplified Least Squares Procedures." *Analytical Chemistry* 36.8 (1964): n. page. Web. 6 Mar. 2016.

6. Parker Pneumatic Division Applications Engineering (Private Communication, August 27, 2015).

7. R. Danny Beets (Private Communication, December 15, 2015).

8. Internal SNL Document, “Documented Safety Analysis for the Annular Core Research Reactor Facility,” Sandia National Laboratories, 2014.

9. Gyftopoulos, E. P., and Gian Paolo. Beretta. "Bulk Flow." *Thermodynamics: Foundations and Applications*. Mineola, NY: Dover Publications, 2005. 360-69. Print.

10. Knight, Erin, Matthew Russell, Dipti Sawalka, and Spencer Yendell. "ValveModeling." *Control Valve Wiki*. University of Michigan, 26 Sept. 2006. Web. 28 Nov. 2015.

11. Internal SNL Presentation, Beets, R. D., “RC/RC Upgrade Project PLRT: RO/RS Training,” Sandia National Laboratories, October 15, 2002.

12. Internal SNL Procedure, Gray, K. T., “ACRR-OP-002 - Pulse Operation,” Sandia National Laboratories, September 16, 2015.

13. Talley, D. G., “Initial Verification and Validation of RAZORBACK – A Research Reactor Transient Analysis Code,” SAND2015-8336, Sandia National Laboratories, September 2015.

14. Internal SNL Calculation, Talley, D. G., “ACRR-CALC-2015-002 Rod Bank Reactivity Curves and Differential Worth Parameters,” Sandia National Laboratories, February 2015.

15. Darren G. Talley (Private Communication, February 29, 2016)

16. Christensen, R. M. *The Theory of Materials Failure*. Oxford: Oxford UP, 2013. Print.

17. Oberg, Erik, Franklin Day Jones, Holbrook Lynedon Horton, and Henry H. Ryffel. *Machinery's Handbook: A Reference Book for the Mechanical Engineer, Designer, Manufacturing Engineer, Draftsman, Toolmaker, and Machinist*. New York: Industrial, 1988. Print.

18. *Aluminum Design Manual: Specifications & Guidelines for Aluminum Structures*. Washington, D.C.: Aluminum Association, 2005. Print.

19. “Unbrako Engineering Guide,” Unbrako, February 2016.

20. Roark, Raymond J., and Warren C. Young. *Roark's Formulas for Stress and Strain*. New York: McGraw-Hill, 1989. Print.

21. ISA-75.01.01-2007 (60534-2-1 Mod), “Flow Equations for Sizing Control Valves,” International Society of Automation, 2007.

22. “Valve Sizing: Technical Bulletin” Swagelok, December 2007.